UNIVERSITY OF CALIFORNIA
RIVERSIDE

Investigation of the Global Record, Taphonomy, Paleobiology, and Paleoecology of the Ediacaran Tubular Morphogroup

A Dissertation submitted in partial satisfaction
of the requirements for the degree of

Doctor of Philosophy

in

Earth and Planetary Sciences

by

Rachel L. Surprenant

June 2024

Dissertation Committee:
Dr. Mary L. Droser, Chairperson
Dr. Nigel Hughes
Dr. Rich Minnich

The Dissertation of Rachel L. Surprenant is approved:

_____

_____

_____

Committee Chairperson

University of California, Riverside

ACKNOWLEDGEMENTS

This research was funded by a Future Investigators in NASA Earth and Space Science Technology research grant (grant no. 80NSSC21K1526), the Lerner Grey Fund for Marine Research, the Desert Research Symposium Reynolds Award, and the Mike Murphy Endowed Field Studies Fund Summer Scholarship. I acknowledge that the Flinders Ranges lie within the traditional lands of the Adnyamathanha people and pay my respect to their Elders past, present, and emerging. We would also like to thank J. and R. Fargher and South Australia's Department of Environment and Water (DEW) (permit to MLD U27143-3) for access to the fossils at Nilpena National Heritage Site. Associated fieldwork was facilitated by S. Evans, J. Gehling, D. Rice, J. Perry, M.A. Binnie, J. Doggett, M. Dzaugis, M.E. Dzaugis, P. Dzaugis, N. Anderson, E. Hughes, I. Hughes, C. Hall, L., C. Casey, D.A. Droser, H. McCandless, W. Weyland, and P. Boan. I would also like to thank H. McCandless, T. Botha, N. Marshall, A. Hoffman, M. Zill, C. Hall, S. Evans, B. Kelly, G. Antell, R. Minnich, N. Hughes, P. Sadler, B. Gaines, R. Dahl, and D. Boyer for their friendship, mentorship, and support throughout my development as a scientist.

Thank you to my committee members N. Hughes and R. Minnich for broadening my knowledge of the fossil record and for providing helpful comments and discussion on the research in this dissertation. Thank you to my advisor Mary Droser for providing me with the inspiration and opportunity to conduct this research. Your unending support on all matters academic and personal made it possible for me to achieve this work and have

aided me in becoming a better paleontologist, teacher, mentor, and human being. To my family, L. Nolan, E. Surprenant, and K. Surprenant, thank you for your patience, love, and support. The curiosity for the world around me that was instilled in me through your example is the foundation of my passion for the Earth sciences and has shaped me into the scientist and person that I am today. I am also eternally grateful for the unwavering support of Raoul Fernandes who has been by my side through it all and never fails to remind me of what really matters at the end of the day.

Text in this dissertation, in part or in full, is a reprint of the materials as it appears in "New insight into the global record of the Ediacaran tubular morphogroup: A common solution to early multicellularity" (Royal Society Open Science, 2024, doi: 10.1098/rsos.231313) and in "Biostratinomy of the enigmatic tubular organism *Aulozoon soliorum*, the Rawnsley Quartzite, South Australia" (Gondwana Research, 2023, doi: 10.1016/j.gr.2023.06.010). The co-author Dr. Mary Droser listed on both publications directed and supervised the research that forms the basis of this dissertation.

ABSTRACT OF THE DISSERTATION

Investigation of the Global Record, Taphonomy, Paleobiology, and Paleoecology of the Ediacaran Tubular Morphogroup

by

Rachel L. Surprenant

Doctor of Philosophy, Graduate Program in Earth and Planetary Sciences
University of California, Riverside, June 2024
Dr. Mary L. Droser, Chairperson

The earliest fossil evidence for complex, macroscopic, community forming organisms on Earth is preserved in the Ediacara biota (575—538 Ma). While placement of Ediacaran taxa within a phylogenetic framework is difficult due to their unique morphologies that are non-analogous to the definitive metazoans of the Phanerozoic, they can be categorized into grades based on body plan similarity, resulting in suites of morphologically similar, but not necessarily phylogenetically related, taxa known as morphogroups. The tubular morphogroup includes all macroscopic, metazoan-grade organisms with hollow and elongate morphologies and is one of the most commonly occurring Ediacaran morphogroups, suggesting that a tubular form was an advantageous morphology for early complex organisms. However, the nature of this advantage is unknown and untestable due to insufficient baseline understanding of the number of genera included in the morphogroup, their temporal ranges, as well as their paleobiological traits and paleoecological strategies. This dissertation develops a foundational understanding of these questions pertaining to the tubular morphogroup

through database generation and analysis, detailed taphonomic investigation, and analysis of growth strategies. Synthesis of the global record of the Ediacaran tubular morphogroup demonstrates that they are the most diverse Ediacaran morphogroup and were key components of Ediacaran ecosystems for ~20 million years longer than was previously appreciated. Detailed taphonomic investigation of the tubular organism *Aulozoon soliorum* from the Ediacara Member of South Australia provides novel insight into the morphology, biomaterials, and paleoecology of this taxon as well as develops a methodology for distinguishing between true morphological features and taphonomically-derived features that that can be leveraged for investigation of other tubular taxa. Study of the growth strategies of the tubular organism *Funisia dorothea* from the Ediacara Member of South Australia demonstrates that, despite a broadly simple form, *Funisia's* growth was highly regulated. Additionally, comparison of *Funisia's* growth strategies with another tubular organism, *Wutubus annularis*, reveals that shared morphology of tubular organisms does not beget developmental or paleoecological similarity. Ultimately, this research develops understanding of what genera, paleoecological strategies, and paleobiological traits are encompassed by the tubular morphogroup and provides novel frameworks for the identification of paleobiologically and paleoecologically meaningful characteristics of individual tubular genera.

TABLE OF CONTENTS

LIST OF FIGURES

INTRODUCTION

CHAPTER 1

CHAPTER 2

CHAPTER 3

APPENDIX B

APPENDIX C

LIST OF TABLES

CHAPTER 2

CHAPTER 3

APPENDIX A

APPENDIX B

INTRODUCTION

The Ediacara biota (575—538 Ma) is a group of globally distributed, predominantly soft-bodied fossils that provide the earliest evidence of macroscopic, complex, community forming organisms on Earth (Droser and Gehling, 2015). Fossils of the Ediacara biota can be divided into three temporally distinct assemblages, the Avalon (575—560 Ma), the White Sea (560— 550 Ma), and the Nama (550— 538 Ma) (Evans et al., 2022), that record an increase in complexity and diversity throughout the terminal Ediacaran (Erwin et al., 2011). Several members of the Ediacara biota have been identified as stem-group metazoans and have been aligned with extant phyla, including Annelida, Cnidaria, and Mollusca (Gehling et al., 2014; Bobrovskiy et al., 2018; Schiffbauer et al., 2020; Evans et al., 2020, 2021; Dunn et al., 2022;). However, many members of the Ediacara biota remain phylogenetically enigmatic and their paleobiological traits and paleoecological strategies are poorly understood (Erwin et al., 2011). This can primarily be attributed to their distinct morphologies that are non-analogous to the definitive metazoans of the Phanerozoic and to their lack of biomineral tissues which lends them to high amounts of taphonomic overprint that can shroud phylogenetically meaningful characteristics.

In the absence of a phylogenetic framework for the Ediacara biota, an effective way in which to group them in order to discern patterns of evolution in these early animal communities is to classify them into morphogroups. Ediacaran morphogroups represent grades of Ediacaran organisms that share a constructional morphology but are not necessarily phylogenetically linked (Dunn et al., 2018; Grazhdankin 2014). The tubular

morphogroup is one of these groupings of Ediacaran organisms, defined as any macroscopic, metazoan-grade organism with a hollow, elongate morphology. This morphogroup is remarkable for its uniquely high abundance (Xiao et al., 2002; Droser and Gehling, 2008; Cai et al., 2012; Wang et al., 2021; Gehling and Runnegar, 2022), its global distribution (Xiao et al., 2016; Selly et al., 2020; Boddy et al., 2022), and its links to metazoan phyla, including Cnidaria, Annelida, and Porifera (Droser and Gehling, 2008; Wood and Kurtis, 2015; Schiffbauer et al., 2020; Yang et al., 2020; Park et al., 2021; Bobrovskiy et al., 2022). These characteristics of the tubular morphogroup indicate that a hollow and elongate morphology was an advantageous body plan for early complex life, but the nature of the paleobiological traits and paleoecological strategies that underlie their success is unclear and the total number of genera within the morphogroup and the temporal distribution of individual tubular taxa are unknown.

This is primarily due to the hollow and simple nature of the genera that comprise the tubular morphogroup which leads to their common preservation as non-descript elongate structures that historically led to their misidentification as trace fossils (Jensen et al., 2006). Upon review of the Ediacaran trace fossil record, the majority of fossils identified as traces were reinterpreted as metazoan-grade tubular body fossils, effectively shifting the perception of the Ediacaran fossil record from one dominated by bilaterian-grade trace makers to one dominated by relatively simple tubular organisms (Jensen et al., 2006). This paradigm shift instilled the significance of tubular organisms within the Ediacara biota but also highlighted a central problem with the morphogroup in that their

hollow and simple morphologies lead to non-descript and taphonomically complex preservation that obfuscates the number of genera that comprise the tubular morphogroup as well as the temporal distribution, paleobiological traits, and paleoecological strategies of individual tubular genera. As a result, current understanding of the tubular morphogroup lacks a robust framework for identifying these key characteristics of the morphogroup, thus it is left with little intrinsic phylogenetic, paleoecological, or paleobiological meaning.

The goal of this dissertation is to address these shortcomings in understanding of the tubular morphogroup through three studies that investigate the tubular morphogroup via three distinct methodologies, including, (1) database generation and analysis for investigation of the total tubular morphogroup, (2) detailed taphonomic investigation of individual tubular taxa, and (3) analysis of growth strategies in individual tubular taxa and comparison of developmental processes between genera. The second and third studies are specimen-based and utilize fossils from the Ediacara Member of the Flinders Ranges in South Australia (Figure 1), which preserve an exceptionally complete record of organisms of the White Sea assemblage. The second study is a detailed taphonomic investigation of the tubular organism *Aulozoon soliorum* which is preserved in multiple localities within and west of the Flinders Ranges (Figure 1a, d-f). The third study investigates the growth strategies of the highly abundant tubular organism *Funisia dorothea* which is also found in multiple localities west of the Flinders Ranges (Figure 1b, c, d).

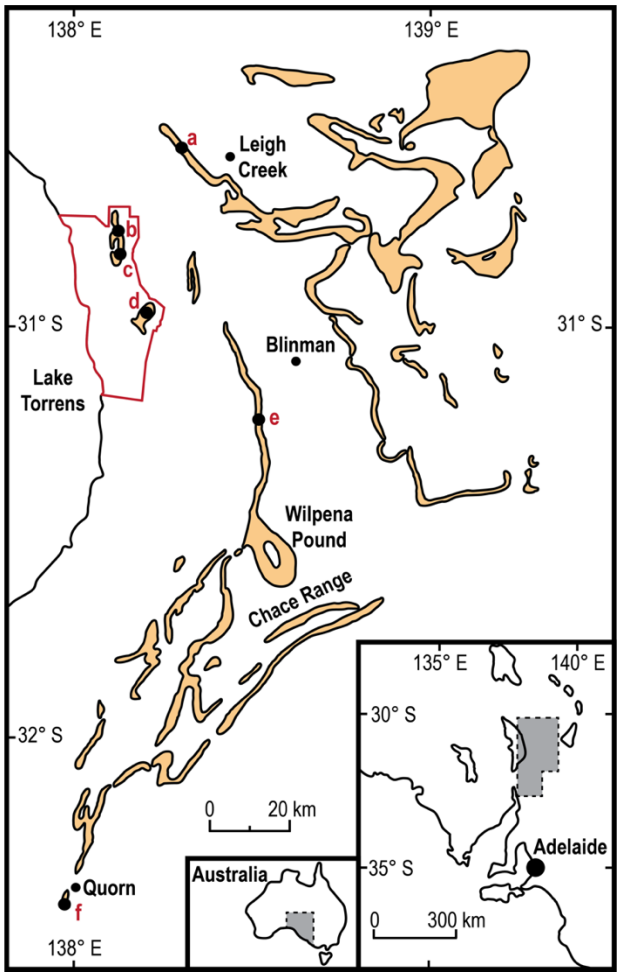

Figure 1. Geographic context of the Flinders Ranges, South Australia, with outcrop of the Pound Subgroup (Bonney Sandstone and Rawnsley Quartzite, including the Ediacara Member) denoted in orange. Nilpena Ediacara National Park is denoted by the red outline. Fossil localities pertinent to Chapters 2 and 3 are labelled letters a-f. (a) Mount Scott Range. (b) The locality formerly known as the Ediacara Conservation Park. (c) the South Ediacara Mine Site. (d) The original Nilpena National Heritage Site. (e) Bathtub Gorge. (f) Devil's Peak. *Aulozoon soliorum* specimens discussed in Chapter 2 are from localities a, d, e, and f. *Funisia dorothea* specimens used for Chapter 3 are from localities b, c, and d.

This dissertation provides the first synthesis of the global record of the tubular morphogroup and highlights several shortcomings in the current understanding of the morphogroup that preclude testing of hypotheses on why a tubular form is the most

common morphology within the Ediacara biota and how the abundance of tubular taxa may have impacted the ecosystems in which they lived. These big picture questions pertaining to the fossil record of the tubular morphogroup motivate the second and third chapters of this dissertation which take a specimen-based approach to create taphonomic and developmental frameworks for the characterization of the paleoecology, paleobiology, and biomaterials of individual tubular genera that can be leveraged to refine understanding of the total tubular morphogroup. Results demonstrate that detailed taxon-based taphonomic and developmental investigations provide a mechanism for determining paleobiologically and paleoecologically meaningful characters in tubular taxa despite their relatively simple morphologies. Ultimately, this dissertation provides novel insight into the fossil record of the tubular morphogroup as a whole, develops understanding of the morphology, paleoecology, and paleobiology of the two most abundant tubular taxa in the Ediacara Member, and provides a framework for investigation of other enigmatic tubular taxa that can be leveraged to refine understanding of the total tubular morphogroup.

CHAPTER 1: NEW INSIGHT INTO THE GLOBAL RECORD OF THE EDIACARAN TUBULAR MORPHOGROUP: A COMMON SOLUTION TO EARLY MULTICELLULARITY

Abstract

The tubular morphogroup is a common component of Earth's first complex, multicellular communities—the Ediacara biota—and offers valuable insight into biological traits that are fundamental to animal life because they have intriguing links to metazoan phyla and are highly abundant in Ediacaran ecosystems. Biomineral tubes (e.g., *Cloudina*) are well described from the Nama assemblage (~550–538 Ma), yielding a relatively detailed understanding of this subset of the morphogroup. Conversely, the non-biomineral tubular taxa of the Nama assemblage, as well as of the older White Sea assemblage (~560–550 Ma), are poorly understood. As a result, the variability of characters that define non-biomineral tubular organisms is unknown and their diversity dynamics throughout the terminal Ediacaran are unconstrained. To test hypotheses related to the diversity, morphological variability and temporal distribution of non-biomineral tubes, a comprehensive database of non-biomineral Ediacaran tubular taxa was compiled. Results demonstrate previously unrecognized morphological disparity in the non-biomineral tubular morphogroup and reveal that it comprises a higher number of genera than all other non-tubular morphogroups in the White Sea and the Nama. Thus, it illustrates that a tubular form dominated Ediacaran ecosystems for considerably longer than previously appreciated and, importantly, was the most common solution to early multicellularity.

Introduction

The Ediacara biota represent the oldest record of complex, community-forming animals and have traditionally been divided into three temporally distinct assemblages, including the Avalon (575–560 Ma), the White Sea (560–550 Ma), and the Nama (550–538 Ma) (Narbonne, 2005, but see Wood et al., 2023). The Ediacaran tubular morphogroup, a suite of organisms characterized by their shared hollow and elongated morphologies, is recognized as a significant component of the Ediacara biota, associated with the White Sea and Nama assemblages, owing to their global distribution (Xiao et al., 2016; Selly et al., 2020; Boddy et al., 2022), high abundance (Xiao et al., 2002; Droser and Gehling, 2008; Cai et al., 2012; Wang et al., 2021; Gehling and Runnegar, 2022) and links to metazoan phyla, including Cnidaria, Porifera, and Annelida (Droser and Gehling, 2008; Wood and Kurtis, 2015; Schiffbauer et al., 2020; Yang et al., 2020; Park et al., 2021; Bobrovskiy et al., 2022).

The common occurrence of a tubular form in the Ediacaran suggests that there was an advantage to this constructional morphology, the nature of which remains unknown. This is further supported by the fact that the tubular morphogroup is one of only four Ediacaran morphogroups (i.e., Arboreomorpha, Erniettomorpha, Rangeomorpha, and tubular organisms) that occur in both the White Sea assemblage and the Nama assemblage. Not only does this demonstrate that tubes were key components of Ediacaran ecosystems but also that the morphogroup persisted across the White Sea–Nama extinction event, which is associated with a loss of 80% of Ediacaran genera and the

extinction of four morphogroups (Evans et al., 2022). Subsequent to the extinction event, the relatively depauperate communities of the Nama assemblage are dominated by an abundant tubular fauna thought to have radiated in and to be uniquely characteristic of the Nama assemblage (Schiffbauer et al., 2016; Darroch et al., 2018; Bowyer et al., 2023; Wood et al., 2023).

The observed radiation of tubular organisms in the Nama assemblage is a well-documented event that has been demonstrated through a series of thorough analyses drawing primarily from the record of biomineral tubular taxa (e.g., Selly et al., 2020; Yang et al., 2020). The number of biomineral tubular genera, their characteristics and their temporal distributions have been well documented, with particularly thorough insight being provided by Selly et al., (2020) (table 1; figure 10) and by Yang et al., (2020) (figures 5, 7). Comparatively little is known about the non-biomineral members of the tubular morphogroup which first appear in the White Sea assemblage and persist into the Nama assemblage. Despite reports of abundant non-biomineral tubes from the Nama assemblage (Wood et al., 2023) and the White Sea assemblage (Gnilovskaya, 1996; Sappenfield et al., 2011; Gehling and Droser, 2013; Ivantsov et al., 2015; Gehling and Droser, 2018; Ivantsov et al., 2019; Ye et al., 2019; Bobrovskiy et al., 2022; Boddy et al., 2022; Gehling and Runnegar 2022; Golubkova et al., 2022; Surprenant et al., 2023), in some cases occurring in such high abundance that they shaped ecosystems by limiting available ecospace (Tarhan et al., 2015; Surprenant et al., 2020), there is no comprehensive understanding of the number of genera that comprise the non-biomineral

subset of the tubular morphogroup, their morphological characteristics or temporal variability. As a result, the radiation of tubes in the Nama assemblage remains uncontextualized by the diversity of the tubular taxa that preceded them, obfuscating the scale and nature of tubular diversification in the terminal Ediacaran.

This study addresses these outstanding questions through the creation and analysis of a database containing all occurrences of non-biomineral Ediacaran tubular organisms. The database is the first comprehensive global study of non-biomineral Ediacaran tubular organisms and is used to accomplish two primary goals geared towards providing novel insight into the non-biomineral tubular morphogroup: (i) identify the number of non-biomineral tubular genera and define the extent of their morphological variability, including gross morphology and external characters and (ii) describe the temporal variability in the number of genera and the constructional complexity of non-biomineral tubular organisms in the terminal Ediacaran.

Results demonstrate a previously unrecognized diversity of gross morphologies and external characteristics in the non-biomineral tubular morphogroup, which is contrary to their common description as exceedingly simple organisms. Additionally, when compared to all other Ediacaran morphogroups, non-biomineral tubular organisms have the highest number of genera in both the White Sea assemblage and the Nama assemblage. The dominance of tubes in both assemblages shows that they made up a significant component of Ediacaran ecosystems for a considerably longer period of time

than has previously been recognized. Notably, it is also found that the diversity of tubular organisms in the White Sea assemblage is broadly similar to the tubular fauna of the Nama assemblage, though there is a recorded increase in the compositional complexity of non-biomineral tubular taxa in the Nama assemblage.

Methods

The database developed for this study was constructed via data mining of peer-reviewed literature published before July 2023 and includes all occurrences of non-biomineral tubular organisms in the Ediacaran fossil record (Appendix A Table 7). The record of biomineral tubes is relatively well documented and well understood (Selly et al., 2020; Yang et al., 2020). The aim of this study is to elucidate the non-biomineral tubular record; thus, only the non-biomineral members of the tubular morphogroup were included in the database. Results from this study provide new data that can be compared with results from previous research on biomineral tubes. This comparison is carried out in this study in order to contextualize the non-biomineral tubular record within the total morphogroup.

The term non-biomineral is here used to describe any tubular organism that is interpreted as having been originally non-rigid organic, rigid organic (e.g., kerogen) or non-biomineral to weakly biomineral. The latter category is included in this study because there is persisting uncertainty about the presence of biomineralization in the tubes categorized as such. The exclusion of biomineral taxa removed the majority of

Cloudinomorphs from this study. However, the non-biomineral Cloudinomorphs (i.e., *Costatubus spp*., *Conotubus hemiannula*tus, *Convolotubus dargazinensis*, *Shaanxilithes ningqiangensis*, *Zuunia chimidtsereni*) were included because their unit-in-unit structure provides an interesting contrast to all other tubular organisms (Selly et al., 2020).

Here, a tubular organism is defined as any metazoan-grade organism with a single hollow and elongate form. Genera included in the database were formally described in the literature as tubular organisms. Any form that was described as 'tubular' but for which a macroalgal or single-cellular interpretation is preferred was excluded from the analysis (e.g., *Liulingjitaenia* (Xiao et al., 2002); *Platysolenites* (McIlroy et al., 2001; Kontorovich et al., 2008). Forms comprised of multiple tubes (e.g., *Ernietta*) or multiple parts including a tube (e.g., *Namacalathus*) are also excluded (Elliott et al., 2016; Shore et al., 2021), because a single tube comprising the entirety of an organism is a distinct and commonly occurring form. Additionally, the definition of a tubular organism used here excludes the taxon *Plexus ricei* (Joel et al., 2014), which has in the past been described as a tubular organism but was re-evaluated by the authors subsequent to the compilation of the database, through which it became evident that *Plexus* is not a true tubular organism as its central axis never fully collapses, indicating that it was not hollow and thus does not fall within the definition of a tube used here. Additionally, the taxon *Thectardis avalonensis* of the Avalon assemblage was excluded from the analysis. Despite the fact that *Thectardis* possesses an overall morphology that is consistent with tubular organisms, it is not described as tubular in the literature, and it is most commonly

grouped with Poriferan taxa, not tubes. While the authors would make the argument that *Thectardis* should be considered a tube based on outstanding definitions of the morphogroup, it was not included.

Individual entries in the database constructed for this study represent the occurrence of a non-biomineral tubular genus in a distinct fossil site or lithological unit (e.g., member or formation). Each entry does not indicate paleoenvironmental, lithological, taphonomic or paleogeographic distinction. Distinct fossil sites are defined as outcrops where tubular fossils occur that have different names and different modern geographic coordinates. These are used to characterize the occurrence of non-biomineral tubes and do not imply paleogeographic distinction.

The occurrence of non-biomineral tubes in paleogeographically distinct localities was identified after data compilation based on the location of each fossil site within its broader locality and associated paleocontinent, informed by reconstructions in Merdith et al., (2021). Disparate paleogeographic locations were determined based on the distance and distribution of paleocontinents, meaning that fossil sites that are estimated to have been associated with different paleocontinents (e.g., Siberia and Baltica; North China and South China) are disparate. Fossil sites that are inferred to have been associated with the same paleocontinents but are found in localities on distinct paleoshorelines or are separated by a large distance are also considered to be disparate (e.g., the Wood Canyon Formation and the Deep Spring Formation are not disparate, but those Great Basin sites

are considered to be disparate from the Miette Group of northwestern Canada despite all occurring on the paleocontinent Laurentia). As such, many distinct occurrences in the database (i.e., individual entries) are found to occur in the same paleogeographic location (Appendix A Tables 5, 7).

Entries in the database are resolved to the species level. However, only four genera are not monospecific (i.e., *Costatubus bibendi*, *C. kirsnovi*; *Saarina hagadorni*, *S. juliae*; *Sinospongia typica*, *S. chenjunyuani*; and *Vaveliksia velikanovi*, *V. svetozarovae*, *V. vana*). Some of these species concepts are based on the occurrence of distinct external characters, so the morphology-based component of this study is resolved to the species level. However, analysis of temporal patterns was conducted at the genus level because the majority of non-biomineral tubular taxa are monospecific, and this is a standard practice in broad-scale analysis of the Ediacara biota. While this obfuscates differences between the species of non-biomineral tubular genera, these species concepts reflect differences in size and external features that do not impact the analyses or results pertaining to temporal patterns in non-biomineral tubes.

Temporal ranges of non-biomineral tubular genera were ascertained through the compilation of the oldest and youngest occurrences of each genus. In many cases, non-biomineral tubes are preserved in formations that have poor geochronological constraints. This uncertainty was addressed by plotting occurrences within the assemblage only,

resulting in an assemblage presence or absence assessment, not a range chart. While many of these organisms are thought to have had shorter temporal ranges, any other illustration of the data would be ignoring occurrences of tubular genera in poorly dated strata and/or presenting inaccurate ranges. For example, *Shaanxilithes* has a short stratigraphic range in China and Namibia, where dates are well constrained, but occurrences in other localities such as the Eastern European Platform, where some strata are less well constrained, call that short range into question. To compare the number of genera that comprise the non-biomineral subset of the tubular morphogroup and how this diversity changed through time relative to other Ediacaran morphogroups (Appendix A Table 6), the database compiled by Evans et al., (2022) was used.

Results and discussion

Diversity

A primary goal of this study was to identify the number of macroscopic, metazoan-grade non-biomineral tubular genera present in the Ediacaran Period. The database compiled for this study contains 108 non-biomineral tubular fossil occurrences, representing 27 genera distributed across 14 paleogeographically distinct locations and 36 formations of the White Sea and Nama age (Appendix A Table 7). The broad paleogeographic distribution of non-biomineral tubular organisms is consistent with previously documented patterns in the entirety of the Ediacara biota and in subsets of tubular taxa (Selly et al., 2020; Boddy et al., 2022; Evans et al., 2022). However, the total number of non-biomineral tubular genera is higher than previously appreciated and is remarkably

high when compared to the other non-tubular Ediacaran morphogroups (Figure 2). The non-tubular morphogroups with the highest number of genera are the Rangeomorpha, Bilateriomorpha and Erniettomorpha with 15, 14 and 10 genera, respectively. At 27 genera, non-biomineral tubes have a 45% higher number of genera than the most diverse non-tubular morphogroup, the Rangeomorpha. This previously unrecognized diversity of non-biomineral tubes demonstrates that a hollow, elongate form was the most common solution to complex life in the Ediacaran and, in conjunction with their high abundance in Ediacaran communities, suggests that this commonly occurring form was advantageous for life in Ediacaran oceans prior to the advent of biomineralization in Cloudinomorphs.

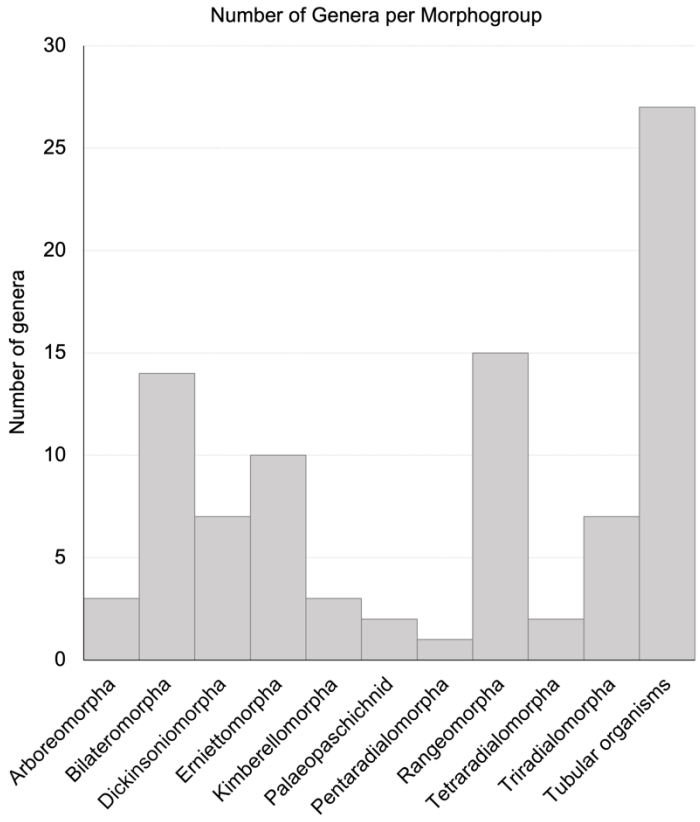

Figure 2. The number of genera in each major Ediacaran morphogroup, including genera present in the Avalon, White Sea, and Nama assemblages.

Morphological disparity

In addition to the identification of the number of non-biomineral tubular genera, this study aimed to describe the extent of morphological variability across non-biomineral tubes, including the assessment of gross morphological variability and diversity of external characters. While the idea that non-biomineral tubes vary morphologically is broadly understood, the extent and nature of this variability have not been characterized. Synthesis of the database reveals a high morphological disparity within the non-biomineral members of the tubular morphogroup despite their shared hollow and elongated forms. Overall morphology can be cylindrical, conical, ovular, or comprised of nested growth units (i.e., Cloudinomorphs). This demonstrates that a cylindrical form is not diagnostic of all non-biomineral tubular taxa and that there is a suite of morphological features that can be used to place non-biomineral tubular taxa within a descriptive framework to provide a more robust definition of the total morphogroup.

Cloudinomorphs, defined as biomineral and non-biomineral tubes constructed of nested and repeating collared cylindrical units, have previously been characterized as a subgrouping of the tubular morphogroup based on gross morphology and growth units (Selly et al., 2020). The remaining non-biomineral tubes have not been similarly classified. To place all tubular taxa within a consistent classification framework that aids in the holistic description of the morphological variation in tubes, new subgroupings for tubular organisms, defined in a manner consistent with the previously established Cloudinomorph grouping, are proposed (Figure 3).

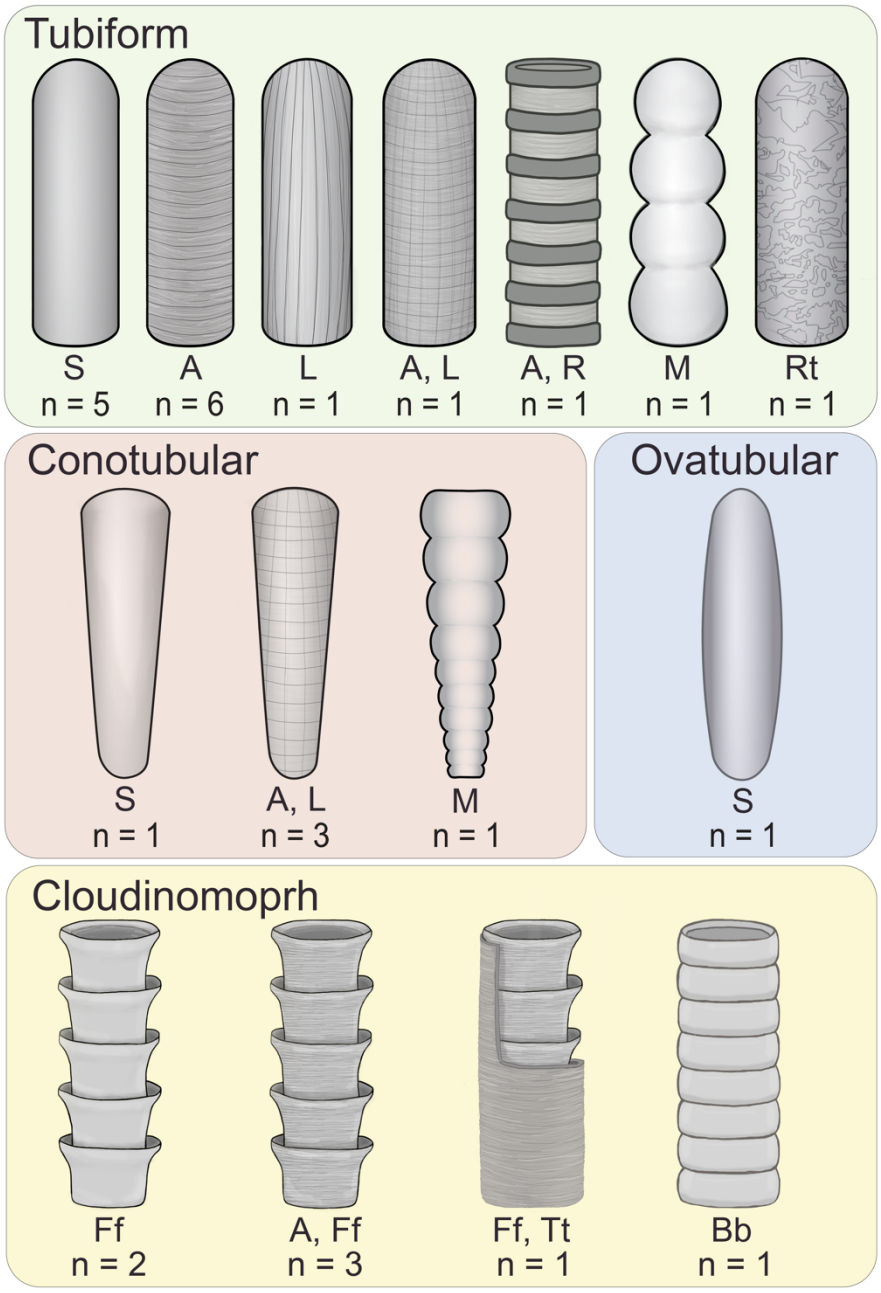

Figure 3. Illustration of the newly proposed form subgroupings and their external characters. N values are the number of genera within each subgrouping that possess the illustrated external features. External feature abbreviations: S, smooth; A, annulae; L, longitudinal striations; R, rings; M, modular elements; Rt, reticulation; Ff, funnel-in-funnel growth units; Bb, barrel-in-barrel growth units; Tt, tube in tube.

The proposed subgroupings include tubiform taxa, which have a cylindrical gross morphology, ovatubular taxa, which have an oval gross morphology that tapers at both ends, and conotubular taxa, which have a conical gross morphology that tapers basally. These groups were defined based on inferred dominant growth pattern, reflective of the fact that tubiform, conotubular, and ovatubular morphologies are necessarily distinct in their dominant growth patterns. Because external characters are not robust indicators of growth patterns in the absence of detailed specimen-based analysis, they were not used to define the subgroupings. These subgroupings do not imply phylogenetic similarity or convergence and are intended to serve solely as an illustrative framework for defining the morphogroup with less generalization. Notably, external features such as annulae and modules do not appear to be characteristic of any one subgrouping. Instead, these features are observed to occur in multiple subgroupings (Figure 3).

It is important to note that these new subgroupings are inclusive of all non-biomineral tubes but perpetuate the central problem with the tubular morphogroup in that it encompasses a prohibitively broad range of biological traits that, even with form-based subgroupings, are not phylogenetically meaningful. Thus, a classification scheme dependent solely on gross and constructional morphology is insufficient for identifying true synapomorphies in the tubular morphogroup. Furthermore, characterization of these subgroupings based on external characteristics (e.g., modules, annulae) can be misleading owing to convergence.

Additionally, neither gross morphology nor external features serve as an accurate proxy for paleoecological strategies. Therefore, the extent of convergence, the phylogenetic affinities and the ecosystem impacts of tubular organisms as a total group remain unresolved and untestable.

Moving forward, the most effective strategy for defining subgroupings of tubular organisms should not aim to define phylogenetic similarity but instead be centered on establishing groups based on paleoecological similarity. This approach allows for the interpretation of the ecosystem impacts of tubular organisms without making untestable assumptions on phylogenetic similarity and has the potential to provide novel insight into the biological traits of tubular organisms as well. To aid in this endeavor, the constructional morphology of tubular organisms should be split into two groupings: tubicolous construction and fluid-filled tubular construction. The former represents an organism living within an external tube with an open aperture and the latter represents an organism consists of a single body wall encompassing a fluid-filled interior with a closed aperture. These are distinct constructional morphologies that could also be convergently evolved but are certainly more paleobiologically and paleoecologically meaningful than other methods of grouping. However, the data collected here reveal a dearth of tubular taxa that are definitively demonstrated to have had a closed or open aperture, and preservation of internal soft tissue is exceedingly rare (Schiffbauer et al., 2020).

As such, the existing understanding of tubular genera precludes the sorting of all tubular taxa into fluid-filled tubular forms and tubicolous tubular forms. That being said, the difference between Cloudinomorphs and all other tubular organisms is, currently, the best constraint on distinguishing between fluid-filled tubular organisms and tubicolous tubular organisms, as the characteristic multi-layered, nested, repeating growth units of Cloudinomorphs are most parsimoniously reconstructed as an external tube housing an organism. However, this is not a catch-all definition because several non-Cloudinomorphs are hypothesized to have had open apertures and internally dwelling organisms (e.g., *Calyptrina striata*) (Bobrovskiy et al., 2022). While the fossil evidence to corroborate these hypotheses is lacking, for example, the documentation of an open aperture is tenuous and there are no internal features preserved, it does cast doubt on the ability of the Cloudinomorph grouping to fully encompass all tubicolous forms.

This calls for a reassessment of known tubular genera with careful consideration of aperture morphology to instill more meaningful subcategories of tubular organisms that can be used to test broader hypotheses pertaining to the role of tubular organisms in terminal Ediacaran ecosystems.

Temporal variability

The second goal of this study was to describe the temporal variability in the number of genera and the constructional complexity of non-biomineral tubular organisms. This analysis is independent of the morphological sub-groupings defined above. When non-

biomineral tubular genera are categorized as occurring in only the White Sea assemblage, only in the Nama assemblage, or in both the White Sea and the Nama assemblages, several newly recognized patterns in their diversity and constructional complexity (i.e., inferred original composition) through time are apparent (Figure 4). Firstly, there are a minimum of 14 non-biomineral tubular genera present in the White Sea assemblage and 15 genera present in the Nama assemblage, with four of the genera from the White Sea assemblage carrying over into the Nama assemblage. Thus, the remarkably high number of non-biomineral tubular genera relative to other morphogroups is upheld within each assemblage. This demonstrates that the total morphogroup originated in and dominated the White Sea assemblage. Therefore, the dominance of the tubular morphogroup is not a signal driven by the radiation of non-biomineral tubes in the Nama assemblage, despite the appearance of novel non-biomineral tubular genera. Instead, the reign of the tubular morphogroup is firmly rooted within the White Sea assemblage, illustrating that a tubular morphology was not a unique solution to the paleoenvironmental conditions or paleoecological strategies of the Nama assemblage but was a long-ranging solution to complex multicellularity in Ediacaran oceans.

Notably, only four genera definitively occur in both assemblages. This constitutes a loss of 71% of tubular genera as a result of the White Sea–Nama extinction event (Evans et al., 2022). This is marginally lower than the ~80% loss of genera calculated by Evans et al., (2022) for all Ediacaran taxa. Non-biomineral tubes additionally record a remarkable recovery after the extinction event, regaining a similar number of genera subsequent to

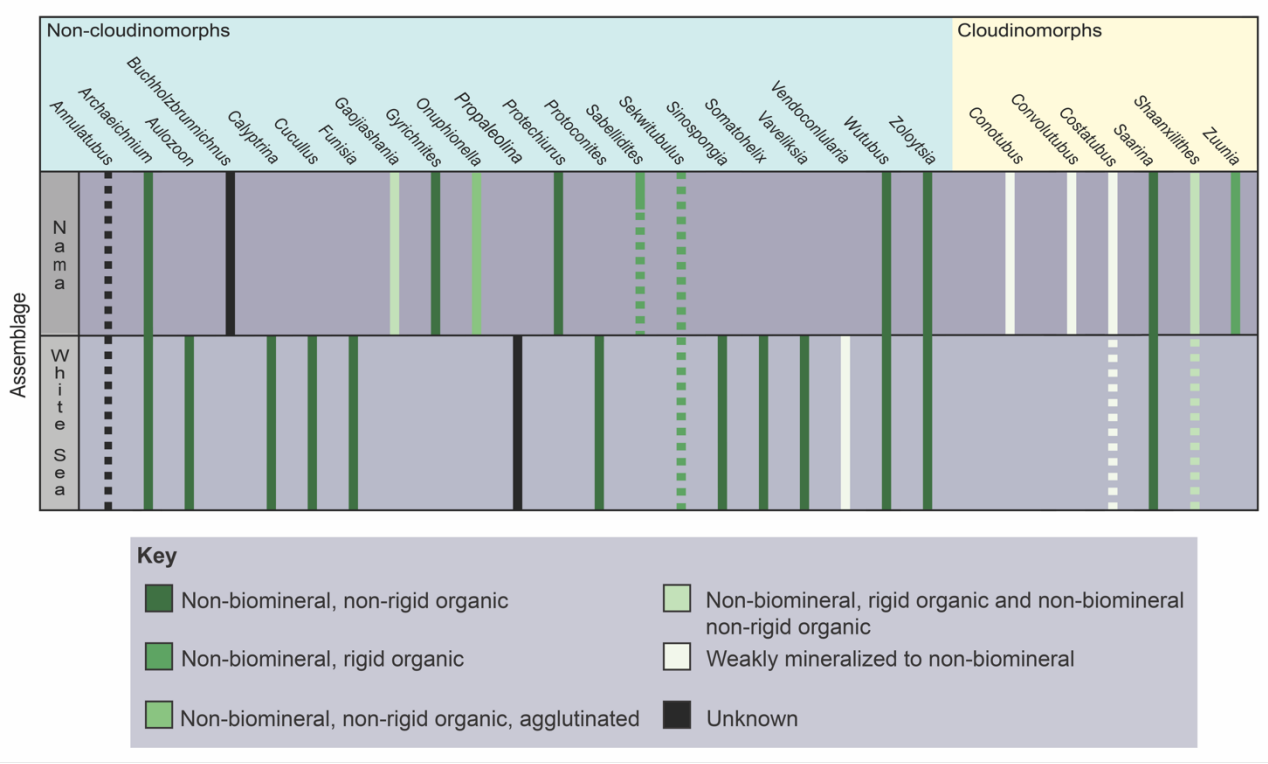

Figure 4. Schematic illustrating the presence or absence of non-biomineral tubular genera in the White Sea assemblage and the Nama assemblage. Dotted lines indicate genera with poor age constraints that potentially occur within the assemblage across which the line is dotted but cannot be definitively placed. Partially dotted lines (e.g., *Shaanxilithes*) represent genera for which some occurrences are well dated (solid lines), but other occurrences are poorly dated and could represent occurrences in the White Sea assemblage or the Nama assemblage (dotted lines). *Sabellidites* is well known to occur only in the terminal Nama assemblage, but there are several occurrences with poor age constraints. The line was dotted throughout the Nama assemblage to reflect this uncertainty but is not extended into the White Sea assemblage given their known restriction to the Nama assemblage. Occurrences represented solely by dotted lines are not considered in the analysis.

the event. This indicates that the extinction did not have a long-lasting effect on the ability of non-biomineral tubular organisms to originate and to dominate Ediacaran ecosystems.

The absence of a large increase in the number of non-biomineral tubular genera in the Nama assemblage calls into question the paradigm of the Nama assemblage as the age of tubes. When non-biomineral tubes are viewed in isolation, they indeed have a comparable number of genera in the White Sea and the Nama assemblages. However, the relatively depauperate Nama assemblage can appear to be uniquely dominated by the tubular morphogroup when relative diversity instead of absolute diversity is considered. The absolute diversity of non-biomineral tubes reported here demonstrates that they are not significantly more diverse in the Nama assemblage than in the White Sea assemblage; instead, non-biomineral tubes lost fewer taxa than the non-tubular Ediacaran morphogroups as a result of the White Sea–Nama extinction event and were more successful in their recovery. When viewed in the context of the total morphogroup, the dominance of tubes in the Nama assemblage does not represent an unprecedented increase in the number of non-biomineral tubular genera but is instead reflective of the radiation of biomineral tubular genera (Selly et al., 2020; Yang et al., 2020), the recovery of non-biomineral tubular genera, and a large decrease in the diversity of non-tubular Ediacaran morphogroups. Thus, the Nama assemblage may well have been the age of biomineral tubes but records no significant change in the dominance of non-biomineral tubes.

While the similarities between the non-biomineral tubes of the White Sea and the Nama assemblages suggest that the non-biomineral tubes were not broadly different between the two assemblages, there is a notably wider range of inferred original tissue compositions in Nama tubes than in White Sea tubes (Figure 4). When genera with unknown original compositions are excluded, 86% of non-biomineral tubular genera in the White Sea assemblage were originally comprised of non-rigid organic material and 14% had weakly to non-biomineral original compositions. In contrast, 43% of non-biomineral tubular genera in the Nama assemblage were originally comprised of non-rigid organic material. The remaining 57% of non-biomineral tubes in the Nama assemblage had either all or some of their body wall comprised of rigid organic material, were agglutinated or were potentially very weakly biomineral to non-biomineral. This is in part driven by the radiation of non-biomineral Cloudinomorphs in the Nama assemblage, but this trend is also reflected in the inferred original compositions of the non-Cloudinomorph tubes (Figure 4). This demonstrates that concomitant with the radiation of biomineral and non-biomineral Cloudinomorphs in the Nama assemblage (Schiffbauer et al., 2016; Selly et al., 2020; Yang et al., 2020), the non-Cloudinomorph tubular taxa were also becoming more complex and diverse in their biological traits.

In addition to changes in inferred original composition, the relative number of non-biomineral Cloudinomorph and non-Cloudinomorph tubular genera also varies between the White Sea and Nama assemblages. In the White Sea assemblage, non-biomineral Cloudinomorphs make up 13% of the total non-biomineral tubular diversity, which rises

to 40% in the Nama assemblage. Concurrent with the increase in Cloudinomorph representation in the Nama assemblage, there is a minor loss in the number of non-Cloudinomorph tubular genera, which go from representing 93% of non-biomineral tubular diversity in the White Sea assemblage to 60% in the Nama assemblage. Despite this, non-Cloudinomorph taxa still make up the majority of non-biomineral tubular genera in the Nama assemblage. When taken together, the persisting dominance of non-Cloudinomorph tubular taxa and their increased variability in original composition in the Nama assemblage illustrate that the total tubular morphogroup, not just Cloudinomorphs, increased in complexity and played a large role in Ediacaran ecosystems during the Nama assemblage.

Conclusion

The compilation of the non-biomineral tubular record reveals several characteristics of the tubular morphotype that bolsters their status as key players in Ediacaran ecosystems, documents a previously unrecognized variability of gross morphology upon the tubular form and extends the range of their role as central components of Ediacaran ecosystems into the White Sea assemblage. This study demonstrates that non-biomineral tubes have the highest number of genera of all Ediacaran morphogroups, both within the Ediacara biota as a whole and within the White Sea and the Nama assemblages. This is consistent with the understanding of tubes dominating the Nama assemblage, but importantly, it documents a previously unrecognized number of non-biomineral tubular genera in the White Sea assemblage. However, non-biomineral tubes of the Nama assemblage are

found to have a higher variability in original compositions than tubes of the White Sea assemblage, indicating that the non-biomineral tubes followed similar patterns in increased complexity as did the biomineral Cloudinomorphs. The patterns revealed here show that, while all tubes increase in complexity in the Nama assemblage, they are characteristic and dominant components of the Ediacara biota beginning in the White Sea assemblage.

It is additionally demonstrated that non-biomineral tubes were highly abundant for a longer period of time than the biomineral forms, leading to the conclusion that biomineralization was not required for the success (i.e., high diversity and abundance) of a tubular form. Thus, the tubular radiation of the Nama assemblage is a continuation of processes that began in the White Sea assemblage, with the perceived rapid increase in tubular forms in the Nama assemblage being a signal driven primarily by biomineral Cloudinomorphs. When viewed independently from the biomineral tubes, non-biomineral tubular organisms dominated the White Sea, persisted across the White Sea–Nama extinction event, and were re-established in the Nama assemblage. This long-ranging diversity of the non-biomineral tubular morphogroup is unmatched by any other non-tubular Ediacaran morphogroups, demonstrating that a tubular form was the most common solution to early multicellularity. Further study of the total morphogroup as well as a detailed study of individual tubular genera is warranted to further elucidate the nature and implications of this long ranging and widespread solution to complex life in Earth's earliest animal ecosystems.

CHAPTER 2: BIOSTRATINOMY OF THE ENIGMATIC TUBULAR ORGANISM *AULOZOON SOLIORUM*, THE RAWNSELY QUARTZITE, SOUTH AUSTRALIA

Abstract

The Ediacara biota (575–538 Ma) are the first macroscopic community forming organisms on Earth, thus providing unique insight into the origins and evolution of complex life. However, the assignment of most Ediacaran organisms to specific phyla and kingdoms remains difficult due to their commonly non-analogous body plans and soft-bodied nature, which often results in the loss of diagnostic features through the processes of death and fossilization. Notably, this taphonomic overprint is not imparted equally to all Ediacaran organisms and is particularly exaggerated for the morphotypic grouping of tubular organisms. This morphogroup is comprised of macroscopic organisms with elongate, hollow, and simple body plans and is the most abundant Ediacaran morphogroup. However, the simple and hollow morphology of tubular organisms results in a broadly low preservation potential. In turn, this commonly limits the reconstruction of in vivo morphology, muddles taxonomic assignment, obfuscates phylogenetic affinities, and inhibits understanding of their broader significance. Fortunately, previous studies of abundant tubular taxa have demonstrated that taxon-level biostratinomic investigations can, in part, account for this low preservation potential. Such studies inform a more complete understanding of the morphogroup, providing novel insight into the paleobiology, paleoecology, and

biomaterials of tubular taxa. To contribute to this biostratinomically-geared assessment of Ediacaran tubular organisms, this study analyzes the preservation of *Aulozoon soliorum*, an abundant tubular organism from the Rawnsley Quartzite of South Australia. This investigation demonstrates that *Aulozoon* is preserved via five preservational modes, which inform a novel in vivo reconstruction of *Aulozoon* as a sessile, fluid-filled, cylindrical organism with a holdfast and a thin, organic, and featureless body wall. The preservational modes identified here additionally inform a taphonomic framework under which *Aulozoon* fossils can be interpreted, thus furthering holistic understanding of the morphogroup-specific preservational variability of Ediacaran tubular organisms.

Introduction

Biomineral and non-biomineral Ediacaran organisms with elongate, hollow, and simple body plans, broadly referred to as tubular organisms, surpass all other Ediacaran morphotypes (e.g., Bilateriomorphs, Rangeomorphs, Dickinsoniomorphs) in abundance (Budd and Jackson, 2016; Schiffbauer et al., 2016; Darroch et al., 2018; Surprenant and Droser, 2024). The common occurrence of tubular organisms within Ediacaran assemblages was initially overlooked due to the misidentification of tubular body fossils as trace fossils (Glaessner, 1969; Seilacher et al., 2003; Seilacher, 2007). Upon systematic reassessment of the Ediacaran trace fossil record, it was found that many of the described Ediacaran trace fossils were body fossils of tubular organisms (Jensen et al., 2006). Thus, demonstrating that the presence of mobile bilaterians in the Ediacaran had been greatly overestimated and the contribution of tubular organisms to Ediacaran

diversity had been greatly underestimated. This paradigm shift established the tubular morphogroup as having the potential to aid in elucidating the connection between the Ediacaran and Cambrian faunas given their newly realized dominance in Ediacaran ecosystems (Schiffbauer et al., 2016) along with their persistence across two purported extinction events in the time leading up to and at the Ediacaran-Cambrian transition (Darroch et al., 2018; Evans et al., 2022). Indeed, some Ediacaran tubular taxa have been proposed to be stem-group metazoans such as annelids (Schiffbauer et al., 2020), cnidarians (Babcock et al., 2005), and poriferans (Xiao et al., 2002), providing several potential links between the enigmatic Ediacaran fauna and the definitive animals of the Phanerozoic.

While the overall dominance and apparent success of tubular taxa at the dawn of animal life has been widely acknowledged for more than a decade (Droser and Gehling, 2008; Sappenfield et al., 2011; Schiffbauer et al., 2016; Wang et al., 2021), the morphogroup remains poorly constrained and is commonly utilized as a catch-all term for simple Ediacaran fossils with no phylogenic links, paleoecological strategies, or paleobiological traits to unite them. The primary roadblock that has enabled this indiscriminate classification practice is the simple nature of tubular organisms as well as their shared taphonomic complexity derived from their hollow and elongate morphologies, which result in the preservation of many fossilized tubular organisms as collapsed and deformed taphomorphs of the original organism (e.g., Xiao et al., 2002; Meyer et al., 2012; Surprenant et al., 2020). These biostratinomic features are exacerbated in originally

nonmineralized tubular organisms such as *Aulozoon soliorum* (Gehling and Runnegar, 2022). As a result, the ability to constrain characters of tubular organisms beyond their gross tubular form is commonly perceived to be limited. Nevertheless, existing taphonomically-geared investigations of tubular taxa have demonstrated that the systematic investigation of tubular forms through a taphonomic, and especially biostratinomic, lens can provide novel insights into the integument strength and structure, growth patterns, life habit, and paleoecological strategies of simple tubular forms (e.g., Sappenfield et al., 2011; Meyer et al., 2012; Surprenant et al., 2020; Shore and Wood, 2021; Wang et al., 2021; Osés et al., 2022), all of which facilitate the development of a more meaningful understanding of the tubular morphotype.

Aulozoon soliorum (Gehling and Runnegar, 2022) is one of many described, yet enigmatic tubular taxa that require a detailed taphonomic description in order to advance understanding of the taxon itself as well as the broader understanding of the Ediacaran tubular morphotype. *Aulozoon* is a large, non-mineralized, nonbranching tubular organism with an elongate and sinuous to broadly looping form. The external surface of *Aulozoon* is largely featureless and smooth, though wrinkles of the integument are common, particularly at points where the tubular body folds or bends (Gehling and Runnegar, 2022). Though it is relatively common in fossiliferous Ediacaran rocks of South Australia, *Aulozoon* evaded formal description until recently due to a long history of contradicting identifications as various forms of back stuffed or mucus lined burrows (Glaessner, 1969; Jenkins, 1995; Seilacher et al., 2003; Seilacher, 2007), and as fungal

rhizomorphs (Retallack, 2007, 2013). Several studies have interpreted *Aulozoon* as a metazoan-grade body fossil (Gehling, 1991; Fedonkin and Runnegar, 1992; Runnegar, 1994; Ivantsov, 2011; Droser et al., 2006), which was confirmed in the formal description of *Aulozoon* by Gehling and Runnegar, (2022).

The recent systematic description of *Aulozoon* definitively demonstrates that it is not a trace fossil through the presentation of morphological observations that indicate *Aulozoon* was comprised of a coherent, flexible body wall, as well as observations of *Aulozoon* fossils exclusively overlying, and never cross-cutting, other Ediacara macrobiota and macroscopic organic mat-related bed textures known as textured organic surfaces (TOS; Gehling and Droser, 2009) (Gehling and Runnegar, 2022). The absence of cross-cutting relationships is one of several features that is critical for distinguishing between tubular body fossils and the back-stuffed or mucus-lined burrows that Aulozoon has been aligned with in the past. Traces produced by known Ediacaran mat-grazing animals, such as *Helminthoidichnites*, are characterized in part by the bisecting (i.e., cross-cutting) of organic structures on the seafloor (Gehling and Droser, 2018). Such ‘‘mining” behavior cannot produce a structure that overlaps TOS and macrobiota as is observed in *Aulozoon*, thus precluding a trace fossil affinity for the taxon. Additionally, the fungal rhizomorph hypothesis was easily rejected by Gehling and Runnegar, (2022) because it is dependent on the interpretation of the Ediacara biota as terrestrial, which has been extensively disproven (Xiao et al., 2013; Runnegar, 2022). In sum, the features reported by Gehling and Runnegar, (2022) firmly establish *Aulozoon* as a monospecific tubular body fossil

and yet, *Aulozoon* remains broadly enigmatic with little understanding of its true morphology, paleoecological strategies, or the nature of its biomaterials. To address these outstanding questions, this study presents a detailed biostratinomic investigation of *Aulozoon* fossils from the Rawnsley Quartzite of South Australia.

Geologic context

Aulozoon soliorum is endemic to the fossiliferous Ediacara Member of the Rawnsley Quartzite in South Australia where it occurs in high abundance at several localities, including Nilpena National Heritage Site (NNHS), the Mount Scott Range, Bathtub Gorge, and Devil's Peak (Droser et al., 2019; Reid et al., 2020; Gehling and Runnegar, 2022) (Figure 1a, d-f). This study uses *Aulozoon* specimens from the listed localities for biostratinomic description of the taxon, providing a large and paleoecologically contextualized dataset that encompasses multiple facies and allows for robust biostratinomic analysis.

The fossiliferous Ediacara Member of the Rawnsley Quartzite, within the Pound Subgroup, is exposed within and west of the Flinders Ranges (Gehling, 2000). The Ediacara Member is located 200–600 m below a basal Cambrian disconformity and is estimated to be between 555 and 550 million years old based on the high number of Ediacaran taxa that it shares with the White Sea region in Russia (Waggoner, 2003; Droser et al., 2006; Grazhdankin, 2014).

In the Ediacara Member, soft-bodied Ediacaran organisms are preserved as casts and molds on the bases of discrete, successive quartzarenite bedding planes (Droser et al., 2019). Each bedding plane represents a single depositional event that instantaneously buried the matground and the associated macrobiota communities, resulting in the casting and molding of the smothered communities on the base of the burial sand body. The persistence of these bedforms as discrete, successive, and texturally homogenous bedding planes through diagenesis is attributed to the organic barrier created by pervasive organic matgrounds along with the early-initiating precipitation of authigenic silica cements enabled by the high silica saturation state of Ediacaran oceans (Tarhan et al., 2016, 2017; Slagter et al., 2021, 2022).

The soft bodied Ediacaran organisms captured by the event deposits that comprise the Ediacara Member are most commonly preserved as either negative hyporelief casts and molds (i.e., a concave fossil on the bed sole) or as positive hyporelief casts and molds (i.e., a convex fossil on the bed sole). The mode of preservation is taxon-specific and is dictated by the structural integrity of the organism. Taxa with tissues that resisted collapse upon burial are found as negative hyporelief external molds on bed soles (e.g., *Dickinsonia spp.*, *Kimberella spp.*), whereas structurally weak taxa that collapsed upon burial are found as positive hyporelief composite molds on bed soles (e.g., *Funisia dorothea*) (Gehling 1999; Joel et al., 2014). Hollow organisms that were infilled with sediment upon burial (e.g., *Aspidella terranovica*) are preserved as positive hyporelief internal molds (Tarhan et al., 2016). The majority of Ediacaran organisms preserved in

the Ediacara Member are characterized by only one mode of preservation. For example, *Dickinsonia costata* body fossils are found only as negative hyporelief external molds (Evans et al., 2017). One exception to this general rule is non-biomineral tubular organisms, which can be preserved as at least four distinct preservational modes due to the robust nature of their bodies while fluid-filled and the corresponding loss of this strength upon fluid evacuation and collapse (Sappenfield et al., 2011; Droser et al., 2019; Surprenant et al., 2020).

Quantitative analyses for this study were carried out solely on specimens from NNHS, located within Nilpena Ediacara National Park. This locality is particularly well-suited for quantitative biostratinomic investigation because it houses 40 excavated fossiliferous bedding planes that are pieced together to reveal up to 40 m^2 of fossilized Ediacaran seafloor (Droser et al., 2019). These bedding planes provide a dataset of multiple populations of *Aulozoon* that are paleoecologically and paleoenvironmentally contextualized and represent preservation under varying substrate conditions (i.e., organic surface development and grain size) as well as varying energetic conditions (i.e., facies). *Aulozoon* is found in two facies at NNHS: the Oscillation-Rippled Sandstone (ORS) facies and the Planar Laminated and Rip-Up Sandstone (PLRUS) facies (Gehling and Droser 2013; Tarhan et al., 2017). The ORS facies records deposition between fair-weather and storm wave base and is comprised of thinly bedded, rippled fine- to coarse grained feldspathic quartzarenite (Gehling and Droser 2013; Tarhan et al., 2017). The

PLRUS facies represents upper sub-wave base canyon fill deposits and is characterized by laterally continuous, planar-laminated fine-grained quartzarenite beds (Gehling and Droser, 2013; Tarhan et al., 2017).

Materials and methods

A total of 254 *Aulozoon soliorum* specimens were examined for this study, 108 of which are from NNHS within Nilpena Ediacara National Park. *Aulozoon* fossils from NNHS occur across 11 excavated bedding planes and on 26 float samples. Qualitative biostratinomic observations and images of specimens were taken from specimens housed in the collections of the South Australia Museum (SAM) and in the field at NNHS, encompassing *Aulozoon* specimens from all listed Flinders Ranges localities (Figure 1). Quantitative analyses were carried out only on specimens from NNHS. Measurements were made using ImageJ software, and data analysis was conducted in R.

Sinuosity of *Aulozoon* from NNHS was calculated by following methods put forth by Shore and Wood, (2021). For each individual, straight-line length and midline length were collected. Straight-line length represents the distance between the midpoint of each terminal end, measured point-to-point with a straight line (Figure 5, purple line). Midline length was found using line segments to measure the distance between end points while remaining on the midline of the tubular body (Figure 5, blue line). Sinuosity was calculated by dividing the midline length by the straight-line length.

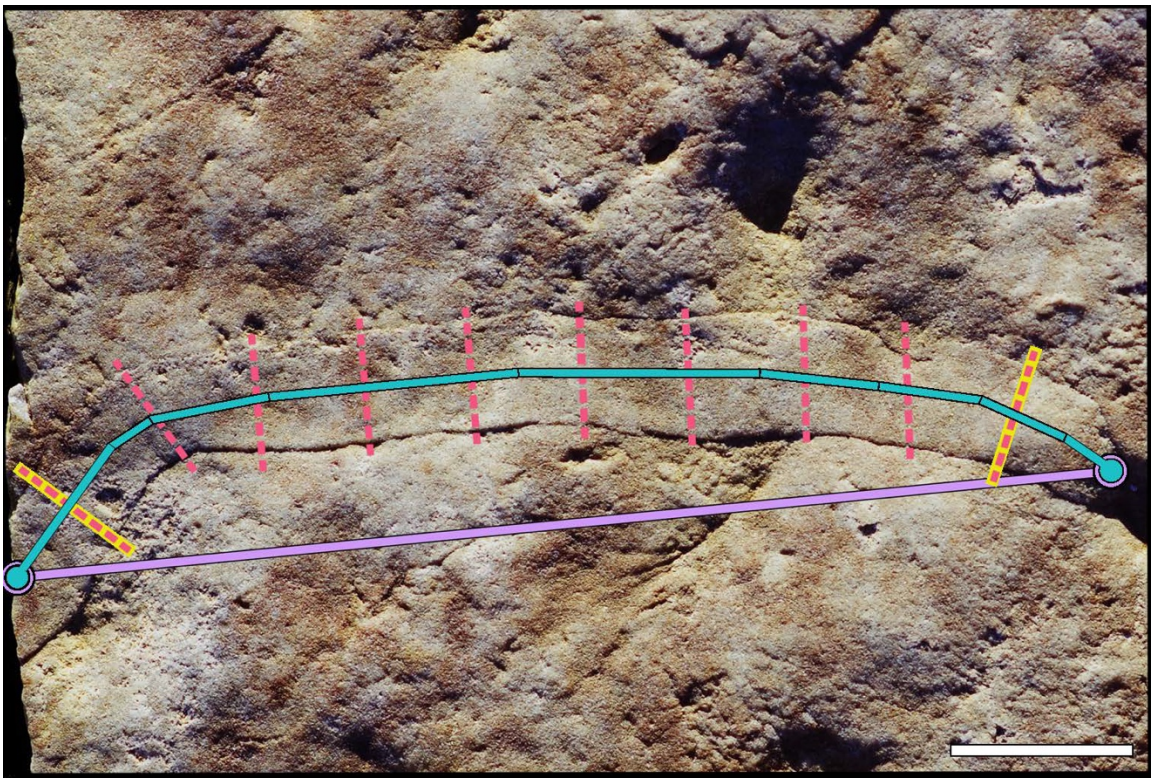

Figure 5. Example of sinuosity and width measurements taken for all *Aulozoon soliorum* specimens included in this study. Red dashed lines represent the ten equally spaced width measurements taken for each individual; highlighted red dashed lines denote the ‘‘left-most” and ‘‘right-most” width measurements utilized to test for directional increases in width. Width measurements were not taken from the last centimeter of each specimen to account for deformation at the ends of the fossil. The blue line represents the midline length of the individual. The purple line represents the straight-line length measured for each specimen, representing the shortest distance between the terminal ends of the individual. Scale = 3 cm.

Widths of *Aulozoon* were collected from images of specimens at NNHS by measuring ten approximately equally spaced measurements across the length of the body (Figure 5, red lines). This was done to account for small-scale biostratinomically-derived width variations resulting from folding, wrinkling and ripping which might result in width values that are greater than or less than the true widths of the tubular bodies depending on where the measurement was taken. The ten width values collected for each *Aulozoon*

specimen were averaged to supply one representative grand mean width for each individual. A grand mean width for the entire *Aulozoon* population was calculated from these representative values.

To identify if there was a progressive increase in width of *Aulozoon* along its length the left-most and right-most width measurements for each *Aulozoon* specimen were compared (Figure 5, highlighted red lines). However, this question is difficult to address because of the lack of complete specimens and the wide range of widths in the *Aulozoon* population at NNHS (Appendix B Figure 26). Therefore, when measuring the difference in width from one end of a specimen to the other, there are multiple caveats that limit interpretations that can be made. Firstly, all *Aulozoon* specimens represent unknown portions of an individual because no complete specimens are known, so it is unclear whether the measurements represent apical, median, or terminal widths. Therefore, data collected from *Aulozoon* specimens at NNHS provide width measurements from different and unknown portions of the body. This is a taphonomic bias that must be acknowledged but cannot be corrected for. Secondly, when *Aulozoon* specimens are oriented horizontally and measurements are taken of the left-most and right-most terminal ends, comparative analyses pick up on variability in the overall size of the *Aulozoon* specimens within the population (i.e., the difference between the smallest and largest individuals regardless of left- or right-most placement) and not the difference between the left-most and right-most widths of each individual. This prevents testing of whether *Aulozoon* tapered from one end to the other. As such, clusters of similarly sized

Aulozoon individuals were identified first so that statistical analyses reflected the significance of the difference between left-most and right-most measurements at the individual level. To address this, a k-means clustering algorithm was applied to the averaged width data of all *Aulozoon* specimens at NNHS to identify clusters of individuals with statistically similar averaged widths so that comparative statistical analyses picked up on width differences between left-most and right-most terminal ends of individuals only, not the overall width distribution of the population (Appendix B Figure 27). Individuals were then sorted into these width groups and a Welch Two sample t-test was run within the size-similar groups to ascertain the significance of the difference between the right-most and left-most widths of individuals.

Size of *Aulozoon soliorum*

Serial width values for *Aulozoon soliorum* provide a grand mean width of 17.29 mm, a maximum width of 32.81 mm, and a minimum width of 6.34 mm. The length of *Aulozoon* specimens ranges from 2.49 cm to 59.08 cm, though it should be noted that none of the *Aulozoon* specimens preserve a complete individual, so these values represent minimum constraints on *Aulozoon* length.

To test whether the width of *Aulozoon* is consistent along the length of the body or if it tapers from one end to the other, three statistically similar width ranges were identified via k-means cluster analysis: 0–14 mm, 15–21 mm, and > 22 mm. Welch Two Sample

t-tests ran for the comparison of left-most and right-most widths of Aulozoon specimens that had been sorted into size-similar clusters resulted in high p-values for all three clusters ($p > 0.05$) (Appendix B Figure 27). This result fails to reject the null hypothesis that the left-most widths are equal to the right-most widths of *Aulozoon*. As such, there is no evidence to support the reconstruction of *Aulozoon* as a tapered form.

There are several remaining questions concerning the overall morphology of *Aulozoon*. However, due to the extensive evidence of deformation in Aulozoon *fossils*, these inquiries must be addressed through a biostratinomic lens to ensure that interpretations are not skewed by taphonomic overprint. The development of a taphonomic framework under which further interpretations of *Aulozoon* can be made is the concern of the remainder of this study.

Biostratinomy of *Aulozoon soliorum*

Spatial relationships

Nine of the beds that preserve *Aulozoon soliorum* at NNHS occur in the ORS facies and two occur in the PLRUS facies. On these bedding planes *Aulozoon* rarely occurs as isolated individuals and are most commonly in populations of at least two individuals. However, *Aulozoon* is never the most abundant taxon preserved on a bedding plane. Overlap and abutting of *Aulozoon* individuals is common, and in highly sinuous individuals, self-overlap is observed (Figure 6).

In line with this, previous studies have described *Aulozoon* fossils as forming a "complex tangle" when found in high abundance on single bedding planes (Gehling and Runnegar, 2022). At locations of overlap, *Aulozoon* always maintain traceable body wall margins with no evidence of cross-cutting relationships (Figure 6b, c), although in rare instances the overlying *Aulozoon* is not preserved after the point of overlap (Figure 6b). *Aulozoon* overlap does not occur to such an extent that it covers entire swaths of bedding plane to create iterative organosedimentary surface textures or textured organic surfaces (TOS), as is observed in populations of the tubular organism *Funisia dorothea* (Gehling and Droser, 2009).

Overlap of *Aulozoon* with other Ediacaran taxa is markedly less common than intra-taxon overlap. The most common association is the overlap of the enigmatic Erniettomorph *Phyllozoon hanseni* by *Aulozoon.* This relationship is observed on surfaces dominated by the benthic prostrate *Phyllozoon*, which is found in association with *Aulozoon* on one bedding plane and on float at NNHS, on several pieces of float from the other Flinders Ranges localities, and is well-documented by Gehling and Runnegar, (2022) on a bedding plane from Bathtub Gorge. On this bedding plane, *Aulozoon* either completely overprints the underlying *Phyllozoon* (Figure 7a) or the *Aulozoon* body is molded to the morphology of the underlying *Phyllozoon*, resulting in a composite mold of the two organisms (Figure 7b). Apart from these two bedding planes and a handful of float pieces there is no repeating association between the two taxa.

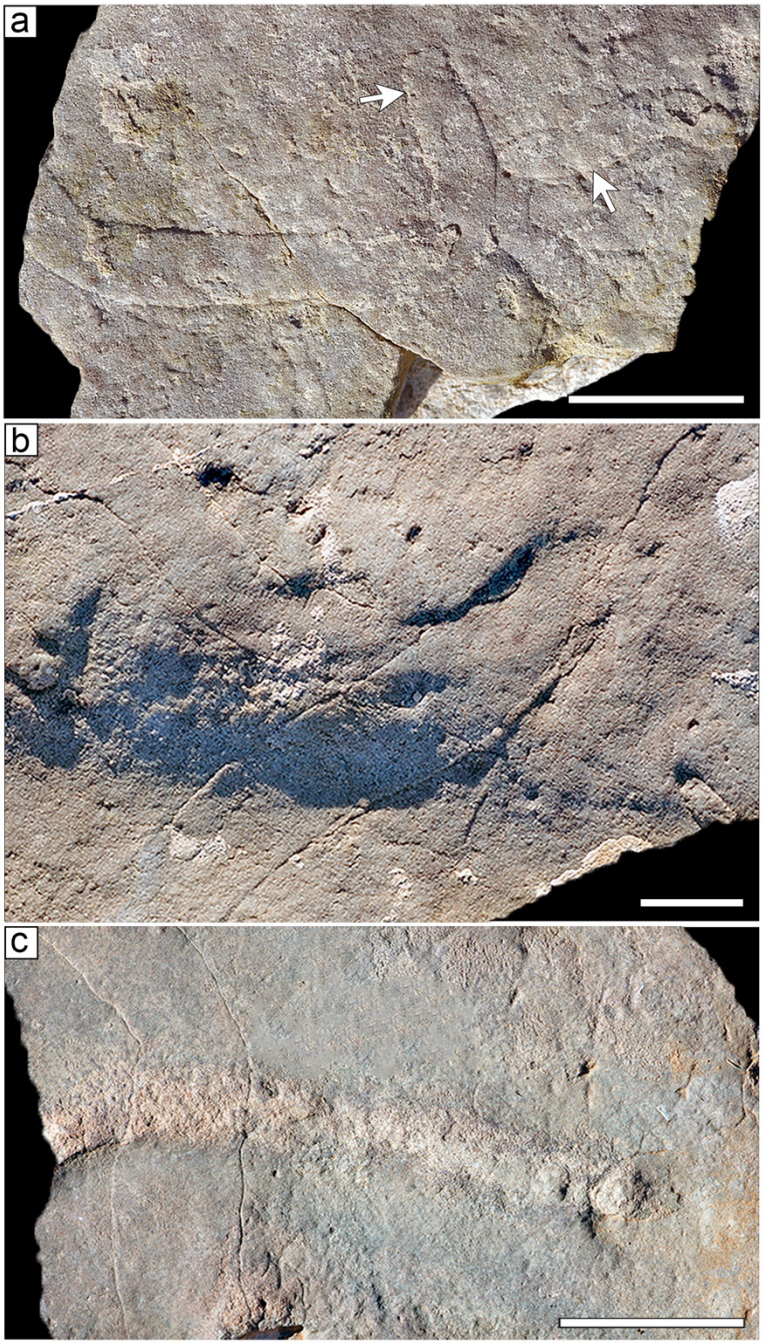

Figure 6. Examples of *Aulozoon soliorum* abutting and overlapping other *Aulozoon* individuals. (a) Two individuals (arrows) abutting each other; the left-most individual additionally exhibits self-overlapping. (b) One larger *Aulozoon* overlapped by a smaller individual, note non-preservation of the overlying individual after the point of overlap. (c) Two overlapping individuals preserved as different preservational modes. Scales a, b = 3 cm; Scale c = 5 cm.

Aulozoon is also observed overlapping mobile organisms, including *Spriggina floundersi* body fossils (Figure 7c), *Dickinsonia costata* body fossils (Figure 7d), and *Dickinsonia spp.* footprints (Gehling and Runnegar, 2022). The overlap of these macrobiota by *Aulozoon* is, however, not common and is observed in only eight specimens.

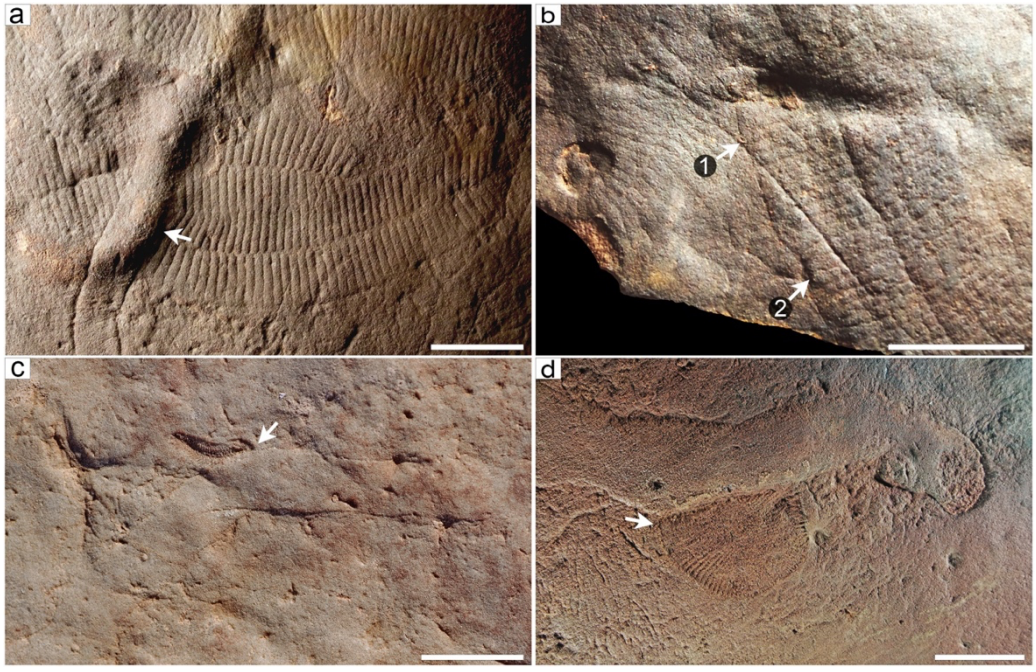

Figure 7. Examples of *Aulozoon soliorum* preserved on top of other Ediacara macrobiota. (a) *Aulozoon* (arrow) overlapping and overprinting *Phyllozoon hanseni*; SAM P58609. (b) *Aulozoon* (arrow 1) preserved on top of a *Phyllozoon* (arrow 2); modules of the underlying *Phyllozoon* impart their structure on the overlying *Aulozoon*, resulting in composite preservation of the two organisms; SAM E05B04. (c) *Aulozoon* overlying and completely overprinting a *Spriggina floundersi* (arrow). (d) *Aulozoon* overlying and completely overprinting a *Dickinsonia costata* (arrow); SAM P14388. Scales = 3 cm.

Preservational modes

Aulozoon soliorum is characterized by five distinct preservational modes that are broadly defined by differences in the nature of the fossil's relief on the bed sole. Identified

preservational modes range from high to low relief convex fossils and from high to low relief concave fossils on the bases of bedding planes (i.e., hyporelief). Convex hyporelief specimens will be referred to as positive fossils whereas concave hyporelief fossils will be referred to as negative fossils for the remainder of this discussion. The extent of relief (low to high) distinguishes between *Aulozoon* fossils that either extend from or are impressed into the bedding plane (positive and negative relief, respectively) by > 2 mm (high relief) and < 2 mm (low relief).

The five preservational modes identified for *Aulozoon* are as follows:

(1) Positive External Casts (Figure 8a): The positive external cast preservational mode of *Aulozoon* is characterized by positive hyporelief with very high relief, extending up to 1.3 cm from the bed sole. This mode of preservation occurs in 14 individuals at NNHS, one in the ORS facies, and 13 in the PLRUS facies, all of which are located on beds characterized by poorly developed TOS. Positive external casts do not have distinct lateral margins and are demarcated by their high relief as well as their elongate and moderately sinuous morphology. The surfaces of positive external casts are commonly characterized by an irregular rough to lumpy texture that is distinct from the surrounding sole surface. When viewed in cross-section there is no observed textural or compositional distinction between the *Aulozoon* cast and the matrix of the casting bed. Positive external casts are easily distinguished from the other preservational modes of *Aulozoon* because of their extremely high positive relief and undefined margins. The only other structure at

NNHS that rivals *Aulozoon* positive external casts in extent of positive hyporelief are stalks of frondose organisms, which are generally of a lower relief and are easily distinguished from convex external casts of *Aulozoon* because *Aulozoon* specimens are always characterized by some extent of sinuosity or irregular margins whereas stalks of frondose organisms are relatively rigid structures with lower levels of sinuosity.

(2) Negative External Molds (Figure 8b): The negative external mold preservational mode of *Aulozoon* is characterized by negative hyporelief molds on bed soles, the extent of the negative relief is up to several millimeters. The margins of negative external molds are distinguished from the bed sole by a sharp transition to negative relief, and the mold itself is smooth with no surface features. The negative external mold preservational mode occurs only in short sections of *Aulozoon* individuals and is therefore never highly sinuous, though generally has some form of broad arching. Negative external molds, which characterize most other Ediacara taxa, are not common in *Aulozoon* and only six individuals at NNHS are characterized by this preservational mode, all of which are associated with moderately to well-developed TOS.

(3) Positive External Molds (Figure 8c): The positive external mold (PEM) preservational mode of *Aulozoon* is characterized by positive hyporelief structures of very low relief, protruding from the bed sole by two millimeters or less and appearing to be almost flush with the bed sole. In cross-section, PEMs are a continuous part of the casting bed, with no textural or compositional distinctions between the two. PEMs can

have well-defined to faint margins, but they always overlie and are distinct from associated TOS. The surface of positive external molds can be smooth and featureless but is generally characterized by folding and wrinkling, and many specimens display surface features consistent with composite preservation of the *Aulozoon* integument and the underlying TOS. The PEM preservational mode can also exhibit high sinuosity and high amounts of deformation such as twisting and ripping.

(4) Internal Molds (Figure 8d): The internal mold (IM) preservational mode is a second, low positive hyporelief mold of *Aulozoon*. IMs are characterized by marginally higher relief than positive external molds, very sharply defined margins, common folds and wrinkles, and high sinuosity. When IMs overlap high relief TOS or macrobiota, they completely overprint the underlying structure. The cross-sectional profile of *Aulozoon* IM preservation was previously demonstrated by Gehling and Runnegar, (2022) through the serial sectioning of an *Aulozoon* specimen. The sectioned specimen demonstrated that the tubular *Aulozoon* fossil was composed of a lens of sediment separated from the matrix by a thin layer of haematitic silt (Gehling and Runnegar, 2022). The sediment infill is a partial infill, forming an irregular oval shaped lens of less than 6 mm thick, that extends for several centimeters of the length of the body and becomes thinner from one end of the specimen to the other. Notably, the infill of the tubular body was shown to be lithologically identical to the burial sand body. The variability of the width of the sediment lens within a single individual that was demonstrated by Gehling and Runnegar, (2022) can also be observed in plan-view in a handful of specimens at NNHS as irregular

lumps and smeared-out ridges on the surface of the *Aulozoon* fossil (Figure 9a, b). These lumps and smeared-out ridges are, however, not a universal or rigorous identification criteria for the IM preservational mode, and in the field, definitive identification can only be achieved for a small number of specimens through observation of fortuitous cross-sections created by natural fractures in the rocks (Figure 9c). While this can result in identification of the preservational mode of an *Aulozoon* fossil at a single point, it does not help to characterize the preservation of the rest of the fossil.

(5) Cast Internal Molds (Figure 8e): The cast internal mold preservational mode of *Aulozoon* is characterized by negative hyporelief fossils with clear margins defined by a sharp change to negative relief relative to the bed sole. Cast internal molds are found in only three *Aulozoon* specimens across three bedding planes and occur only within a small length of individual *Aulozoon* tubes. Given their similarity in relief, distinguishing between the cast internal mold preservational mode and the negative external mold preservational mode is not straightforward. One potential distinguishing feature is the reported presence of wrinkling and creasing on cast internal molds when an internal mold is forcibly removed from the bed sole (e.g., Gehling and Runnegar, 2022). The deformational features in cast internal molds reported by Gehling and Runnegar, (2022) are entirely absent in the negative external mold preservational mode of *Aulozoon* and thus could help in distinguishing between the two preservational modes. However, the occurrence of wrinkling in cast internal molds is not observed at NNHS, indicating that wrinkles are an imperfect marker features for distinguishing between the two

preservational modes. The development of sequential taphonomic scenarios for the negative external mold and cast internal mold preservational modes later in this discussion provides insight into expected scenario-specific features that will help to distinguish between these two preservational modes.

It is more helpful to view these two preservational modes as two ends of a sliding scale of sediment infill extent, one end member being the PEM preservational mode (i.e., no infilled sediment) and the other end member being the IM preservational mode (i.e., partial infill) (Figure 9c). The taphospace between the two endmembers represents varying amounts of sediment infill. *Aulozoon* specimens preserved in low positive hyporelief can be placed at some point within this sliding scale but their preservational mode cannot be definitively classified without destructive sampling. It is additionally important to note that extent of sediment infill has been demonstrated to vary across the length of single individuals, meaning that a single *Aulozoon* fossil with low positive hyporelief will occupy multiple spots on the sliding scale between the PEM and IM preservational modes (Figure 9c, d). Due to the considerable gray area that exists between the PEM preservational mode and the IM preservational mode in most specimens, the two preservational modes are not differentiated from each other in field observations and are thus combined as the positive external mold/internal mold (PEM/IM) preservational mode for this discussion.

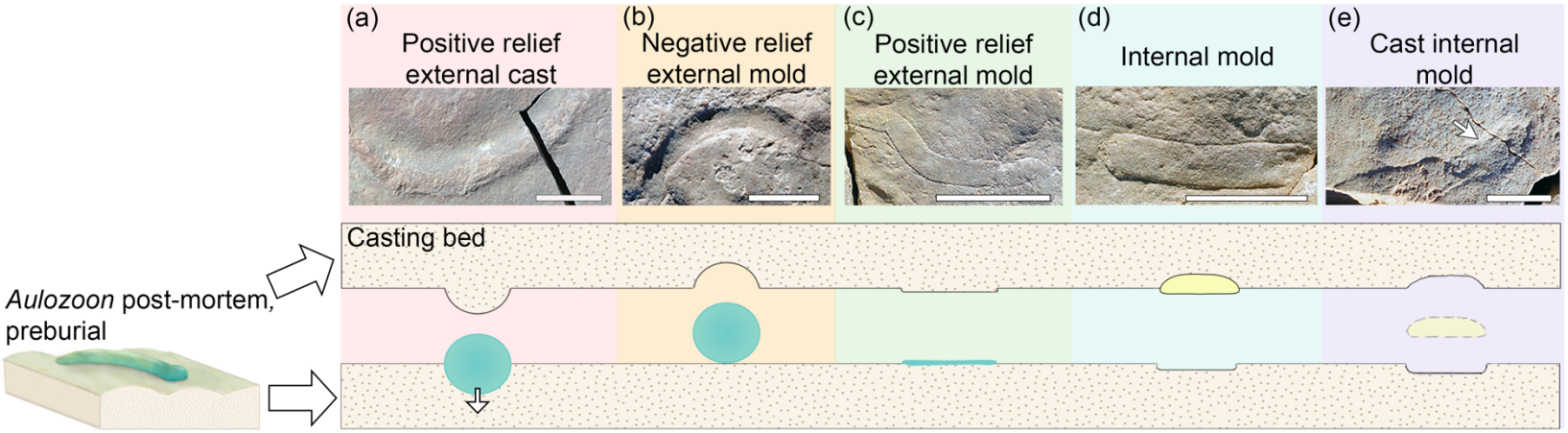

Figure 8. Simplified schematic of the five preservational modes observed in *Aulozoon*, the inferred preservational processes associated with each preservational mode, and fossil examples from Nilpena National Heritage Site. All fossils are preserved on the bases of bedding planes (i.e., hyporelief). Teal shading of hypothetical cross-sections denotes a non-collapsed *Aulozoon* whereas yellow shading represents sediment that has infilled the *Aulozoon* body cavity. The *Aulozoon* post-mortem, preburial image depicts an *Aulozoon* lying flat on the seafloor for illustrative purposes, this does not reflect hypothesized life habit. (a) Positive relief external cast preservational mode, wherein the individual is preserved as a high positive hyporelief structure, suggesting that upon burial the organism was pushed down into the sediment. (b) Negative relief external mold preservational mode, in which the individual is preserved as a negative hyporelief structure, indicating that upon burial the organism resisted collapse and was molded by the overlying sediment. (c) Positive relief external mold preservational mode, wherein the organism was preserved as a low positive hyporelief structure, suggesting that upon burial the organism collapsed and resulted in the composite preservation of both body walls on the bed base. (d) Internal mold preservational mode, wherein the preserved fossil is a low positive hyporelief mold comprised of sediment that partially infilled the *Aulozoon* body cavity during burial. (e) Cast internal mold preservational mode, this preservational mode indicates the former presence of an internal mold that was subsequently lost to unknown late diagenetic processes. Scales = 5 cm.

Multipart preservation

Multipart preservation, in which a single individual exhibits two or more distinct preservational modes, is characteristic of tubular organisms (Sappenfield et al., 2011; Surprenant et al., 2020). *Aulozoon soliorum* fossils exhibit several forms of multipart preservation, reflecting combinations of the four distinct preservational modes (i.e., PEM/IM and cast internal mold; PEM/IM and negative external mold; PEM/IM and positive external cast) (Figure 10). Of the *Aulozoon* at NNHS, 16% are characterized by multipart preservation (Table 1).

	Preservational mode(s)	N
Single-type preservation	Positive external mold/internal mold	81
	Positive external cast	9
Multipart preservation	Positive external mold/internal mold + Positive external cast	5
	Positive external mold/internal mold + Negative external mold	6
	Positive external mold/internal mold + Cast internal mold	7
Sum		108

Table 1. The number of occurrences of single-type preservation and the number of occurrences of distinct combinations of multipart preservation in *Aulozoon soliorum* fossils at Nilpena National Heritage Site. Note that negative external molds occur only in association with positive external mold/internal mold (PEM/IM) preservation and that cast internal molds occur only in association with PEM/IM preservation.

While the transition between the PEM and IM preservational modes is classified as multipart preservation and can be clearly observed in rare cases (Figure 10a), the inability to reliably identify this transition type precludes the inclusion of this multipart preservational type as a discrete form of multipart preservation in Table 1.

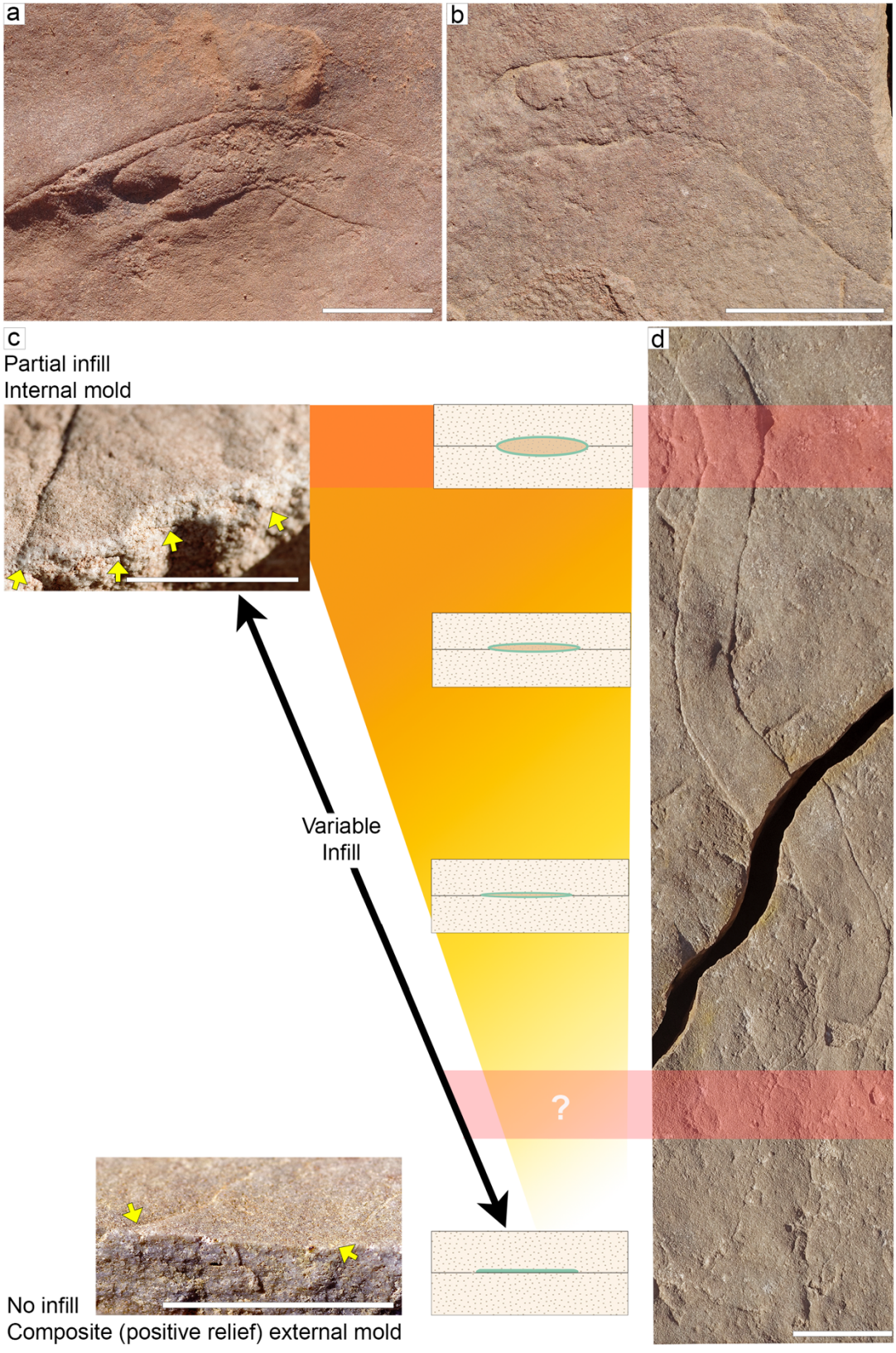
a
b
c
Partial infill
Internal mold
d
Variable
Infill
?
No infill
Composite (positive relief) external mold

Figure 9. Illustration of the variable extent of infill in internally molded *Aulozoon soliorum* specimens. (a) *Aulozoon* specimen preserving a transition from an internal mold (right) to a negative relief external mold (left), note the lobate nature of the transition where sediment infill ceases. (b) *Aulozoon* specimen preserving a transition from an internal mold to a positive relief external mold, this transition is characterized by patchy sediment infill that appears as irregular lumps on the fossil surface. (c) Schematic of the nature of variable sediment infill in internally molded *Aulozoon* specimens; the highest extent of infill is represented at the top with an example from Nilpena National Heritage Site wherein the body is partially infilled with sediment. The extent of sediment infill can decrease from this point until there is no infill and the fossil is preserved as a positive relief composite external mold, this is demonstrated at the bottom of the schematic with a corresponding fossil example. (d) Image of an *Aulozoon* specimen that has variable relief, suggesting a tapering of sediment infill from the top of the image to the bottom, red lines correlate the preservation of this fossil to the extent of infill, this is constrained for the top-most portion of this fossil due to the presence of a rock fracture and is inferred from fossil relief at the bottom of the sample, though the infill extent at this portion of the fossil is ultimately not known, so its placement on the scale of variable infill is estimated and denoted with a question mark. Scales a-c = 1.5 cm, scale d = 3 cm.

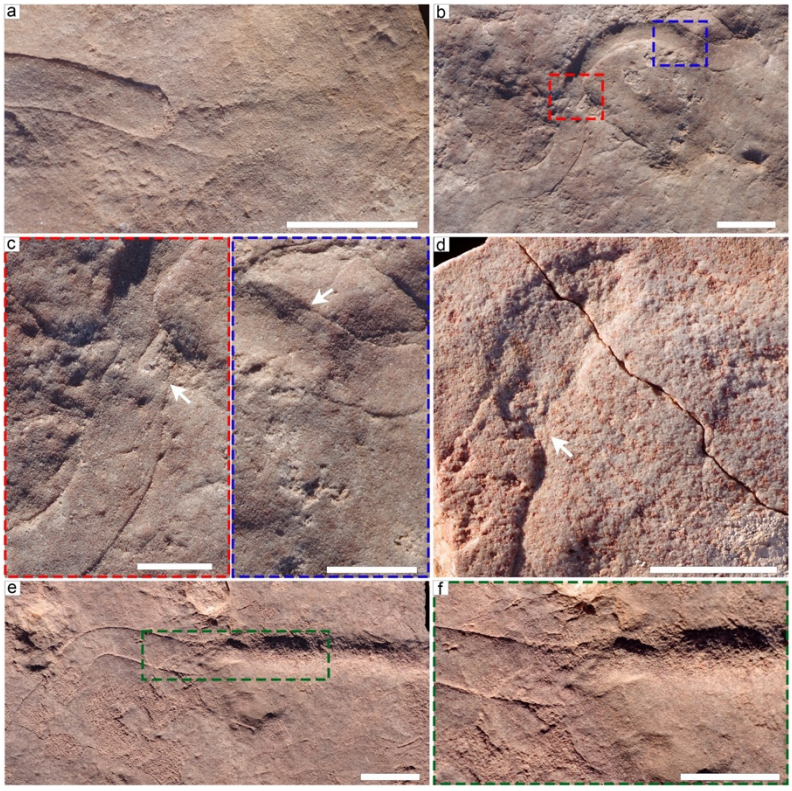

Figure 10. Examples of *Aulozoon soliorum* specimens at Nilpena National Heritage Site that exhibit multipart preservation. (a) *Aulozoon* fossil that clearly preserves the transition from internal mold (left) to positive external mold (right), as is demarcated by the transition from a higher relief well-defined body (left) to a lower relief poorly defined body (right). Note that at the point of transition there is a ridge extending across the body, which is rounded and granular, consistent with tapered sediment infill. (b) *Aulozoon* specimen that transitions from positive external mold/internal mold (PEM/IM) preservation on the left to negative external mold preservation in the middle and then back to PEM/IM preservation on the right-hand side; red and blue boxes denote the location of magnified images in c. (c) Magnified view of the left-hand (red) and right-hand (blue) transition from PEM/IM preservation to negative external mold preservation. Arrows denote the point of transition, which are characterized by short longitudinal folds of the fossilized integument. (d) *Aulozoon* specimen preserved as an internal mold which transitions to a cast of an internal mold (arrow), note exposure of the infilled cross-section and angular nature of the infill termination at the point of transition. (e) *Aulozoon* that is preserved as a PEM/IM (left) that transitions to a positive relief external cast (right); green box denotes location of magnified image in f. Note the change in the definition of the body wall margins, which is sharp and clear in the PEM/IM section but is diffuse in the positive external cast section. (f) Magnified view of preservational transition in e. Note constriction of the body at the point of transition accompanied by irregular sediment ridges and integument deformation. Scales a, b, d = 3 cm, scale e, f = 2.5, scales c = 1.5 cm.

It should be noted however that all examples of multipart preservation include the PEM/IM preservational modes, meaning that it is likely that many of these specimens represent the co-occurrence of three preservational modes (e.g., PEM, IM, and negative external cast). Notably, several specimens clearly transition from an IM to negative relief external molds or positive relief external casts, and in this transition a cross-section of the infill is revealed, allowing for definitive identification of IM preservation at that single point (Figures 9a, 10d). This does not guarantee that PEM preservation will not be present elsewhere along the length of the tube, so these specimens are still classified as the combined PEM/IM preservational modes.

In other examples of multipart preservation, the transition between preservational modes can be gradational in nature, demarcated by a decrease in relief of the fossil and a decrease in definition of the fossil margins (Figure 9d). For example, in the transition from positive external cast to PEM/IM preservation, there is a corresponding transition from no distinct margins in the positive external cast portion to clear marginal distinctions in the PEM/ IM portion (Figure 10e, f). More commonly, however, the transition between preservational modes corresponds with a clear ridge of either folded integument or infilled sediment, depending on the nature of the transition (Figure 10b-d). This ridge can be either a single positive relief structure extended across the body or a series of successive positive relief folds (e.g., Figure 10c).

The transition between PEM/IM and cast internal mold preservation is not characterized by similar ridges but is instead characterized by a jagged and differentially weathered transition point, reflecting the late-stage diagenetic loss of the internal mold to reveal the underlying cast (Figure 10d).

Occurrence of the five preservational modes of *Aulozoon* as components of multipart preservation ensures that each preservational mode reflects a true taphomorph of *Aulozoon* and is not a distinct, unrelated taxon. This is particularly important for the accurate identification of positive external casts as *Aulozoon* fossils because they are otherwise relatively featureless and difficult to definitively identify, but their common attachment to undoubted *Aulozoon* PEM/IM preservational modes allows for their definitive identification as *Aulozoon* fossils even in the absence of multipart preservation. Notably, the cast internal mold and negative external mold preservational modes occur only in specimens that have multipart preservation.

Given the aforementioned identification criteria and acknowledging the presence of multipart preservation, the PEM/IM preservational mode is found to be the most common taphomorph of *Aulozoon*, occurring in all but nine specimens at NNHS. While markedly less common, the frequency of occurrence of the remaining three preservational modes, from highest to lowest, is positive external casts, negative external molds, and cast internal molds (Table 2).

Preservational mode	N
Positive external mold/internal mold	99*
Positive external cast	16
Cast internal mold	5
Negative external mold	6

Table 2. Number of times each preservational mode is observed in *Aulozoon* specimens at Nilpena National Heritage Site. N represents the number of occurrences, including specimens with multipart preservation, as such some individual specimens are listed more than once in this table. * 55 out of these 99 specimens have confirmed internal mold preservation.

Deformation

Integument deformation is common in *Aulozoon*; of the 108 individuals at NNHS only 18 had no preserved evidence of body wall deformation such as wrinkling, folding, and ripping. This is consistent with preservation of specimens from other localities in the Flinders Ranges. Notably, there are a handful of morphologically distinct deformation features that repeat across multiple *Aulozoon* individuals. While the consistent expression of these features could indicate that they are true morphological features and not the expression of deformation dictated by integument thickness and biomaterial strength, these repeating features are not exclusively present in the best-preserved individuals where the finest resolution of morphological details are expected to be preserved. Instead, repeating features are observed in poorly preserved specimens of *Aulozoon* and in well-preserved specimens, so ridges, wrinkles, folds, and rips are interpreted as biostratinomic features.

Deformation features are common in all preservational modes of *Aulozoon* except for in negative external molds, which never preserve deformation features. In the remaining preservational modes (i.e., positive external casts, PEM/IMs, and cast internal molds) there are four primary forms of deformation that are commonly found co-occurring in specimens of *Aulozoon*:

(1) Marginal creasing: Folds and wrinkles that are oriented sub-perpendicular to perpendicular to the tube midline and originate at the tube margin but do not extend past the midline (Figure 11a, b).

(2) Surface creasing: Folds and wrinkles that are oriented sub-perpendicular to perpendicular to the tube midline, originating at the body margin and extending at least to the midline but commonly extending across the entire width of the tube (Figure 11c-f). In some instances, surface creasing can cover the entire body of the *Aulozoon* (Figure 11c). The most pronounced cases of surface creasing are associated with the twisting and folding of *Aulozoon* (Figure 11f).

(3) Linear creasing: Folding or wrinkling that is roughly parallel to sub-parallel to the midline of the tube. These features do not originate at the tube margin and can be located close to the midline or can be parallel to the outer tube margin (Figure 12a-d).

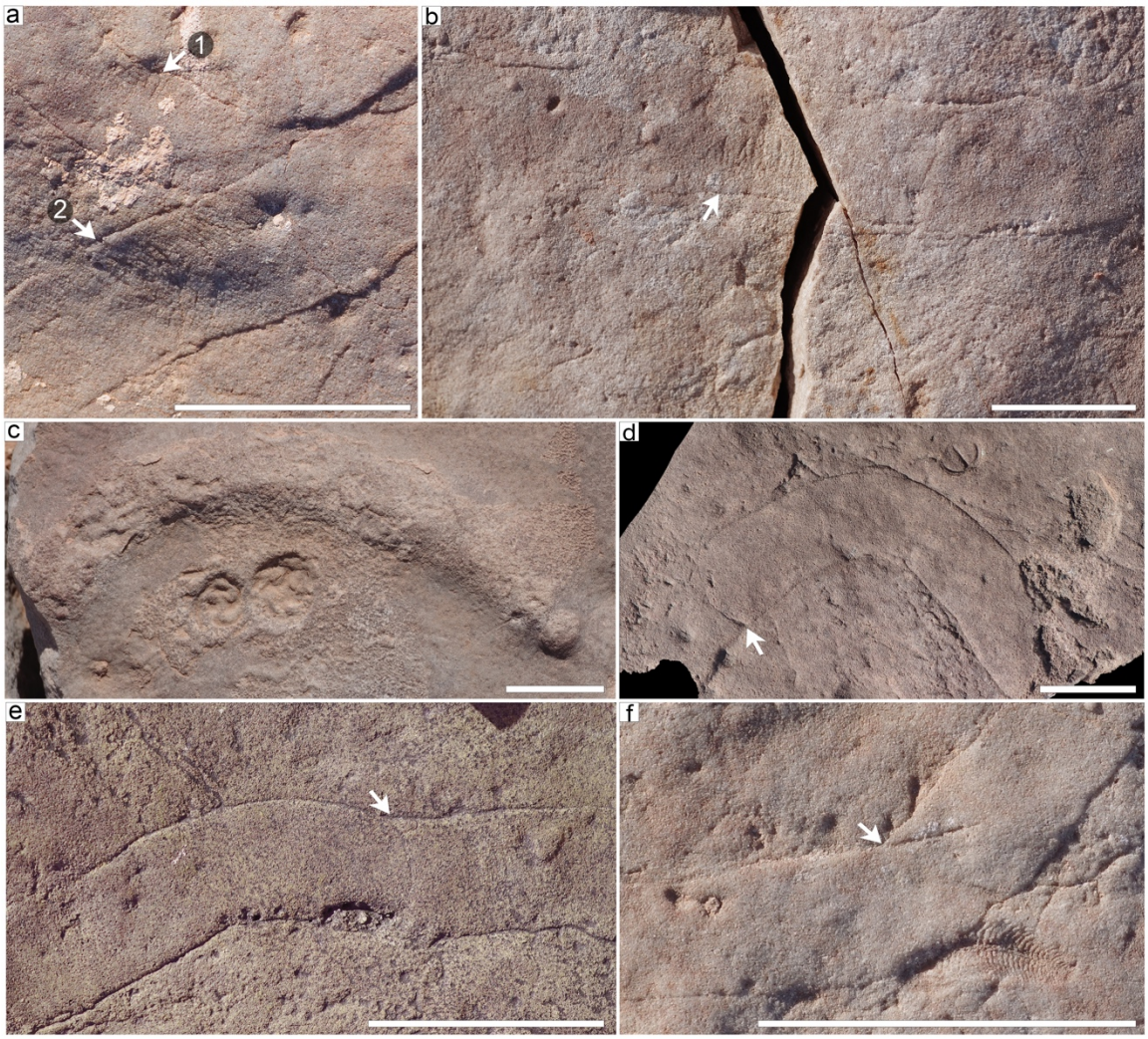

Figure 11. Examples of deformation patterns observed in *Aulozoon soliorum*. (a) Example of marginal creasing in overlapping specimens, denoted by arrows 1 and 2. (b) Example of marginal creasing (arrow). (c) Example of a form of surface creasing observed in *Aulozoon* wherein integument forms almost reticulated creasing patterns across the fossil surface. (d) A form of surface crease that is a single isolated, curved ridge extending across the *Aulozoon* (arrow). (e) A second example of isolated, curved ridge surface creasing (arrow). (f) Example of surface creasing derived from folding of the *Aulozoon* body wall. Scale a = 1.5 cm, scales b, c = 3 cm, scale d = 3.5 cm, scales e, f = 5 cm.

(4) Margin irregularity: Irregular lateral margins that range in morphology from undulatory, rounded protrusions and inversions to rips preserved as non-repeating angular irregularities in the body wall (Figure 12e-h).

Marginal creasing is observed in 47% of *Aulozoon* specimens at NNHS and occurs primarily in PEM/IM preservational modes but is also observed in one specimen preserved as a convex external cast nearing a point of preservational mode transition. Marginal creasing is otherwise primarily located at points of bending in PEM/IMs but are also more common in *Aulozoon* specimens that are preserved on top of well-developed, high relief TOS (e.g., Figure 11a, b) or at points of overlap between tubes (Figure 11a, arrow 2).

Surface creasing occurs in 73% of the *Aulozoon* specimens at NNHS. One common type of surface creasing that is observed in PEMs/IMs is the presence of a meniscate ridge that crosscuts the width of the tubular body (Figure 11d, e). When a meniscate ridge occurs, a minor decrease in tube width (> 2 mm) is observed on one side of the ridge.

There is, however, no consistent pattern in the convexity of the meniscate ridge and the width of the tube. For example, when viewed horizontally and studied from left to right, some specimens have a convex meniscate ridge (i.e., when viewed from left-to-right the ridge is like the letter ‘‘C”) and the leftmost part of the tubular body preceding the ridge is narrower than the right-most portion occurring after the ridge (Figure 11d).


a
b
c
d
e
f
g
h

Figure 12. Additional examples of deformation patterns in *Aulozoon soliorum*. (a) A specimen of *Aulozoon* with a deep linear crease running sub-parallel to the body wall margin (arrow). (b) Example of an *Aulozoon* with extensive linear creasing leading up to termination of preservation (right), grooves are poorly defined, are sub-parallel to the body wall, and are discontinuous. (c) Linear creasing (arrow) running sub-parallel to the body wall. (d) Linear creasing in two *Aulozoon* specimens which parallel the body wall for the majority of its length, creating a double margin effect defined here as margin mirroring creasing. (e) Example of an *Aulozoon* specimen with an irregular margin, the arrow denotes a sharp, V-shaped irregularity in the body wall indicative of ripped integument. (f) *Aulozoon* specimen with a broadly undulatory body wall in the center of the fossil and extensively ripped integument at the terminal ends of the fossil. (g) *Aulozoon* fossil preserving margin irregularity in the form of small scale, rounded protrusions (arrow) that are irregular in size and spacing. (h) *Aulozoon* specimen that preserves larger scale body wall undulations (arrow) that are irregular and are associated with overlap of a high relief textured organic surface and another *Aulozoon*. Scales a, b, f, g = 3 cm, scale c = 2.5 cm, scale d, h = 5 cm, scale e = 1.5 cm.

Alternately, when observed in this same orientation, other specimens exhibit a concave meniscate ridge (i.e., when viewed left-to-right the ridge is like the letter ‘‘C” written backwards) and the leftmost proceeding portion of the tubular body is narrower than the right-most portion of the tubular body after the meniscate ridge (Figure 11e). This feature is, at face value, intriguing and suggestive of some form of segmentation. However, if these meniscate ridges were a true morphological feature there would be a consistent relationship between the convexity of the ridge and the width of the tube on either side of the ridge so that regardless of orientation, the convexity of the ridge and its relationship to body width is consistent. Instead, it is found that the convexity of the meniscate ridges have no consistent relationship to tube width and are therefore interpreted as biostratinomically-derived creases potentially related to integument deformation during injection of sediment. Other examples of surface creasing do not have consistent, repeating morphologies and occur variably as the result of the high relief underlying TOS, of general collapse and burial-related deformation (Figure 11c), and of general deformation through folding and twisting (Figure 11f).

Linear creasing is the least common deformation type, occurring in 19% of *Aulozoon* specimens of the PEM/IM and positive external cast preservational modes. Linear creases are either deep, roughly straight, and negative relief features (e.g., Figure 12a, c) or shallow, poorly defined, and non-straight creases (e.g., Figure 12b).

Extensive, non-straight linear creasing can occur so prevalently that it completely covers the tube surface in irregular creases that are subparallel to the long axis of the tube and often correspond to the twisting or shredding of the tube leading up to the termination of preservation (Figure 12b).

Linear creases also take the form of two distinct and repeating fold types, one being the aforementioned deep negative relief longitudinal grooves that run parallel to subparallel to the midline for a portion of the tube (Figure 12a, c) and the other being margin mirroring creases that manifest as positive relief ridges running along the outermost margin on one or both sides of the tube (Figure 12d). Deep longitudinal grooves were described by Gehling and Runnegar, (2022) as a common feature in *Aulozoon* fossils from Bathtub Gorge. However, this feature is uncommon at NNHS and is observed in only seven specimens. Additionally, the deep longitudinal grooves do not have a consistent length or depth of negative relief, which, along with their rarity indicates a biostratinomic origin. Margin mirroring creases are observed in 15 PEM/IM individuals at NNHS (Figures 8a, 12d). These crease types have sharp, deeply negative margins and can either occur continuously for the full preserved length of a tube, occur once along a small length of a tube, or occur multiple times, discontinuously along the margin of a tube. Ridges generated by margin mirroring creases are between 0.57 and 7.27 mm wide and range from short lengths of 7.51 mm to the entire length of the preserved tube, up to 110 mm. The relief of these ridges is equal to, to marginally higher, than the relief of the main tube.

The termination of the margin mirroring crease can either end abruptly in a blunt, squared off edge or can taper off to join the main margin. The ridge itself can be a smooth, linear feature or a more irregular and undulous feature.

Margin irregularity features are highly irregular deformation patterns that characterize the entirety or part of the length of a tube's external margin. Breaches occur as rips or undulations in the integument wall; 4% of PEM/IM *Aulozoon* specimens preserve ripping, half of which also preserve body wall undulations. 63% of PEM/IM *Aulozoon* specimens preserve body wall undulations, only 3% of which have rips. Therefore, the majority of *Aulozoon* specimens that preserve ripping also preserve body wall undulations, but the majority of specimens with body wall undulations do not preserve ripping. Signatures of a ripped integument are straightforward in that they are characterized by jagged and irregular edges (Figure 12e, f). Ripped *Aulozoon* integument occurs only in the PEM/IM preservational modes and can be a small, isolated rip (Figure 12e) to extensive tearing (Figure 12f). Undulations are highly irregular but are characterized primarily as a departure from the straight-line wall margin (e.g., Figure 10e). Undulatory margins are only preserved in PEM/IMs and range from small-scale repeating protrusions of the body wall (e.g., Figure 12g) to larger isolated protrusions from the straight-line margin (e.g., Figure 12h). Undulations are not always mirrored on both sides of the tube, they do not exhibit regular spacing or sizes, and they do not extend across the surface of the tube. Undulations commonly correspond with the decreased definition of tube margins and decreased overall relief of the *Aulozoon* fossil, but there

are specimens with well-defined margins, moderate relief, and undulous margins (Figure 12h). Interestingly, margin irregularities do not directly correlate with the extent of surface, marginal, and linear creasing in that specimens with rips and undulous margins can have no other signs of deformation. Conversely, specimens with high amounts of creasing almost always have undulous margins in at least a portion of the body (e.g., Figure 11a, b, d-f).

Terminations

A complete specimen of *Aulozoon soliorum* preserving true morphological features at both ends has yet to be identified. The longest known specimen is one meter in length and does not preserve terminal ends with clear morphological features (Gehling and Runnegar, 2022). This lack of clear original terminal morphology in *Aulozoon* specimens is also observed at all localities, and it is likely that many preserved terminal ends of *Aulozoon* represent deformational features and not the true morphology of *Aulozoon* at its base and apical end. In this discussion the word ‘‘terminations” refers solely to the end of preservation of the fossil and does not imply the presence of features that represent true in vivo morphology.

Terminations of *Aulozoon* are not commonly observed because the rock slab often fractures before the body fossil ends, cutting off one or both ends of the organism. At least one terminal end is preserved in 81% of *Aulozoon* specimens at NNHS, 48% of which preserve terminations at both ends of the tube. There are no observed examples of

negative external molds with terminations because they are always either cut off by a slab fracture or located within the middle of an individual with multipart preservation and the terminal ends of the tube are characterized by a different preservational mode. As such, only the PEM/IM, cast internal mold, and positive external cast preservational modes are discussed below. Within these preservational modes, *Aulozoon* terminations have morphologically consistent and repeating forms which are preserved as positive hyporelief features, here classified as seven distinct termination types:

(1) Circular (Figure 13a): Three specimens at NNHS are preserved with a circular structure ranging in diameter from 1.03 to 1.68 cm, narrower than the preceding *Aulozoon* body, at one end of the fossil. Two of these *Aulozoon* fossils are preserved as positive external casts and one is a PEM/IM. Circular terminations never occur on both ends of an individual, are smooth, featureless, and have sharp to diffuse margins. The circular structure itself is preserved in high positive hyporelief similar to that of *Aulozoon* positive external cast fossils. Circular termination structures are always separated from the tubular body by a millimeter-wide ridge of sediment, but the repeated proximity of the circular termination, its consistent alignment with the tubular body, and similarity in its relief to the relief of the tubular body indicate a direct connection between the two structures.

(2) Rounded (Figure 13b): Rounded terminations define *Aulozoon* ends that are convex and have smooth, sharply defined margins. A total of 17 *Aulozoon* terminations are

characterized by rounded terminations. There is no change in tube width leading up to rounded terminations. Rounded terminations occur in the PEM/IM, cast internal mold, and positive external cast preservational modes, but are most commonly observed in PEM/IM preservation.

(3) Smooth Blunt (Figure 13c): Smooth blunt terminations are flat (i.e., not convex or rounded) and have smooth, sharp margins. A smooth blunt termination can either be relatively flat, forming a right angle where it joins the body margin, or it can be diagonal, meeting one side of the body margin at an obtuse angle and the other at an acute angle. The width of the body at the point of the smooth blunt termination is consistent with the width of the rest of the body. 24 *Aulozoon* specimens have at least one smooth blunt termination. This termination type is absent in positive external cast preservational mode, rare in the cast internal mold preservational mode and common in the PEM/IM preservational modes.

(4) Rough Blunt (Figure 13d): Rough blunt terminations are the second most common termination type. A total of 33 *Aulozoon* specimens at NNHS, all of which are classified as PEM/IM preservational modes, have a rough blunt termination. Rough blunt terminations are similar in overall shape to smooth blunt terminations and the junctions of the terminal end display similar angles with the body walls. However, rough blunt terminations do not have smooth margins. Instead, the terminal margin of a rough blunt end is jagged and irregular.

The roughness of this termination type does not propagate past a few millimeters from the termination and does not impact body width. The margins of rough blunt terminations can be sharply defined or low relief and poorly defined.

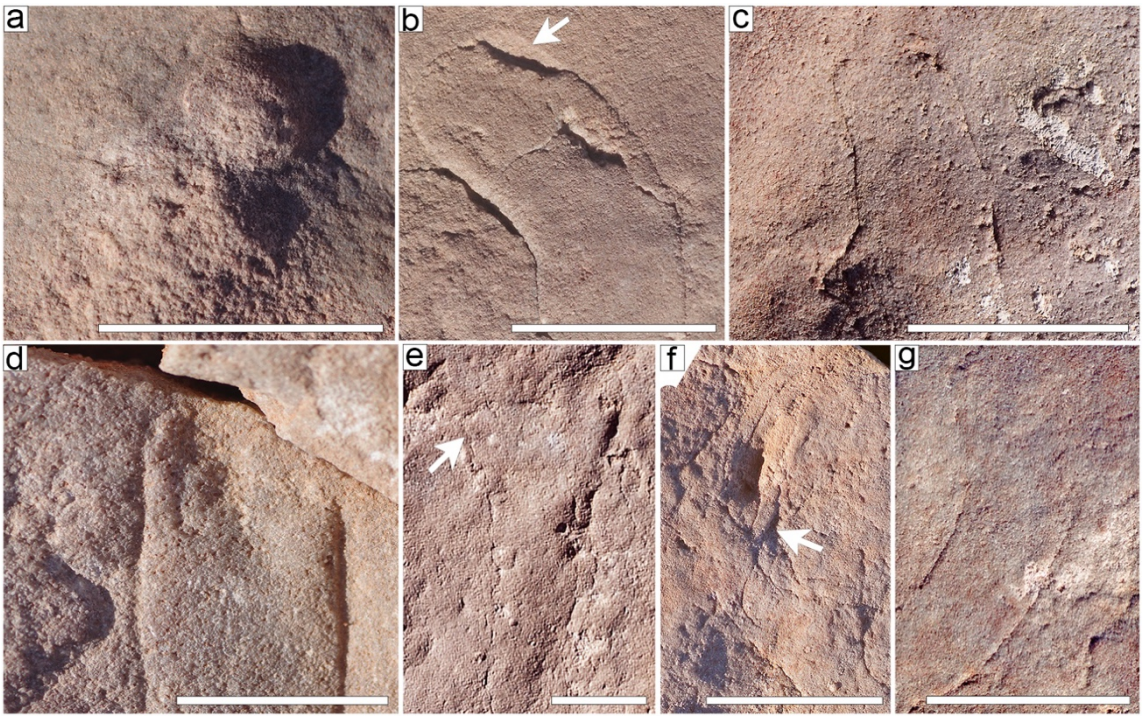

Figure 13. Examples of all observed termination types in *Aulozoon soliorum* fossils from Nilpena National Heritage Site. (a) Circular termination type. (b) Rounded termination type with partially exposed cast of an internal mold (arrow). (c) Smooth blunt termination type. (d) Rough blunt termination type. (e) Flared termination type (arrow). (f) Ripped termination type (arrow). (g) Diffuse termination type. Scales a, b, c, e, g = 3 cm, scale d, f = 1.5 cm.

(5) Flared (Figure 13e): Flared terminations are observed in five individuals at NNHS, all of which are classified as PEM/IM preservation. Flared terminations are characterized by an increase in width beginning about one to three centimeters before the end of preservation. The widest point of the flared termination ranges from 12 to 27 mm wider

than the preceding tubular body. This change in width creates a funnel-shaped terminal end with margins that range from well-defined and sharp to diffuse. Margins can either be smooth or highly undulous and are often a combination of both smooth and undulous. The relief of flared terminations is generally equivalent to the relief of the preceding body, but it can also have a higher positive relief than the rest of the preserved tube. In four of the specimens with flared terminations, the flared section is immediately preceded by an irregular surface crease trending perpendicular to the tube midline (Figure 13e, arrow). Each side of the flared termination is straight to moderately arched; the length and shape of the flare is not mirrored across the midline. The surface of the flared termination ranges from extensive surface wrinkling to completely featureless. The terminal margin of a flared end is only preserved in two specimens, the remaining three are terminated prematurely by fractures in the rock. In the two specimens where it is preserved, the terminal margin is clearly defined and undulous.

(6) Ripped (Figure 13f): Ripped terminal ends occur in seven PEM/IM *Aulozoon* and can take several forms depending on the severity of the rip, ranging from pinched off, to frayed, to shredded. In some instances, severely ripped ends propagate longitudinal wrinkles away from the termination and into the body (e.g., Figures 12b, 13f). Regardless of rip severity, ripped terminations always correspond with change in width, relative to the main body width, at the point of rupture. However, width change in the ripped portion of an *Aulozoon* individual is not consistent and can be either an increase or decrease in width relative to the preceding tube.

(7) Diffuse (Figure 13g): Diffuse terminations are the most commonly occurring type of termination in *Aulozoon*, characterizing the terminations of 35 PEM/IM and convex external cast individuals. The distinguishing characteristic of diffuse terminations is the absence of a clearly preserved terminal end. Instead, the lateral margins of the tube become less and less defined and the relief of the tube decreases until the tube is indistinguishable from the sole surface.

It is evident that certain preservational modes are prone to certain termination types (Figure 14a). No single termination type is largely dominant in terms of number of occurrences (Table 3), and there are no common co-occurrences of termination types in specimens with two preserved ends (Appendix B Table 8). Notably, there are no examples of tubes with two ripped ends, two flared ends, or two circular ends. The PEM/IM preservational modes exhibit all seven termination types. The cast internal mold preservational mode never preserves circular, flared, or ripped terminations. However, only two specimens preserve cast internal molds with terminations, one is a rounded termination and the other is a smooth blunt termination. The termination type data presented for cast internal molds then should not be interpreted as an indicator of population-level biostratinomic patterns. Positive external cast termination types are also limited in that they do not preserve flared or ripped terminations and are primarily characterized by diffuse and circular terminations.

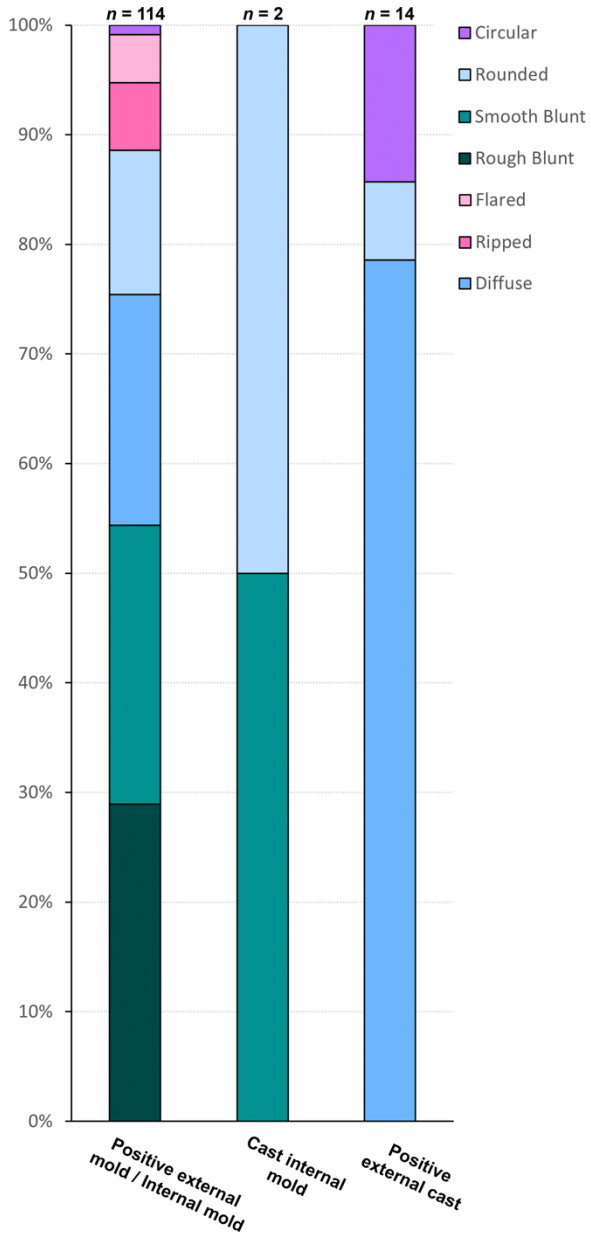

Figure 14. Percent occurrence of termination types in different preservational modes of *Aulozoon*. Negative external molds are excluded from this figure because they occur exclusively in multipart preservation and do not exhibit true terminations.

Termination type	No. occurrences	% frequency
Circular	3	2
Rounded	17	13
Smooth blunt	24	18
Rough blunt	33	25
Flared	5	4
Ripped	7	5
Diffuse	35	27

Table 3. Number of occurrences and frequency of all seven *Aulozoon* termination types.

Termination type does not appear to be correlated with the extent of deformation or the overall preservation of the body. *Aulozoon* fossils can have wrinkled bodies and undulous margins and have well-defined terminations such as circular, rounded, or smooth blunt terminations (Figures 10a, d, 11c, 12e). Conversely, *Aulozoon* can have minorly wrinkled bodies and smooth, well-defined margins and have poorly defined terminations such as diffuse, flared, or ripped terminations (Figures 10a, 12b, f). In these cases, the majority of the body exhibits relatively good preservation but the body wall approaching the end that exhibits diffuse, flared, or ripped terminations becomes more undulous and wrinkled. In this sense, the terminal end type only corresponds to localized preservational fecundity and not whole-body preservation. This is not to say, however, that there are no specimens that exhibit extensive wrinkling and diffuse, flared, or ripped terminations, because those specimens are also observed.

Discussion

At NNHS there are minor differences in preservation of *Aulozoon soliorum* between the ORS and PLRUS facies, namely the positive external cast preservational mode is most common in the PLRUS facies and is rare in the ORS facies. This suggests that the preservation of positive external casts is potentially linked to paleoenvironmental factors. Otherwise, taphonomic features of *Aulozoon* are consistent across facies and localities, indicating that other preservational features of *Aulozoon* most likely reflect variables unrelated to the paleoenvironment, such as original biomaterial strength and biological traits, rather than differing energy regimes, paleoenvironments, or grain sizes of the casting beds. The synthesis of these biostratinomically-linked features allows for the establishment of several hypotheses on the taphonomic pathways, morphology, biomaterials, and life mode of *Aulozoon*.

Taphonomic models

The five preservational modes of *Aulozoon soliorum* exhibit distinctions in type (i.e., positive or negative) and height of relief, cross-sectional appearance, and surface deformation. These distinctions suggest that each preservational mode reflects one or several distinct taphonomic pathways. A combination of taphonomic and geologic evidence is utilized to propose multiple scenarios that would hypothetically result in the observed preservational modes of *Aulozoon*. Some preservational modes can be explained by multiple, equally plausible taphonomic scenarios. In such cases, a single taphonomic pathway cannot be assigned to each preservational mode, though scenarios

that are most likely can be identified. Given that there is no evidence for internal structures in *Aulozoon* and that the organism is preserved in both high relief and as collapsed specimens, taphonomic scenarios presented here model *Aulozoon* as having been fluid-filled. This is consistent with models proposed for taphonomically similar tubular organisms (e.g., Sappenfield et al., 2011; Surprenant et al., 2020).

The high positive relief of the positive external cast preservational mode requires that the organism was embedded in the seafloor by several centimeters either during life and burial or during burial only. Therefore, at the time of burial, the *Aulozoon* individual was either already living as an infaunal organism or was fluid-filled and robust enough to be impressed into the underlying sediment by the weight of the burial sand body. Evidence for an infaunal life mode in *Aulozoon* is lacking, with no supporting evidence apart from the minimal support provided by positive external cast preservation. Additionally, the high abundance of PEM/IM preservation indicates that *Aulozoon* individuals preferentially collapsed or were infilled upon burial and were deposited on top of the organic mat, which is not consistent with an infaunal life habit. Further, the common occurrence of *Aulozoon* overlapping and abutting other *Aulozoon*, macrobiota, and TOS requires that *Aulozoon* overlay benthic organisms and is inconsistent with an infaunal life habit. Therefore, the second explanation for positive external cast preservation, which invokes the impression of a robust, fluid-filled tube into the underlying sediment upon burial, is preferred. In this proposed scenario, an *Aulozoon* tube filled with some form of fluid (e.g., saline) is buried within a section of the seafloor that has a poorly developed,

non-rigid organic surface, allowing for the fluid-filled *Aulozoon* to be pressed into the underlying sand body (Figure 15ai-aii). Shortly after burial and impression of the fluid-filled tube into the underlying sediment, the tube collapsed, likely due to a combination of post-mortem decay and pressure from the overlying bed, leaving a void space in the underlying sand body that was then filled by the overlying sediment (Figure 15aiii). This results in the preservation of a highly positive relief external cast on the base of the burial event herein referred to as positive external cast preservation.

In this context, the characteristic irregular surface texture of positive external casts (e.g., Figure 11c) can be attributed to the rupture and collapse of the *Aulozoon* tube, which would have resulted in the decaying integument being pushed to the bottom of the external mold created by the impression of the once fluid-filled tube. This partially decayed integument would then be cast on the base of the overlying sand body as it moved to fill the void space left by the ruptured tube. Therefore, it would be expected that the surface of a positive external cast of *Aulozoon* would be highly wrinkled and irregular because the texture reflects the preservation of decayed integument over the original external mold. Thus, full surface wrinkling in positive external casts of *Aulozoon* is likely related to the degradation of the body wall and does not correspond to the original texture of the *Aulozoon* tube. Notably, these full surface wrinkles found commonly on positive external casts of *Aulozoon* only occur rarely on PEM/IM preservation, suggesting that collapsed and infilled individuals were sometimes subject to decay processes prior to or after final burial.

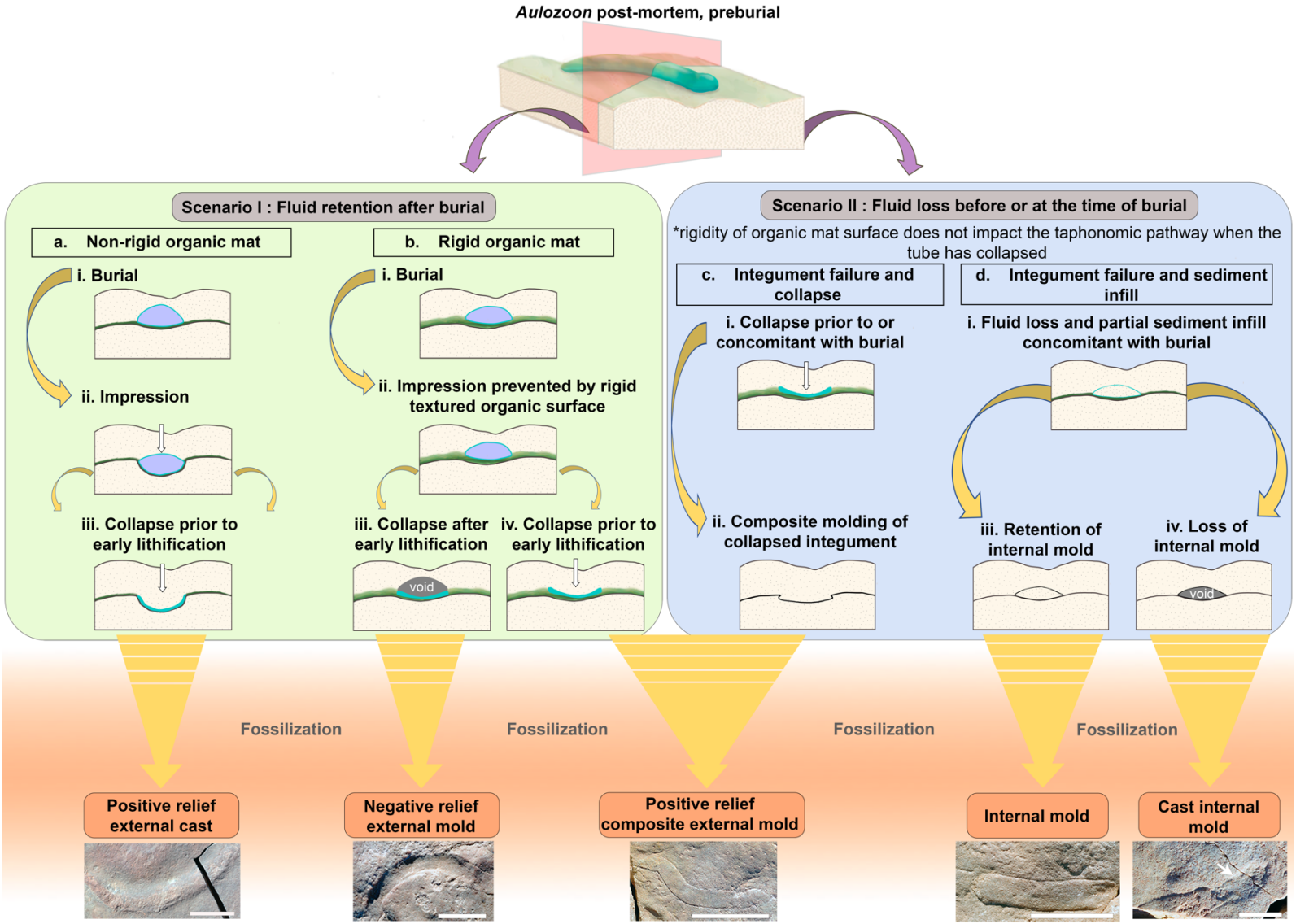
Aulozoon post-mortem, preburial
Scenario I : Fluid retention after burial
a. Non-rigid organic mat
i. Burial
ii. Impression
iii. Collapse prior to early lithification
b. Rigid organic mat
i. Burial
ii. Impression prevented by rigid textured organic surface
iii. Collapse after early lithification
void
iv. Collapse prior to early lithification
Scenario II : Fluid loss before or at the time of burial
*rigidity of organic mat surface does not impact the taphonomic pathway when the tube has collapsed
c. Integument failure and collapse
i. Collapse prior to or concomitant with burial
ii. Composite molding of collapsed integument
d. Integument failure and sediment infill
i. Fluid loss and partial sediment infill concomitant with burial
iii. Retention of internal mold
iv. Loss of internal mold
void
Fossilization
Fossilization
Fossilization
Fossilization
Positive relief external cast
Negative relief external mold
Positive relief composite external mold
Internal mold
Cast internal mold

Figure 15. Schematic demonstrating the different taphonomic pathways represented by each preservational mode of *Aulozoon soliorum*. The *Aulozoon* post-mortem, preburial image depicts an *Aulozoon* lying flat on the seafloor for illustrative purposes, this does not reflect hypothesized life habit. Note that some preservational modes can be achieved through several disparate scenarios. In this schematic, teal represents *Aulozoon* integument, purple represents a fluid filled *Aulozoon*, and light yellow represents *Aulozoon* that have been infilled by sediment. (a) Demonstration of the taphonomic pathways that are possible if *Aulozoon* retained its internal fluid after burial and was deposited on a non-rigid organic mat. (ai.) Burial of the *Aulozoon* and retention of fluid. (aii.) Fluid is retained and the *Aulozoon* body remains robust, because the organic surface is not forming a rigid barrier, the *Aulozoon* is impressed into underlying sediment due to the weight of the overlying sediment. (aiii.) *Aulozoon* collapses after impression resulting in a positive relief external cast because the non-collapsed tube created an external mold in the underlying sediment that was subsequently cast by the overlying sediment that moved to fill the void left by the collapsed tube. Note that the collapsed integument is impressed into the top surface of the positive relief external cast. (b) This scenario considers how a non-collapsed *Aulozoon* tube would be preserved if deposited on top of a rigid organic mat. (bi-ii.) Upon burial the fluid filled *Aulozoon* cannot be impressed into the underlying sediment because of a resistant and rigid organic mat. (biii.) Buried *Aulozoon* collapses after the onset of early lithification, resulting in the preservation of a negative relief external mold. (biv.) *Aulozoon* collapses before early lithification, overlying sediment moves to fill the void left by the collapsed tube and results in the preservation of a positive relief composite external mold. In scenario II the variable taphonomic pathways followed for collapsed and infilled *Aulozoon* are explored, because these scenarios are dependent on the loss of tube rigidity during collapse which would preclude impression or molding of the tube's external surface, the rigidity of the organic mat is negligible. (ci-ii.) *Aulozoon* collapses and loses internal fluid prior to or concomitant with burial. This results in the impression of the collapsed body wall into the underlying mat and fossilization of a low positive relief composite external mold. (di.) *Aulozoon* loses fluid and is partially injected with sediment prior to or at the time of burial. The body wall remains as an organic barrier between the casting bed and the internally injected sediment, thusly preventing complete amalgamation. (dii.) If the internal mold remains intact through late-stage diagenesis and excavation the resulting fossil is an internal mold of *Aulozoon*. (diii.) If the internal mold is lost to currently unknown late-stage diagenetic processes the resulting fossil will be the cast of the internal mold created at the time of burial. Scales = 5 cm. Illustrations not to scale.

While other explanations for the positive external cast preservational mode are possible (e.g., positive external casts and negative external molds could be the only *in situ* *Aulozoon* and thus are the only ones able to retain fluid), the model proposed here is consistent with its facies dependent distribution, its exclusive occurrence on bedding planes characterized by poorly developed TOS, and its characteristic full surface wrinkling.

Similarly to positive external casts, the relief of negative external molds necessitates that *Aulozoon* was a robust structure that could resist collapse upon burial if fluid was retained. However, the high negative relief of negative external molds indicates that instead of being impressed into the seafloor by the weight of the newly deposited sand body (as in the positive external cast scenario), negative external molds result from the newly deposited sand body being draped over the fluid-filled tube and molding its external surface (Figure 15b). This preservational model is supported by the absence of deformational features on negative external molds, which would not be expected to be present in the mold of a non-collapsed specimen. In this scenario, a potential reason for the inability of the fluid-filled tube to be impressed into the underlying sediment is the presence of rigid, well-developed TOS that, through a combination of biostabilization and baffling, likely served as a barrier preventing the *Aulozoon* tube from being pressed into the underlying sediment (Cuadrado et al., 2011). Nevertheless, the tube would have remained a robust structure between the TOS and the burial sand body, resulting in the molding of the tube's external surface on the base of the event deposit as a negative

hyporelief external mold (Figure 15biii). This scenario is consistent with observations at NNHS wherein positive external cast preservation is found exclusively on beds with poorly developed TOS while negative external mold preservation is found solely on beds with well-developed TOS. Importantly, this proposed scenario requires that the *Aulozoon* tube remained robust until after the overlying bed had been stabilized through early-initiating precipitation of silica cement (Figure 15biii), a process that has been experimentally demonstrated to create a scaffolding over organic surfaces at a pace that precedes significant amounts of soft tissue decay (Slagter et al., 2021, 2022). If the tube were to collapse prior to early lithification the overlying sand body would move to fill in the void space, resulting in a PEM (Figure 15biv).

The preferred taphonomic scenarios for the positive external cast and the negative external mold preservational modes invoke the development level of TOS as a key constraint on the ultimate preservational mode of *Aulozoon*. However, there are several other potential explanatory variables including thickness of the casting bedform and facies-related energy differences that could also be cited as potential taphonomic controls. To test the potential role of each of these taphonomic controls, two *Aulozoon* dominated bedding planes, 1T-F and WS-TBEW, are compared (Droser et al., 2019). 1T-F is a bedding plane in the ORS facies that has a thickness of several centimeters and a mature or well-developed TOS. WS-TBEW is a bedding plane in the PLRUS facies that is less than 1 cm thick and has a low maturity or poorly developed TOS. 1T-F preserves 31 *Aulozoon* specimens which are characterized by PEM/IM preservation. 13% of those

specimens have multipart preservation showing transitions from PEM/IM to negative external mold preservation. WS-TBEW preserves 29 *Aulozoon* specimens, 62% are PEM/IMs only, 17% are multipart preservation of PEM/IMs and positive external casts, and 21% are positive external casts only. This comparison reveals a distinct pattern in preservational mode abundance, wherein positive external cast preservation is common on WS-TBEW but absent on 1T-F. This pattern can potentially be attributed to one or multiple of the three identifiable differences between the two beds: TOS development, bed thickness, and facies-related energy levels.

If the high abundance of positive external cast preservation on WS-TBEW is attributable to facies-related energy level differences, one would expect to see the high positive relief casting of other collapse-resistant taxa preserved in the PLRUS facies. However, the PLRUS facies as a whole is not characterized by the highly positive relief preservation of *Aulozoon* and other macrobiota. Instead, this occurrence is restricted to two bedding planes in the PLRUS facies that also preserve similarly unique preservational modes of other taxa. For instance, on WS-TBEW the rare flipping and high positive hyporelief preservation of the bases of *Tribrachidium heraldicum* is observed (Hall et al., 2015). Therefore, positive external cast dominated bedding planes are interpreted as unique preservational environments in which the impression of resistant organisms was more favorable than on other beds at NNHS. These unique preservational environments are not consistent across the whole PLRUS facies and are therefore not closely linked to the energetic conditions of the facies.

Additionally, in this hypothetical scenario wherein facies related energy levels are responsible for preservational differences, one would expect a corresponding absence of positive external cast preservation in the ORS facies as a result of a lower energy paleoenvironment, precluding the deep impression of robust taxa into the underlying seafloor. This hypothesized pattern is not consistent with observations at NNHS in that positive external cast preservation is not entirely absent in the ORS facies, though it is rare, indicating that the energetic conditions of the ORS facies did not preclude high positive relief preservation. Therefore, facies related energy levels cannot be invoked as an explanation for the preservation of positive external casts of *Aulozoon*.

Elimination of facies-related energetic difference leaves bed thickness and TOS development as two potential explanatory variables for the unique abundance of positive external casts on WS-TBEW. If bed thickness was the driving force behind preferential preservation of positive external casts on WS-TBEW and of negative external molds on 1T-F, the necessary hypothesis would be that the thicker the bed, the stronger the compressive force, and the more likely that a fluid-filled *Aulozoon* would be impressed into the underlying sediment to create a positive external cast. Alternately, the higher compressive forces generated by a thicker bedding plane could lead to higher rates of collapse, but the presence of negative external molds on thick beds precludes this explanation. Under the hypothesis that a thicker bed would lead to higher rates of impression into underlying sediment, it is predicted that positive external casts would be more abundant on thick beds than on thin beds. This is the opposite of what is observed at

NNHS. WS-TBEW is a thin bed with a high abundance of positive external casts whereas 1T-F is a very thick bed with no positive external casts and a higher abundance of negative external molds, thus falsifying the hypothesis that positive external cast preservation and negative external mold preservation is driven by bed thickness. Therefore, the nature of the TOS is the single explanatory variable remaining. This is consistent with observations of a poorly developed TOS on WS-TBEW and a contrastingly well-developed TOS on 1T-F (Droser et al., 2022). This, in conjunction with observations that WS-TBEW also preserves similarly unique taphonomic modes of other taxa, indicates that WS-TBEW preserves a unique paleoenvironment characterized by a soft, nonrigid TOS which allowed for the deep impression of organisms into the seafloor. This hypothesis is consistent with the TOS type present on beds where convex external cast preservation occurs as well as with the broader understanding of TOS dynamics at NNHS (Gehling and Droser, 2009).

Given the low relief and frequency of deformation in *Aulozoon* PEMs, the corresponding taphonomic model must invoke some form of fluid loss and collapse (Figure 15c). As such, the proposed model entails that the *Aulozoon* tube is ruptured and loses its internal fluid as a result of preburial death or as a result of the high energy storm event that ultimately deposited the casting sand body. After the loss of fluid, the *Aulozoon* individual is buried and flattened, resulting in the low positive hyporelief composite preservation of both sides of the tubular body wall on the base of the burial sand body (Figure 15cii). Another potential way in which the PEM preservational mode could occur

is if a fluid filled *Aulozoon* tube was deposited on a well-developed TOS and buried prior to collapse (Figure 15b) but then collapsed rapidly post-burial before the overlying sand body had stabilized (Figure 15biv). In this scenario the buried, fluid-filled tube would have been on the way to becoming a negative external mold, but because the overlying sand body was not stabilized at the time of collapse the negative hyporelief external mold would have been obliterated by the downward movement of the sediment to fill the void space left by the collapsed tube. The downward movement of the sediment would then result in the molding of the collapsed tube, forming a low positive relief composite external mold (Figure 15biv). In this second scenario a higher frequency of deformational features in the resulting fossil is expected. In practicality, individual PEMs of *Aulozoon* cannot be assigned to either scenario, but both are likely potential taphonomic pathways to be considered.

Given the cross-sectional evidence of sediment infilling *Aulozoon* tubes at variable thicknesses in the IM preservational mode, the proposed taphonomic scenario for IMs must invoke rupture and partial infill of a portion of the tubular body (Figure 15d). Within this model, the *Aulozoon* tube would have been severed or ripped before or during burial, resulting in the loss of internal fluid. After this, the ruptured tube would have been infilled by storm surge sediment, evidenced by the synlithological composition of *Aulozoon* infill and casting bed matrices (Gehling and Runnegar, 2022). The variable thickness of infill from one end of a tube to the other and meniscate surface creasing support this model by indicating that infill was directional, as would be expected in storm

surge-mediated infilling. After this initial partial infill of the *Aulozoon* body cavity and final burial, the sediment infill persisted through diagenesis as a discrete lens of sediment that is partially amalgamated to the sole of the casting bed, but distinct from the matrix due to the thin organic barrier derived from the *Aulozoon* integument, resulting in a positive hyporelief internal mold (Figure 15dii).

The taphonomic models for both the PEM and IM preservational modes are consistent with the observed abundance of deformational features in those preservational modes. Both preservational modes underwent collapse, which is linked with wrinkle structures (Jensen et al., 2006), and it is parsimonious to infer that the irregular infill of a tubular organism would result in the deformation of the surrounding integument. Specifically, it is observed that the orientation and morphology of margin mirroring creases, a form of deformation that occurs solely in PEM/IM preservational modes, are consistent with the variable collapse and infill of a hollow structure (e.g., Figure 9a).

The cast internal mold preservational mode reflects a taphonomic scenario in which an IM was formed at the time of death and burial of the *Aulozoon* individual (Figure 15d), but that internally molded sediment was subsequently lost through late-stage diagenetic processes that are, as of yet, enigmatic (Figure 15diii). However, following understanding of organic surfaces functioning as barriers to amalgamation of lithologically homogenous bedforms in the Ediacara Member (Tarhan et al., 2015), it is parsimonious to infer that an IM would not be fully amalgamated to a bed sole because of the integumentary barrier

between the infill and the matrix. The late-stage loss of an unamalgamated IM would therefore result in a negative hyporelief cast of an internal mold of *Aulozoon*. This taphonomic model is supported by multiple instances of the clear late-stage removal of an IM to reveal a cast internal mold (Figures 10d, 13b). Additionally, Gehling and Runnegar, (2022) report that in some cases, a removed IM will also reveal integument wrinkle marks on the underlying cast internal mold, though this is not observed directly at NNHS.

Given these taphonomic scenarios, several features can be identified to distinguish between the cast internal mold and the negative external mold preservational modes of *Aulozoon*, a concern that was identified earlier in this discussion. Cast internal mold and negative external mold preservational modes are only observed in specimens with multipart preservation. Because there is always another preservational mode associated with cast internal mold and negative external mold preservation, they can be distinguished by characterizing the transition between the preservational modes in an individual. The way in which these transitions manifest align with their respective preservational scenarios because they alternately represent early taphonomic processes and late-stage diagenetic processes. These are distinct processes in which integument as well as casting and molding sediment are expected to behave differently. In this context, if the preservational mode transition is smooth and folded with no jagged edges (e.g., Figures 9a, 10b, c) it can be diagnosed as a negative external mold because that transitional morphology reflects plastic deformation of a flexible integument, consistent

with the negative external mold taphonomic scenario proposed here. Alternately, if the transition is jagged or has an appearance of differential weathering across the preservational transition it can be diagnosed as a cast internal mold (e.g., Figures 10d, 13b), because under the proposed taphonomic model for cast internal molds the process of infill loss occurs at a late diagenetic stage and is not related to soft tissue deformation. Therefore, a transition to a cast internal mold should appear as a brittle fracture of the fossil surface. These criteria work well for multipart preservation in *Aulozoon*, but if isolated negative relief specimens of *Aulozoon* are uncovered in further excavations their preservational mode should not be diagnosed in the absence of multipart preservation.

Biomaterials

The differential preservation of *Aulozoon soliorum* as a robust structure impressed into the underlying or overlying sediment body and as a collapsed, deformable structure on the sole of the casting bed indicates that *Aulozoon* was fluid-filled in life and either retained fluid or deflated upon death and burial. However, the majority of *Aulozoon* individuals are classified as taphomorphs derived from tube collapse whereas those that reflect fluid retention are markedly rarer (Table 2). Thus, while *Aulozoon* was capable of fluid retention after burial, the taxon preferentially collapsed upon death and burial. Notably, the preservational modes that reflect fluid filled *Aulozoon* (i.e., positive external casts and negative external molds) exhibit distinct taphonomic signatures from those preservational modes that reflect collapsed or partially infilled *Aulozoon* (i.e., PEM/IMs).

This is namely seen in the absence of creasing and margin irregularity in negative external molds and the absence of margin irregularities and marginal creasing in positive external casts. The absence of certain deformational features in these two preservational modes starkly contrasts the occurrence of some form of deformation in 98% of PEM/IM *Aulozoon* fossils. Cast internal molds, with the exception of one specimen described by Gehling and Runnegar, (2022), do not preserve deformational features, so they are not included in the following discussion.

The taphonomic disparity between the negative external mold and positive external cast preservational modes and the PEM/IM preservational mode exemplifies that much of the structural integrity of *Aulozoon* was derived from its fluid-filled body cavity. It is pertinent to note however, that although a fluid filled *Aulozoon* appears to have been robust enough to be pushed into underlying sediment and molded by the overlying casting bed without preserving deformational features, it was not rigid. Instead, we observe that sinuosity is present in the positive external cast and negative external mold preservational modes (Figure 8a, b), which is consistent with some extent of flexibility of the *Aulozoon* body even when fluid filled. Regardless, the prevalence of creases and marginal breaches in PEM/IM preservation indicates that collapsed integument had lower structural integrity and was more prone to deformation than integument that was fluid-filled. It is also observed that the extent of deformation in PEMs of *Aulozoon* is impacted by the topography of the underlying surface, with underlying surface features mirrored by

the *Aulozoon* integument in 38 specimens at NNHS (e.g., Figure 16). This further supports the hypothesis that *Aulozoon* integument was very thin and suggests that the patterns of deformation in the PEM/IM preservational mode can provide insight into the baseline integrity of the *Aulozoon* integument.

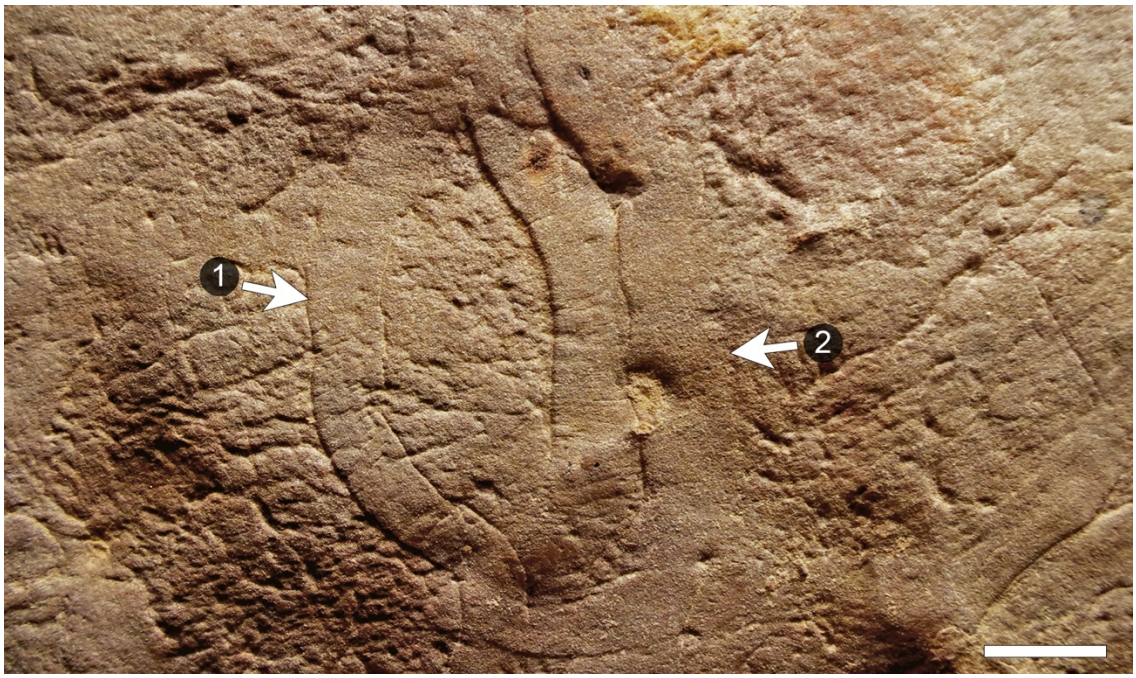

Figure 16. Example of *Aulozoon soliorum* overlying high relief textured organic surface. Morphology of the *Aulozoon* is either impacted by the underlying topography (arrow 1) or completely overprints the underlying textures (arrow 2); SAM P40573. Scale = 3 cm.

Prior to interpreting the structural properties of *Aulozoon* integument, it must be determined which features reflect pre- or syn-burial mechanical deformation of the integument and which reflect decay or degradation of the integument to prevent conflation of integument structure and integument recalcitrance. In this context, decay and degradation refer to post-death and post-burial aerobic breakdown of the *Aulozoon*

integument. The sole deformational feature that can be linked to integument degradation state in *Aulozoon* is the extensive full-surface creasing in positive external cast preservation and some PEMs/IMs. Previous studies have demonstrated that the sharpness of margins in another abundant tubular organism at NNHS, *Funisia dorothea*, correspond with the decay state of the fossil (Surprenant et al., 2020). This does not appear to be the case with *Aulozoon*, in which it is observed that the sharpness of the tube margin does not necessarily correspond to the overall preservation state of the fossil. In fact, it is common to observe margin irregularities, such as undulations, protrusions, and rips, in one portion of the tube and sharp, well-defined margins with no deformation in another portion of the same tube (Figure 9d). If margin irregularities were indicators of decay, it is expected that they would impact the whole tube in a relatively consistent manner and would correspond with overall less detailed preservation. This relationship between margin irregularity and overall *Aulozoon* preservation is not observed. As such, margin definition is taken to reflect the response of *Aulozoon* integument to biostratinomic factors other than decay, such as uneven topography of the underlying TOS, uneven sediment infill, and lifted edges. TOS underlying *Aulozoon* is observed to underprint the fossil, imparting its texture onto the overlying tubular body fossil and resulting in the uneven draping of the tube on the seafloor, thus resulting in margins that are undulatory (Figures 7b, c, 16). At points of transition from IM to PEM preservation, on the select number of specimens that preserve this feature clearly, the thinning of sediment infill corresponds with a high level of margin irregularity (Figures 9d, 10a), thus demonstrating a second mechanism for non-decay related irregularity in margin definition. It has additionally been demonstrated in

Dickinsonia costata fossils at NNHS that the storm surge-related wedging of sediment under an organism at the time of burial will result in the non-preservation of the section of the body that was lifted by the sediment (Evans et al., 2015). This is a potential third explanatory variable for undulatory margins of *Aulozoon*, wherein small portions of the integument at the margin of the tube could have been lifted at the time of burial.

Other deformational features that could be conflated with decay include surface, marginal, and linear creasing of *Aulozoon*. There is, however, no clear link between abundance of creases and overall poor preservation of *Aulozoon*. Additionally, these creases occur preferentially in PEM/IM preservation and are entirely absent in the negative external mold preservational mode. This pattern indicates that surface, marginal, and linear creasing in *Aulozoon* were absent when the organism was alive, and that the common creasing structures are deformational features related to the underlying topography as well as collapse and variable infill of the tube during burial. In this context, margin rips and ripped terminal ends of *Aulozoon* are interpreted as extreme signs of deformation.

The non-decay related deformational features of *Aulozoon* best characterize collapsed taphomorphs of *Aulozoon* and include margin irregularity, linear creasing, marginal creasing, and surface creasing—except for the pervasive surface creasing that is unique to positive external casts. In synthesis these features indicate that once *Aulozoon* lost its internal fluid, the integument became highly deformable. However, deformation varies in

intensity across single tubes and ripped integument is rare, indicating that while fluid loss resulted in a loss of body rigidity it did not result in the loss of integument cohesion or resistance to brittle fracture (i.e., *Aulozoon* integument did not disintegrate after fluid loss, it simply became highly prone to deformation). This loss of rigidity as a result of fluid loss is additionally reflected in the common preservation of *Aulozoon* populations as ‘‘tangled heaps” (Gehling and Runnegar, 2022). This form of preservation indicates that after fluid loss *Aulozoon* tubes lost structural integrity. However, these heaped tubes retain distinctly defined margins for tens of centimeters of the tube length. The retention of this preservation potential despite loss of rigidity supports interpretation of *Aulozoon* integument as a coherent, though easily deformed, organic structure.

The preponderance of plastic deformation in PEMs/IMs of *Aulozoon* is one of several lines of evidence that indicates that the integument of *Aulozoon* was very thin. This interpretation is also supported by three independent lines of evidence: (1) IMs are partially adhered to the bed sole and in cross-section are shown to be separated from the matrix of the casting bed by a sub-mm thick haematitic barrier. The barrier itself reflects the presence of a thin organic structure at the time of burial and the partial adherence of the IM indicates that this organic barrier was not very thick, which would have resulted in minimal, instead of partial, adherence to the bed sole (Tarhan et al., 2017; Droser et al., 2022); (2) Body wall undulations in *Aulozoon* are more common and more pronounced on specimens that are preserved on top of a well-developed, variable relief TOS. Such a relationship between the edges of a fossil and the underlying surface is expected only in

the preservation of a non-robust structure that was thin enough to be impacted by the underlying surface, therefore providing evidence for a very thin and malleable integument of *Aulozoon*; 3) TOS patterns and macrobiota structures are commonly found to underprint PEMs of *Aulozoon* (Figures 7a, 16). Together these features are indicative of a thin integument that molded itself to the structure of the underlying surface and had little inherent structural integrity.

The thinness of the *Aulozoon* integument has several taphonomic implications, primarily in that thin organic structures are characterized by low recalcitrance (Hancy and Antcliffe, 2020). The overall clear preservation of *Aulozoon*, however, is difficult to reconcile with such a thin and hypothetically difficult to preserve integument. Additionally, the deformation state and clarity of preservation in single individuals of *Aulozoon* is found to be variable across the length of the tube. This is not common for individual fossils at NNHS, which can generally be characterized by a single preservational state and indicates that there is some factor other than decay and baseline integument strength, which are processes that should affect the whole fossil equally, at play across the length of individual *Aulozoon*.

One explanation for these patterns in *Aulozoon* preservation is that the majority of *Aulozoon* fossils identified as PEM/IM preservational modes actually have some extent of sediment infill, and true PEM preservation, wherein only the collapsed body walls are preserved, is rare. While this hypothesis cannot be directly tested without the serial

sectioning of several *Aulozoon* individuals with differing preservational modes, margin definitions, and reliefs, it is consistent with taphonomic evidence presented here. A handful of *Aulozoon* fossils are found to preserve clear and undoubted transitions from IM preservation to PEM preservation across the length of the individual (Figures 9d, 10a). In these specimens the internally molded portion is characterized by smooth, sharp margins and is completely overprinting the underlying TOS. In these specimens, as the relief of the internally molded section decreases, presumably transitioning to thinner infill and then to complete composite external mold preservation, diminished sharpness of the tube margin, presence of margin undulations, and the under printing of the TOS is observed. This preservational gradient within single collapsed specimens of *Aulozoon* demonstrates that thinner sediment infill is correlated with increased TOS-related deformation and decreased clarity of the fossil margins.

This demonstrates that a thinner or absent sediment infill results in higher impact of underlying TOS and poorer preservation of the tubular organism. This is further supported by the variable ability of *Aulozoon* fossils to overprint macrobiota that it is preserved on top of. In some instances, the morphology of the underlying organism is impressed upon the overlying *Aulozoon* integument, resulting in composite preservation of the two organisms (e.g., Figure 7b). In another instance, an *Aulozoon* fossil overlaps and completely overprints a *Dickinsonia costata* fossil (Figure 7c, d).

The inconsistent overprinting of underlying macrobiota can be explained by a thin integument that was variably infilled by sediment, wherein thicker sediment infill resulted in complete overprinting of underlying structures and thinner to absent sediment infill resulted in the under-printing of underlying structures on the thin integument of *Aulozoon*.

This hypothesis is additionally supported by the patterns observed in the *Aulozoon* termination types. Only two of the seven termination types, rough blunt and diffuse, are characterized by a gradational decrease in preservational clarity over the space of several millimeters. Rough blunt terminations are similar in morphology to transitions between PEM and IM preservation (Figures 9d, 10a, 13d), suggesting that the termination of tubes as rough blunt ends reflects the end of sediment infill and subsequent non-preservation of the remainder of the composite tube. This relationship is demonstrated well in Figure 10a wherein it is clear that sediment infill ceases, corresponding with a rough blunt transition, followed by a decrease in fossil relief and sharpness of tube margins ending in a diffuse termination. This suggests that towards diffuse ends sediment infill tapered out gradually, resulting in decreased definition of the tubular body until no sediment remained and the remaining integument was too thin to be preserved. Diffuse terminal ends are the most common termination type in the PEM/IM preservational modes.

The common occurrence of diffuse ends is consistent with the hypothesis that infill occurred directionally in *Aulozoon* during the burial storm surge and that one end of the tube would have to be characterized either by abrupt cessation of infill or gradually tapered infill and a corresponding loss in preservational definition.

This model is additionally supported by the conspicuous absence of the preservation of a complete *Aulozoon* specimen. If preservation of collapsed *Aulozoon* specimens was bolstered by internal infill and rare without infill, it would be expected that only the portions of the tubular body closest to the location of integument rupture and infill would be preserved well. The process of infilling *Aulozoon* tubes appears to have been unidirectional, therefore the distal-most ends of a collapsed individual would be unlikely to be preserved. As such, the absence of full *Aulozoon* individuals might be attributable to the low preservational potential of *Aulozoon* integument. If the integument was robust without a secondary taphonomic process required to stabilize it, complete specimens should be preserved commonly and would not be absent from the fossil record. The sum of this evidence provides good support for the hypothesis that *Aulozoon* preservation was facilitated by sediment infill and that in the absence of infill the thin integument of *Aulozoon* was not easily preserved.

Morphology

Evidence presented here supports the previously described morphology of *Aulozoon soliorum* as an elongate, tubular organism that had a circular cross-section in life (Gehling and Runnegar, 2022). Beyond this broad constraint on *Aulozoon* morphology, much about the true form of *Aulozoon* is unknown. This study enables three outstanding questions about the basic morphology of *Aulozoon* to be addressed: (1) What, if any, external features did *Aulozoon* possess; (2) was the common sinuosity of *Aulozoon* present *in vivo* or is this a biostratinomic feature; (3) what did the terminal ends of *Aulozoon* look like?

Data presented here strongly supports the interpretation of external features observed in *Aulozoon* fossils (i.e., marginal irregularity, linear creasing, surface creasing) as deformational or decay features. Additionally, the absence of surface features on negative external mold preservational modes of *Aulozoon* is significant in that it is the single preservational mode that molds the non-collapsed external surface of *Aulozoon* as it would have been in life. Therefore, evidence presented here indicates that, in life, *Aulozoon* possessed a smooth body wall.

Another tubular organism at NNHS, *Somatohelix sinuosus*, is characterized by a sinuous form. The sinuosity of *Somatohelix* is oriented around a symmetrical axis and it exhibits consistent patterns in the location of folding relative to sinuosity, suggesting that the organism possessed a helical morphology in life (Sappenfield et al., 2011). *Aulozoon* is

similarly characterized by a sinuous form, but this sinuosity is not oriented around a symmetrical axis and there are no consistent patterns in folding location. Further, calculated sinuosity values for *Aulozoon* fossils indicate that most individuals are characterized by no sinuosity (S = 1) and no other sinuosity value characterizes a majority of individuals (Appendix B Figure 28). As such, the observed sinuosity of *Aulozoon* fossils is interpreted to have been derived from a high plasticity of the integument in life along with a lack of structural integrity after death and fluid loss. This indicates that *Aulozoon* did not a have a secondary structural organization and that departure from a straight, cylindrical form is derived from integument flexibility.

To further understand *Aulozoon's* true morphology, the question of what the true terminal ends of *Aulozoon* looked like must be grappled with. To answer this question, it is first necessary to interpret what preservational scenario each termination type of *Aulozoon* reflects.

The ripped termination type is relatively straightforward in that it reflects the termination of *Aulozoon* preservation through the mechanical deformation and failure of the integument. This termination type has no consistent morphology and clear signatures of extensive deformation (i.e., twisting, shredding), thus ripped terminations are definitively characterized as a biostratinomic feature, not as a true morphological feature.

The diffuse and rough blunt termination types are interpreted to reflect the preservation of the tube ceasing as a result of waning sediment infill. Diffuse terminations are the most common termination type of *Aulozoon* and are proposed to reflect the gradual decrease in sediment infill towards the end of the tube. This termination type does not form a sediment or integumentary ridge but is associated with a decrease in fossil relief from the bed sole and a decrease in definition of tube margins towards the diffuse termination.

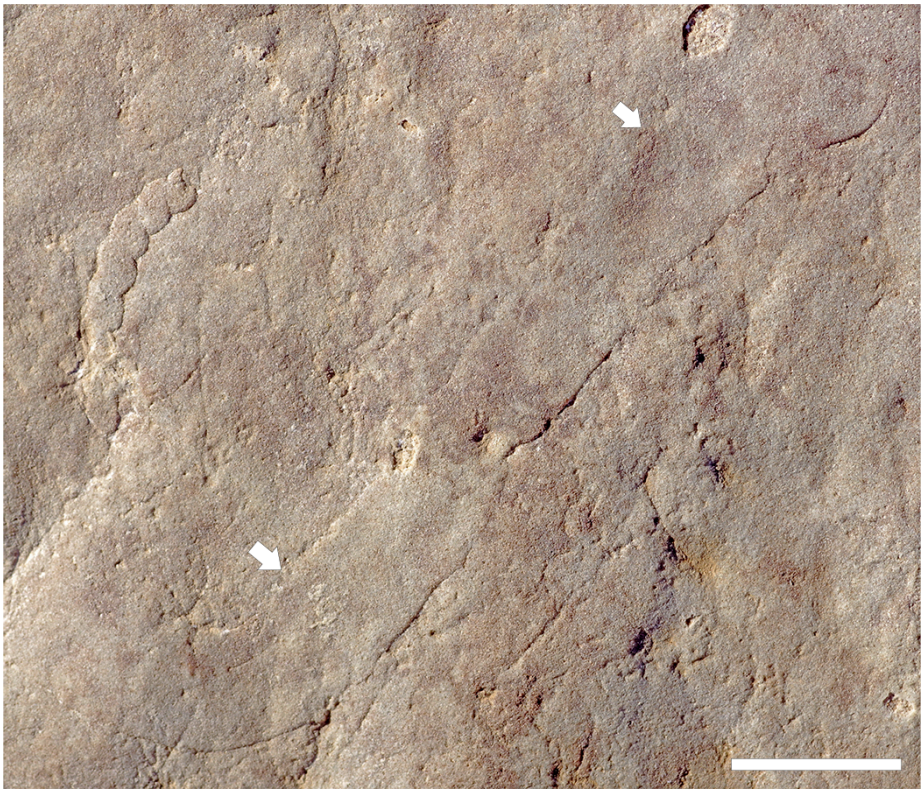

Figure 17. *Aulozoon soliorum* specimen that exhibits variable body margin relief and definition at different points in the fossil that do not represent termination of the tube. The body wall in the leftmost portion of the fossil (arrow) is clear and well defined, whereas the body wall in the rightmost portion of the fossil (arrow) is faint and poorly defined. Note that the other side of the fossilized tube is well defined across its whole length. Scale = 3 cm.

The transition from well-defined to poorly defined tube margins within single specimens is observed both at the terminal ends of *Aulozoon* and in the middle of specimens (Figure 17). This indicates that such preservational irregularity is characteristic of the *Aulozoon* integument as a whole and is not restricted to the organism's terminal ends. As such, diffuse terminations are most likely not an indication of a less recalcitrant terminal end but of variable underlying topography and extents of sediment infill.

Rough blunt terminations are commonly accompanied by surface creasing and likely reflect an abrupt end to the sediment infill, potentially due to kinks in the tubular body as is reflected by associated creasing. In specimens with rough blunt terminations, the cessation of infill is proposed to have prevented the preservation of the remainder of the tubular organism as a composite PEM. In some instances, a rough blunt morphology is observed at the transition point between IM preservation and other preservational modes in individuals with multipart preservation (Figure 10c). This is consistent with the interpretation of rough blunt terminations as the abrupt cessation of sediment infill because the two scenarios can be viewed as contrasting instances in which sediment infill is stopped and either the non-infilled integument is not preserved (i.e., rough blunt termination) or non-infilled integument is preserved (i.e., rough blunt transition). In this context, rough blunt terminations reflect biostratinomic features, not true morphological features.

Smooth blunt terminations are characterized by their sharp and smooth definition. This pattern is observed only at terminal ends of *Aulozoon* and the abrupt nature of this termination is most parsimonious with the lifting of the tubular body and subsequent non-preservation of the portion that has been lifted (*sensu* Evans et al., 2015). While this process should result in a preferred orientation of lifted specimens reflecting the current direction, the way in which *Aulozoon* are preserved as complex tangles precludes the ability to test this hypothesis. The preservation of these terminal ends is, however, entirely consistent with the lifting and non-preservation of the *Aulozoon* tube. As such, the smooth blunt termination type is interpreted as a biostratinomic feature.

Circular termination types display a consistent morphology and size. In addition to this, their high positive hyporelief preservation is akin to that of positive external cast preservation but is not linked to TOS development. This suggests that these circular structures were anchored under the mat, serving as holdfast.

Rounded termination types are characterized by a sharp and smooth terminal margin, for which there are two plausible explanations. The first explanation is related to observations of mid-tube meniscate surface creases observed in several specimens of *Aulozoon*. While these mid-tube creases are demonstrated to represent biostratinomic and not true morphological features, they are similar in expression to rounded terminations. As such, it is possible that rounded termination types also reflect some change in infill of *Aulozoon*. This is consistent with the observation that the mid-tube meniscate ridges are

always accompanied by some extent of relief change, which would be expected with changes in the level of infill. In the case of rounded terminal ends, however, this cessation of infill resulted in the non-preservation of the remaining tubular body. If this is the same process proposed for rough blunt terminations, the morphologies of the terminations would be similar. However, if the *Aulozoon* integument was infilled from one direction the thin, deformable tissue might have become folded as a result of injection and would thus create a smooth rounded ridge. A second equally plausible explanation for rounded terminations is the presence of a holdfast that was not preserved. In this scenario, if *Aulozoon* was attached to the seafloor by a holdfast, as is evidenced by the circular termination type, there is potential for the tubular body to be preserved while remaining connected to the holdfast but not preserving the structure itself. In this context, an *Aulozoon* individual that had lost its fluid but was still connected to its holdfast would plausibly have folded over the holdfast upon burial, thusly preventing preservation of the holdfast itself (i.e., a circular termination) and instead resulting in the preservation of the body wall as a rounded terminal structure. Here, preservation of the holdfast is not achieved, and the rounded termination reflects the point of attachment but not the holdfast structure itself. These two models establish rounded terminations as primarily biostratinomically controlled features.

Flared termination structures are characterized by a large increase in width from the tubular body, variable margin definition, moderately high positive hyporelief, sharp terminal ends (i.e., not diffuse), and a cross-body ridge preceding the flared portion. This

combination of features provides support for both a true morphological and a biostratinomic origin for this termination type. On one hand a biostratinomic origin appears to be parsimonious, in that the flared portion could reflect a deformed and ripped terminal end of the *Aulozoon* individual. This is consistent with the observed decrease in definition of the margin of the flared end nearing its final termination. However, many features of flared terminations are not consistent with a biostratinomic origin. If this termination type were to reflect a deformed and ripped end of an *Aulozoon* tube, the thin and torn *Aulozoon* integument would be expected to be preserved as a low positive hyporelief structure due to the demonstrated thinness of the body wall. However, flared ends can be found as high positive relief structures, sometimes reaching higher positive reliefs than the preceding PEM/IM tubular body fossil. This indicates that the flared structure was a relatively robust structure that was able to be impressed further into the underlying TOS than the preceding tubular body. This is not expected of deformed *Aulozoon* integument, which is demonstrated here to be preserved in a relief similar to that of the tubular body. Additionally, ripped terminal ends are observed to have no consistency in shape, with some ripped portions being more shredded and twisted and others being torn and stretched. In contrast to this, flared terminal ends exhibit a consistent morphology and a consistent increase in width from the tube body. Further, the repeated presence of a cross-body ridge just before the flared terminal end is potentially suggestive of a true morphological feature. This pre-flare ridge along with the robust nature and general consistent shape of the flared portion could potentially indicate that flared terminal ends represent a true morphological feature. This does not, however,

preclude the possibility that the structure is purely biostratinomic and reflects a broadly shredded terminal end. Currently only two complete flared terminations are known, preventing a deeper investigation into the origin of this terminal structure. At this time, both models are upheld as potential explanations for the flared terminations of *Aulozoon*.

Considering that the majority of *Aulozoon* termination types reflect biostratinomic patterns, it remains unclear what the end of the tubular organism looked like and whether it was flared and housing a form of feeding apparatus (Figure 18a) or sealed and rounded off (Figure 18b). It is, however, clear that *Aulozoon* possessed a holdfast at the base of its tubular body (Figure 18b). The emerging image of *Aulozoon* is one of a smooth, elongate, cylindrical organism anchored within the sediment. Though the apical-most end of *Aulozoon* remains enigmatic, comparison of left-most and right-most width measurements of *Aulozoon* provide no evidence to support systematic changes in width from one end of the tube to another and thus should be characterized as a broadly cylindrical form with a consistent width along its length. The sum of these features informs a novel morphological model for *Aulozoon* (Figure 18). In this model, *Aulozoon* was a flexible, fluid-filled, tubular organism with a circular cross-section (Figure 18c) and a circular holdfast at one end (Figure 18d) that was narrower in diameter than the tubular body. The apical end of the *Aulozoon* tube remains enigmatic (Figure 18a, b).

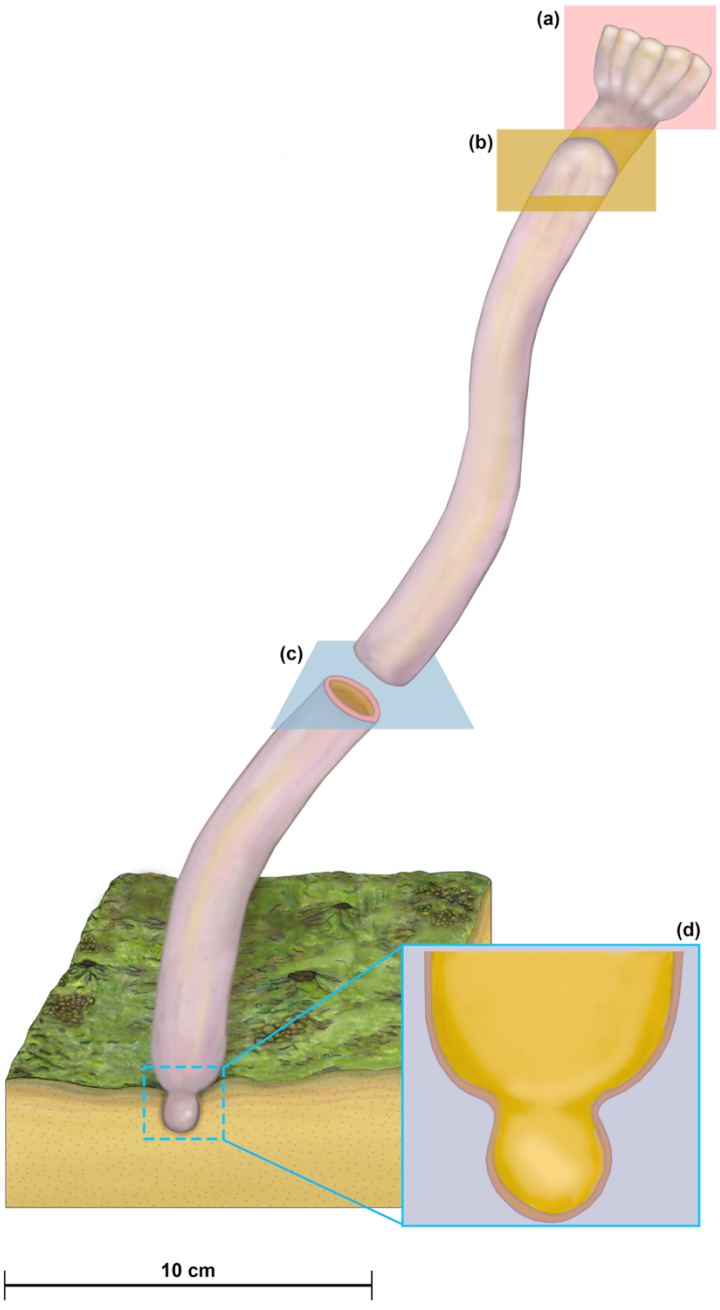

Figure 18. Reconstruction of *Aulozoon soliorum* in life informed by data presented here. (a) One potential true terminal end of *Aulozoon*, a flared termination. (b) A second hypothesized terminal end of *Aulozoon*, a rounded and closed off termination. (c) Cross section of *Aulozoon* in the middle of the tube, illustrating thin body wall (pink) and hollow, fluid-filled interior (orange). (d) Terminal holdfast embedded in the sediment. Note hollow interior (orange) and thin body wall (pink).

Paleoecology

Based on the data presented here, several hypotheses on *Aulozoon soliorum* life mode can be tested. The presence of a holdfast in *Aulozoon* establishes it as a sessile, benthic organism that was anchored under the mat-sediment interface. This allows for the rejection of a pelagic life mode for *Aulozoon*. While a completely infaunal lifestyle has also been rejected for *Aulozoon*, the unique preservation of *Aulozoon* as positive external casts could be hypothesized to reflect a semi-infaunal lifestyle wherein a section of the tubular organism was exposed in the water column and the other section was infaunal. A semi-infaunal life mode is consistent with positive external cast preservation, with the abundance of PEM/IM preservation, and with the presence of multipart preservation wherein a positive external cast transitions to a PEM/IM. However, if part of the *Aulozoon* body was under the sediment and the other part was in the water column, sharp turns in multipart preservation at the transition between the positive external cast and the PEM/IM preservational modes would be expected because one side would be subject to the current and the other would be anchored in the sediment. Such sharp transitions are not observed, nor is the current alignment of PEM/IM preservational modes. Therefore, this hypothesis is not supported by the data presented here and the most plausible mechanism for positive external cast preservation is the presence of non-rigid TOS.

The elimination of pelagic and infaunal life modes for *Aulozoon* leaves two hypotheses: *Aulozoon* lived prostrate on the seafloor or *Aulozoon* lived upright in the water column. If *Aulozoon* were to have lived flat on the seafloor in tandem with the mat, *Aulozoon* would

only overlie other organisms when transported or disturbed by a burial event and, when *in situ*, would have diffuse margins indicative of the organism growing into the mat. While the specimens of *Aulozoon* that overlie other macrobiota are rare enough to support the hypothesis that all *Aulozoon* were prostrate and only overlapped macrobiota when transported, the remaining evidence does not support a prostrate life habit, namely in that there are no specimens of *Aulozoon* that have diffuse margins along the entirety of the tube. This type of diffuse margin is expected if they were growing into the mat. Even specimens associated with a holdfast, and are thus definitively in situ, do not exhibit evidence of growth in tandem with the mat.

Instead, features consistent with an upright life habit, such as overlap with other taxa and TOS, as well as sharp tube margins indicating that the tubular body was deposited on top of the mat, characterize *Aulozoon*. An upright life mode is additionally consistent with the presence of a fluid-filled central body cavity extending the length of the *Aulozoon* tube, which is supported by the variable collapse and non-collapse of *Aulozoon* reflected by the five preservational modes. A fluid-filled interior would have provided a source of neutral buoyancy to keep *Aulozoon* suspended in the water column despite an integument with little inherent structural integrity (Bamforth and Narbonne, 2009). The presence of a fluid, such as saline, instead of gas in the central cavity of *Aulozoon* is consistent with the mechanism through which modern benthic marine invertebrates maintain buoyancy (e.g., saline filled body cavities of sea anemones) (Barnes et al., 2009). Therefore, *Aulozoon* is reconstructed as a sessile, benthic tubular organism that was fluid-filled and neutrally

buoyant in the water column (Figure 18). Given that the fluid-derived buoyancy of *Aulozoon* was supporting a thin, non-rigid body wall it is likely that the organism did not stand entirely upright (i.e., vertical) in the water column but was orientated sub-diagonally to the seafloor. Thus, the exact form of *Aulozoon* in the water column would have most likely been controlled by current intensity and direction.

The absence of definitive fossil evidence of the apical-most end of *Aulozoon* precludes speculation as to how it may have sustained itself. However, an upright benthic lifestyle in shallow water is parsimonious with suspension feeding.

Affinities

Data presented here further confirms a body fossil origin for *Aulozoon soliorum*, but characterization of *Aulozoon* beyond this broad classification remains difficult. The large size of *Aulozoon* in addition to the absence of branching, striae, and rhizoids on the holdfast structure in *Aulozoon* precludes a macroalgal affinity (Xiao and Dong, 2006). Alternate interpretations, such as *Aulozoon* being an egg sack are intriguing, but ultimately inconsistent with data presented here, including size range of *Aulozoon*, its lack of consistent associations with other macrobiota, and the absence of other macroorganisms preserved inside of *Aulozoon*.

The broad classification of *Aulozoon* as a potentially metazoan-grade organism raises the question of the relationship of *Aulozoon* to crown- and stem-group metazoans. Previous studies have attempted to place *Aulozoon* into such classifications, citing similarities with

several fossil and living species including *Vittstudivermis annularis* from the earliest Cambrian in China (Gehling and Runnegar, 2022) and the extant vestimentiferan annelid *Riftia pachyptila* (Runnegar, 1994). However, these taxa are defined by features such as external ornamentation and biomineralization which are inconsistent with the characteristics of *Aulozoon* described here. As with most Ediacaran organisms, no direct comparison is perfect and therefore the synonymization of *Aulozoon* with younger or extant genera is not supported. Further, the overall lack of features present in *Aulozoon* fossils precludes assignment to the phylum level. However, authors have invoked the common alignment of Ediacaran tubular taxa with phylum Annelida (Moczydłowska et al., 2014; Budd and Jackson 2016; Schiffbauer et al., 2020; Yang et al., 2020) as justification for the establishment of an annelid affinity as the null hypothesis for *Aulozoon* (Gehling and Runnegar, 2022). While the affinity of all Ediacaran tubular taxa is well beyond the scope of this research, there is no evidence to support the hypothesis that tubular forms are monophyletic, and therefore the identification of other tubular taxa as potential annelids provides no support for an annelid affinity of *Aulozoon*.

Furthermore, observations made during this investigation provide no evidence to support an annelid affinity for *Aulozoon*. The structure of *Aulozoon* as a non-segmented and hollow organism negates this hypothesis.

In addition to those primary lines of evidence, the observations presented here do not support the reconstruction of *Aulozoon* as the sheath of a tube-dwelling organism or as an organism possessing organs or musculature. Thus, the null hypothesis of an annelid affinity is rejected, and the alternative hypothesis of an unknown affinity is supported.

Conclusion

Through this systematic taphonomic investigation, *Aulozoon* is reconstructed as a large tubular organism that possessed a broad cylindrical morphology and a smooth, straight body wall. This study identifies the presence of a holdfast at the base of the *Aulozoon* body and provides evidence for a fluid-filled body cavity. Thus, *Aulozoon* is interpreted as a sessile organism that lived upright in the water column and derived its buoyancy from fluid within its hollow body cavity. The morphology of *Aulozoon's* apical most end remains enigmatic, though this study identifies two potential morphologies: a rounded termination or a flared termination. Further, the patterns of deformation observed in *Aulozoon* are consistent with a very thin body wall that is here demonstrated to be preserved most clearly when the body is infilled with sediment. The emerging picture of the integumentary structure of *Aulozoon* is distinct from that of other tubular taxa preserved in the Rawnsley Quartzite and provides a way forward for distinguishing between taxa that are otherwise simple and difficult to distinguish. As such, the interpretation of the Ediacaran tubular fossil record through such a comparative taphonomic lens appears to be essential to the further resolution of the tubular fossil record and the interpretation of their evolutionary significance.

CHAPTER 3: GROWTH STRATEGIES OF THE HIGHLY ABUNDANT EDIACARAN TUBULAR ORGANISM *FUNISIA DOROTHEA*

Abstract

The Ediacara biota (575—538 Ma) are the first complex, multicellular, and community forming organisms on Earth and provide the earliest evidence for metazoan life. An exceptionally complete and extensive record of these early animal communities is preserved within the Ediacara Member (~555—550 Ma) of South Australia. *Funisia dorothea* is a metazoan-grade tubular organism that is the most abundant organism in the Ediacara Member by an order of magnitude and is characterized by a hollow, elongate body constructed of uniserially repeating modular elements. The high abundance of *Funisia* led it to shape the ecosystems around it and its occurrence in densely packed aggregates of similarly sized individuals is consistent with reproduction via spatfall, representing some of the earliest evidence of sexual reproduction in multicellular organisms. Thus, *Funisia* represents a broadly significant Ediacaran organism and one of few taxa that provides insight into the paleobiological traits of the Ediacara biota. This study investigates size changes in *Funisia* modular elements to provide further insight into the paleobiology of this organism through the development of a holistic growth model. Results demonstrate that the growth strategies of *Funisia* were highly regulated to maintain consistent modular element sizes along the length of an individual and a broadly cylindrical form. The growth model proposed here is compared with the preestablished growth model for another Ediacaran tubular organism comprised of uniserially repeating

modular elements, *Wutubus annularis*, demonstrating that the two taxa follow distinct developmental processes, and have disparate autecological strategies, despite a shared constructional morphology.

Introduction

Fossils of the Ediacara biota (574—538 Ma) represent the first macroscopic, complex, and community forming organisms on Earth, with many members likely representing stem-group metazoans (Droser and Gehling, 2015; Evans et al., 2020; Schiffbauer et al., 2020; Evans et al., 2021; Dunn et al., 2021, 2022). The Ediacara Member (~555—550 Ma) of South Australia preserves an exceptionally complete and extensive record of these early animal communities (Droser et al., 2019, 2022). Of the fossil genera known from the Ediacara Member, *Funisia dorothea*, a metazoan-grade tubular organism characterized by its non-mineralized and hollow form constructed of serially repeating modular elements, is the most abundant by an order of magnitude (Droser and Gehling, 2008; Surprenant et al., 2020). Not only did the high abundance of *Funisia* lead it to limit available ecospace, thus shaping the ecosystems around it (Surprenant et al., 2020**)**, but the common occurrence of *Funisia* in densely packed aggregates of similarly sized individuals is consistent with reproduction via spatfall, representing some of the earliest evidence of sexual reproduction in multicellular organisms (Droser and Gehling, 2008). These characteristics of *Funisia* establish it as a key player in Ediacaran ecosystems of the Ediacara Member as well as a genus that provides novel insight into the paleobiology of the Ediacara biota. In addition to being a prominent member of the ecosystems

preserved within the Ediacara Member, *Funisia* is also one of the most abundant members of the tubular morphogroup, a globally distributed group of organisms that share a hollow and elongate body plan that can be cylindrical, conical, ovular, or comprised of nested growth units depending on the taxon (Droser and Gehling, 2008; Surprenant et al., 2020; Surprenant and Droser, 2024). The tubular morphogroup is broadly significant because it is the most commonly occurring multicellular body plan in the Ediacaran Period and has been invoked as a partial driver of purported ecosystem changes that led to the extinction of the Ediacara biota at the Ediacaran-Cambrian boundary (Schiffbauer et al., 2016; Darroch et al., 2018).

The modular construction of *Funisia* makes it one of few members of the Ediacara biota whose morphology lends itself to the analysis of growth strategies. Other modular, soft-bodied Ediacara taxa, such as *Dickinsonia costata, Charnia masoni,* and *Wutubus annularis*, have been studied for the nature of their growth and have been placed within a unifying, though not phylogenetically informative, framework that describes their development via the relative contributions of insertional growth (i.e., the addition of new modular elements) and inflational growth (i.e., the expansion of existing modular elements into three-dimensional space) (Braiser et al., 2012; Chen et al., 2014; Evans et al., 2017; Dunn et al., 2021). While current understanding of *Funisia* holds that its populations grew via synchronous aggregate growth, as is evidenced by its common occurrence in densely packed populations of similarly sized individuals (Droser and Gehling, 2008), the growth strategies of *Funisia* individuals are not known.

This study develops a growth model for *Funisia* that is consistent with pre-existing growth models for other modular Ediacaran taxa to better contextualize this highly abundant taxon within the Ediacara biota as a whole and to allow for comparison with other modular tubular organisms.

Geologic background

Funisia dorothea is endemic to South Australia and is found only in the Ediacara Member of the Rawnsley Quartzite, within the Pound Subgroup (Figure 1), where it is the most commonly occurring taxon by an order of magnitude (Droser and Gehling, 2008; Surprenant et al., 2020). The Ediacara Member is located 200 to 600 m below a basal Cambrian disconformity and is well-known for its preservation of the soft-bodied Ediacara biota as casts and molds on the bases of successive and discrete quartzarenite bedding planes (Droser et al., 2019). These fossils are best known from Nilpena Ediacara National Park, located to the west of the Flinders Ranges (Figure 1).

Specimens used for this study are from three localities within Nilpena Ediacara National Park: the former Ediacara Conservation Park and the original Ediacara fossil discovery site (Figure 1b), the South Ediacara Mine Site (Figure 1c), and the original Nilpena National Heritage Site (NNHS) (Figure 1d). *Funisia* specimens from the Ediacara Conservation Park and the South Ediacara Mine Site that were used for this study are housed in the collections of the South Australia Museum (SAM); all of these specimens are preserved on small slabs that have been removed from their bedding plane context.

Funisia specimens from NNHS are located both within SAM collections as small slabs as well as on excavated and reconstructed bedding planes of up to 40 m^2 that remain in the field, including beds TB-S1, TB-BRW, WS-JDB, WS-MAB, and LV-FUN (Droser et al., 2019). NNHS houses 40 fossiliferous bedding planes, each of which represents a single depositional event that rapidly buried the matground and the associated macrobiota communities (Droser et al., 2019, 2022). The organisms that were buried by these depositional events were subsequently preserved as casts and molds on the bases of the burial sand bodies, which remain as discrete and excavatable bedforms due to the organic barrier created by pervasive organic matgrounds and early initiating precipitation of authigenic silica cements (Tarhan et al., 2016, 2017; Slagter et al., 2021, 2022, 2024). This has allowed for the systematic excavation and reconstruction of over 100 square meters of fossiliferous bedding planes that preserve Ediacara organisms within their facies and paleoecological context (Droser et al., 2019).

Materials and methods

Funisia dorothea is reconstructed as a hollow, fluid-filled organism that was anchored to the seafloor with a holdfast and stood upright in the water column (Droser and Gehling, 2008). As a result of its hollow morphology, *Funisia* is preserved under four distinct preservational modes that reflect the non-collapse, collapse, or sediment infill of the organism (see Surprenant et al., 2020 for a comprehensive overview). The preservational mode that reflects collapse of *Funisia* upon burial occurs as positive hyporelief external molds on the bases of bedding planes (Figure 19). Specimens included in this study were

limited to the collapsed preservational mode because it is the most commonly occurring type of *Funisia* fossil and is one of only two preservational modes that preserve modular elements. The other preservational mode that preserves modular elements is the negative hyporelief external mold, reflecting the non-collapse of *Funisia* and the molding of its external surface in negative relief on the base of the bedding plane (Surprenant et al., 2020). While this non-collapsed preservational mode is ideal for studying growth strategies in *Funisia,* because the modular elements preserved via this pathway are not collapsed and are thus subject to the least amounts of deformation, it is too rare to be utilized for robust analysis.

In contrast, modular elements of the collapsed preservational mode of *Funisia* are fundamentally impacted by soft-bodied deformation which has the potential to skew size data. Therefore, a primary assumption of this study is that by using only one preservational mode (i.e., the collapsed preservational mode), biostratinomic overprint will be more or less equally imparted on all specimens. This allows for the comparison of modular element size across individuals despite the influence of collapse and compaction on the shape of modular elements. For this reason, only data pertaining to the size of modular elements in *Funisia* were collected. Shape data were not considered because this is more likely to represent collapse-related deformation, not growth-related changes in morphology.

Biostratinomic overprint was additionally controlled for by only measuring specimens that preserve at least three modular elements with clearly defined margins on all sides, and modular elements that exhibited clear signs of stretching, tearing, bending, or folding were not included in this study (Figure 19b).

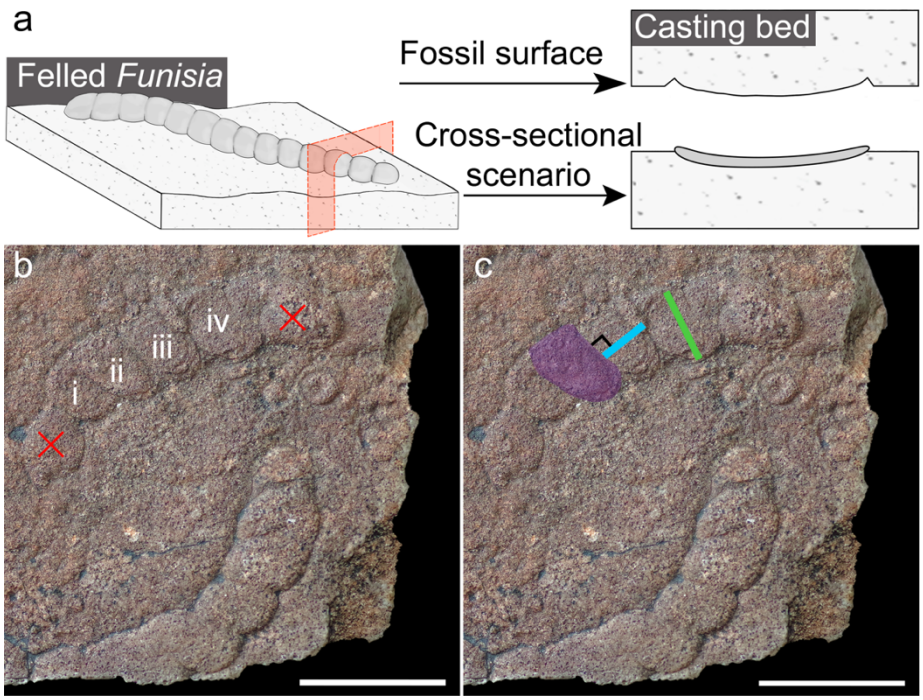

Figure 19. (a) Schematic illustration of the preservational model for *Funisia dorothea* fossils preserved as positive hyporelief relief external molds (i.e., the collapsed preservational mode); the red shaded region in the left-most illustration denotes the location of the cross-sections shown in the right-most illustration. Adapted from Surprenant et al., (2020), illustration is not-to-scale. (b) Example of *Funisia* specimens and modular elements that were deemed suitable and not suitable for inclusion in this study (SAM P41508); the specimen at the bottom of the slab was not included due to a lack of well-defined modular elements, and the specimen at the top of the slab was included in this study, but not all of its modular elements were suitable for analysis because they show clear signs of deformation. Excluded modular elements are denoted by red crosses and included modular elements are labelled i-iv, denoting the order in which they were measured. (c) Demonstration of area (purple shaded region), length (blue line), and width (green line) measurements that were taken for all modular elements suitable for analysis. Scale bars b, c = 2 cm.

To curate a dataset that could be used to assess growth processes in *Funisia,* thousands of specimens from the excavated beds at NNHS and the collections at SAM were reviewed. Based on the above specimen criteria, a total of 51 *Funisia* were selected for analysis. These specimens include small (width (W) = 2 mm—6 mm) (Figure 20a), intermediate (W = 6 mm—10 mm) (Figure 20b), and large (W = 10 mm—14 mm) (Figure 20c) *Funisia*. This wide range of sizes provides a useful dataset for comparing modular element size change throughout growth. On average, selected specimens preserved five modular elements, with a maximum of 12 modular elements per individual. A total of 237 modular elements were measured. Each specimen was photographed, and measurements were taken in ImageJ. Data collected from each specimen included total number of preserved modular elements as well as width, length, and area of each modular element (Figure 19c). Data analysis was conducted in R.

While the number of specimens selected for this study is sufficient for testing hypotheses on growth strategies, the relatively low number of specimens suitable for analysis compared to the total number of known *Funisia* fossils (N > 1,000) highlights the rare preservation of well-defined modular elements in *Funisia* (Surprenant et al., 2020). This is related to their hollow morphology and common collapse upon burial, as well as to the dense packing of individuals in *Funisia* populations, which results in high amounts of overlap. Both of these factors that leads to lower resolution of fine morphological details such as modular element boundaries (Surprenant et al., 2020). In addition to the rarity of well-preserved modular elements, the preservation of complete *Funisia* including an

abapical end with a holdfast and a determinant apical end is rare, even in well-preserved individuals with clear modular elements. Therefore, assessment of the total length and the total number of modular elements preserved in an individual is not possible through direct observation of fossil material. Because of this, measured modular elements cannot be identified as “apical-most” or “abapical-most” and all results presented in this study represent an unknown portion of the specimen’s total body length. To denote the relative placement of modular elements along the length of a single specimen, each modular element was assigned a number. This number reflects the location of the modular element

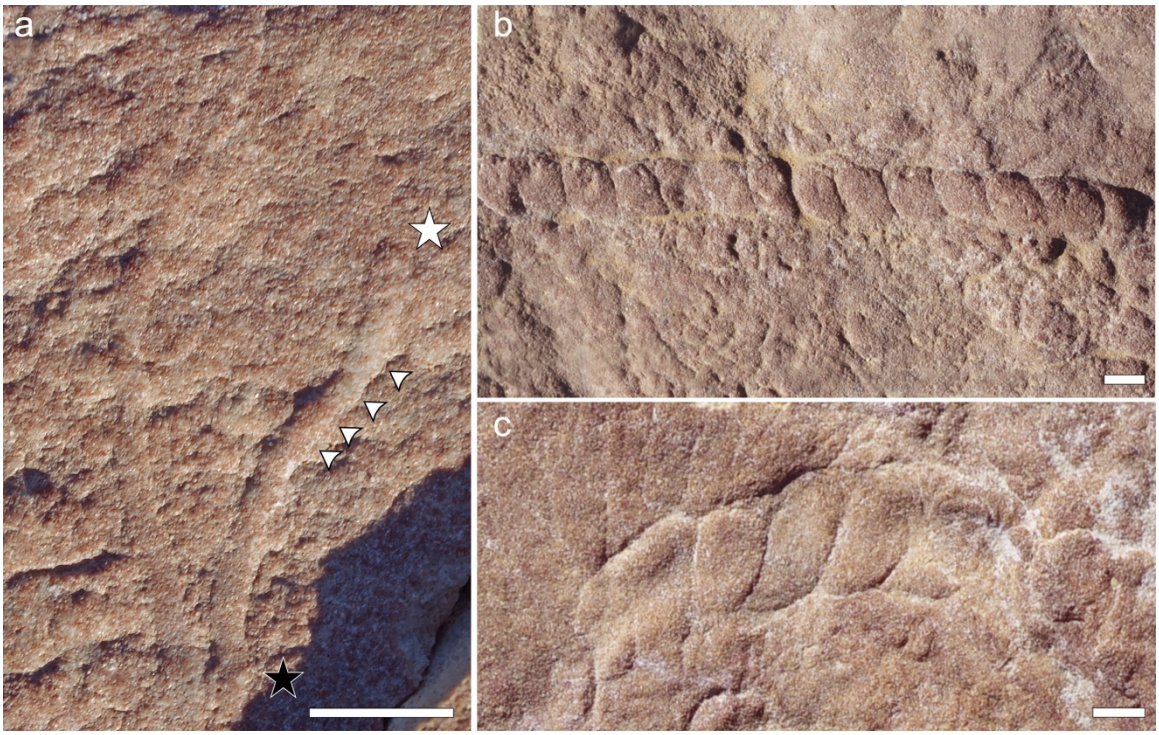

Figure 20. (a) The two smallest known *Funisia dorothea* specimens, the right-most specimen preserves an apical end (white star), an abapical end (black star), and four modular elements (arrows). (b) Intermediate sized *Funisia* preserved with no bending. (c) Large sized *Funisia* with the widest known modular elements. All specimens are preserved on bed LV-FUN at NNHS. Scale bars = 5 mm.

along the length of the individual when the specimen is oriented horizontally. The left-most modular element was always measured first and is thus designated as modular element one. Subsequent modular elements are numbered two, three, and so on to encompass all well-preserved modular elements. For example, in Figure 19b, the left-most modular element that is suitable for analysis (i.e., not deformed) is designated number one and the following intermediate elements are numbered two and three while the right-most element is numbered four. The left-most and right-most modular elements are referred to as the first and last measured modular elements, respectively. These numerical designations are used solely to demonstrate the size variability in elements relative to their placement along the length of the individual and do not imply apical- or abapical-most placement.

In recognition of the limitations considered above, this study aims to assess the nature of growth in *Funisia* through the comparison of size ratios of modular elements within individuals and between small, medium, and large individuals. The former addresses whether modular element size varies consistently along the length of an individual whereas the latter addresses the nature of modular element size change in different growth stages. Combined, these two lines of evidence provide a holistic view of *Funisia* growth processes.

Results

Modular element size within individuals

To test whether modular elements in *Funisia dorothea* are size-similar along their length or if they taper from one end to the other, the area of all well-preserved modular elements in 21 *Funisia* specimens was measured. This represents a subsample of the full dataset of 51 specimens because only specimens that were preserved with minimal to no bending were used for this analysis (e.g., Figure 20a, b) while those with prominent bending were not used (e.g., Figure 20c). Use of only straight to minimally bent *Funisia* allows for comparison of the area of modular elements in an individual without skewing of modular element area by localized soft-bodied deformation.

The distribution of modular element areas in the 21 selected individuals demonstrates a prominent clustering of modular element area values in all specimens, especially those within the small size classes (Figure 21). However, several *Funisia* specimens have modular elements with substantially higher or lower areas than the modular elements that are clustered (e.g., specimens K, O, and Q, Figure 21), clearly demonstrating some variability in modular element area within individuals. Importantly, this range of modular element areas is not correlated with the relative placement of the modular elements along the length of the individual. Most notably, the first and last measured modular elements do not consistently plot with the smallest or largest areas. Instead, area values are observed to be randomly distributed relative to their location along the length of an individual, with some of the first and last measured modular elements clustering with

intermediate modular elements (e.g., specimens E-H, M, and Q, Figure 21) and others plotting away from the clustered values (e.g., specimens L, N, and S, Figure 21). Additionally, some of the area values that are notably smaller or larger than the other clustered values represent intermediate modular elements (e.g., specimens L, O, and Q, Figure 21). Overall, this demonstrates that the range of modular element areas within individuals does not reflect a consistent variation in modular element size along the length of an individual, rather, the variability in modular element area appears to be random along the length of an individual and is most prominent in intermediate and large individuals.

Modular element size across individuals

To visualize the relationship between modular element length and width throughout different growth stages of *Funisia* (i.e., in small, medium, and large individuals), the length and width of all modular elements in the 51 selected specimens were measured to provide an average modular element length to width ratio for each specimen (Figure 22). The average width of modular elements is found to increase linearly with average length (R^2 squared = 0.78), and a linear regression model supports a statistically significant correlation between the two variables ($p < 2.2\ e^{-16}$). Notably, the length of modular elements does not increase equally with width, and the slope of the linear regression model is less than one, indicating that length of modular elements increased at a slower rate than width.

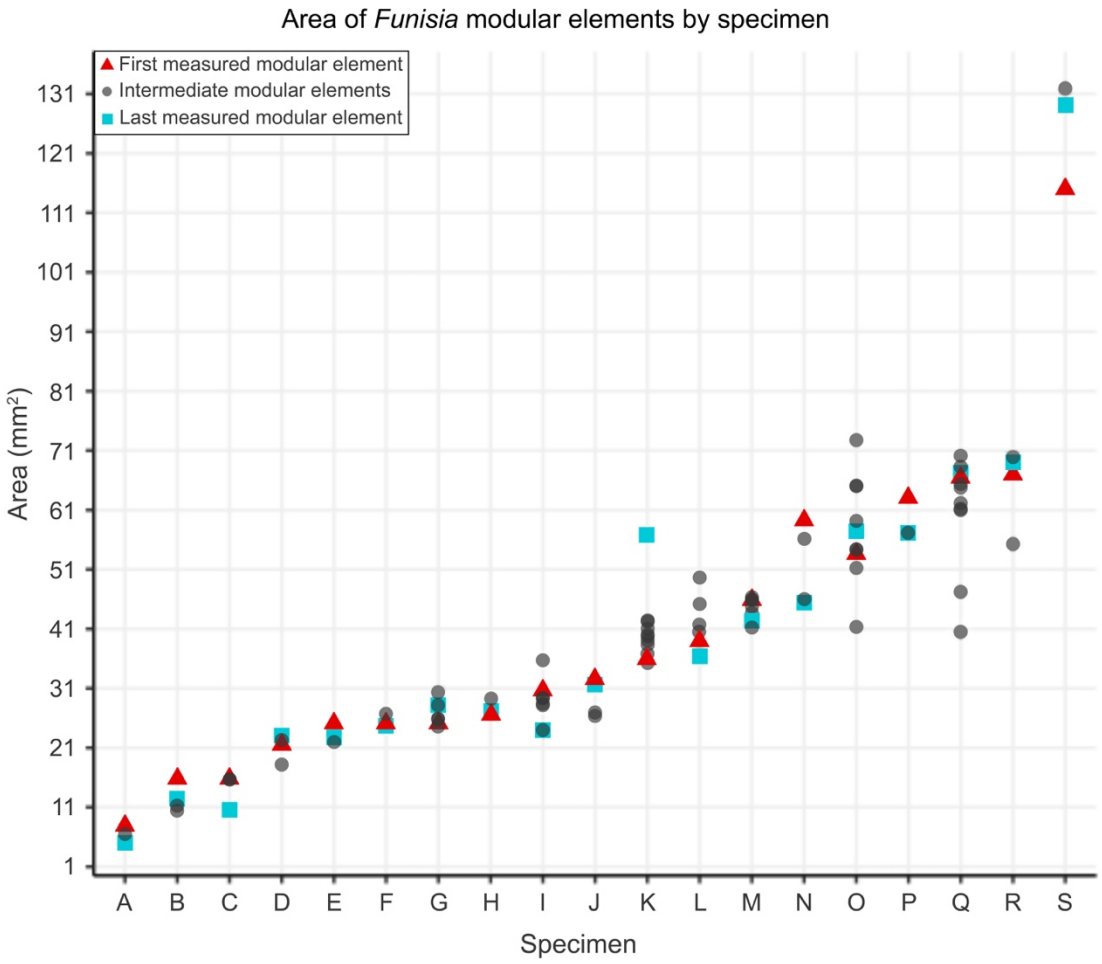

Figure 21. Area of individual modular elements by *Funisia dorothea* specimen. Modular elements located in the middle of a specimen (i.e., intermediate modular elements) are represented by gray circles; circles that are darker gray represent overlapping area values of two or more modular elements. See Appendix C Figure 29 for the relative placement of intermediate modular elements in each specimen.

Discussion

Variation in the widths of *Funisia dorothea* included in this study demonstrates that there is a wide range of size classes within the dataset (Figures 20-22), providing the opportunity to analyze how the dimensions of *Funisia* modular elements changed with

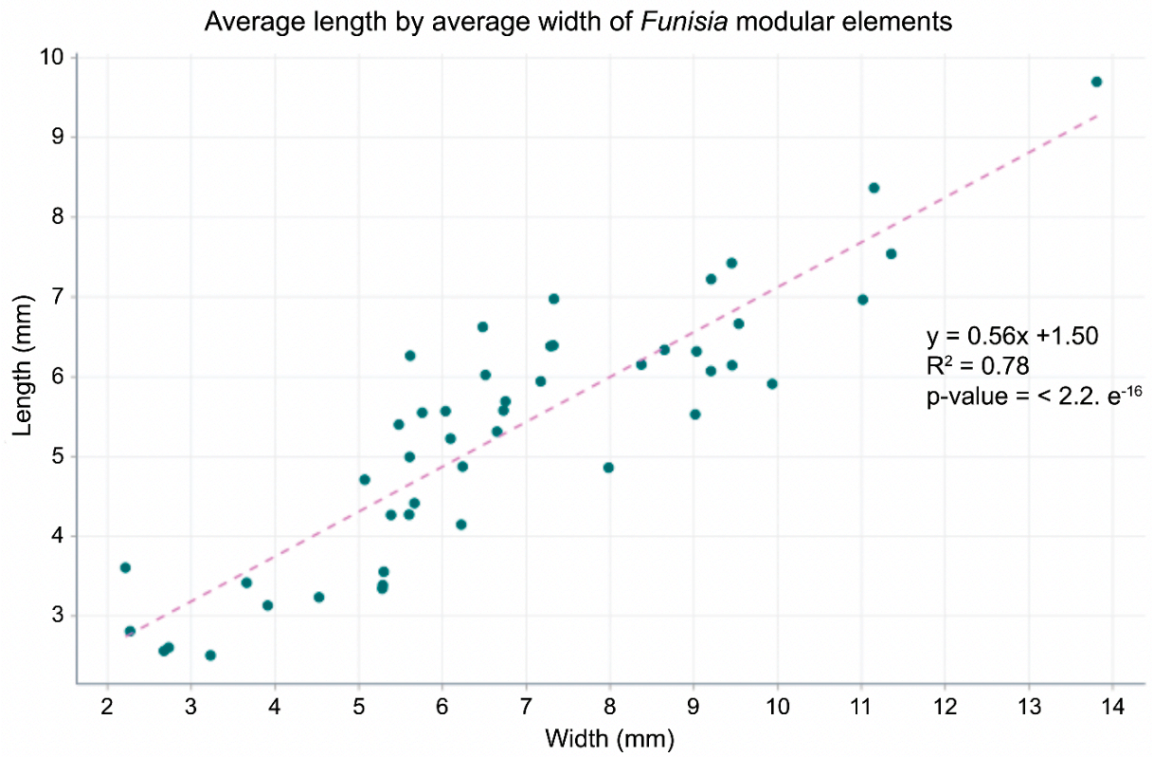

Figure 22. Average length by average width of modular elements in *Funisia dorothea.*

size and allowing for the development of a novel growth model for this highly abundant tubular taxon. It is important to first note that the observed differences in size are not necessarily related to age of the organism, as there is no constraint on whether paleoenvironmental factors such as available ecospace, organic mat type and maturity, or nutrient availability may have limited or encouraged growth of Ediacara taxa (Droser et al., 2022). Regardless of the reason for growth (i.e., age or resource availability), the nature of size change should be consistent across *Funisia* specimens, allowing for the testing of hypotheses on the relative contributions of inflational and insertional growth.

Inflational growth

Results from this study demonstrate that inflation of modular elements (i.e., expansion into three-dimensional space) played an important role in the growth of *Funisia* (Figures 21, 22). The wide range of modular element widths and lengths (W = 2.2—13.8 mm, L = 3.6—9.7 mm) as well as areas (Figures 21, 22) demonstrates that growth of *Funisia* did not proceed solely through the insertion of modular elements that had a consistent size from the time of initial establishment. The inflational growth of *Funisia* is additionally consistent with the morphology of their holdfasts (Figure 23). When found in isolation, *Funisia* holdfasts are circular, but they are more commonly preserved as closely packed, sub-circular structures exhibiting symmetrical flattening of shared edges, often appearing to have a honeycomb-like pattern. Not only is the symmetrical flattening of shared edges consistent with synchronous growth in *Funisia* clusters, but it also indicates that *Funisia* expanded into the horizontal plane throughout growth.

Further, the linear relationship observed between average length and width of *Funisia* modular elements demonstrates that the inflation of modular elements was consistently regulated throughout growth so that width increased more quickly than length (Figure 22). The maintenance of a consistent width to length ratio, with a greater width than length, of modular elements would have allowed *Funisia* to maintain an overall cylindrical and elongate morphology while ensuring the stability of the organism's hydrostatic skeleton as it extended up into water column.

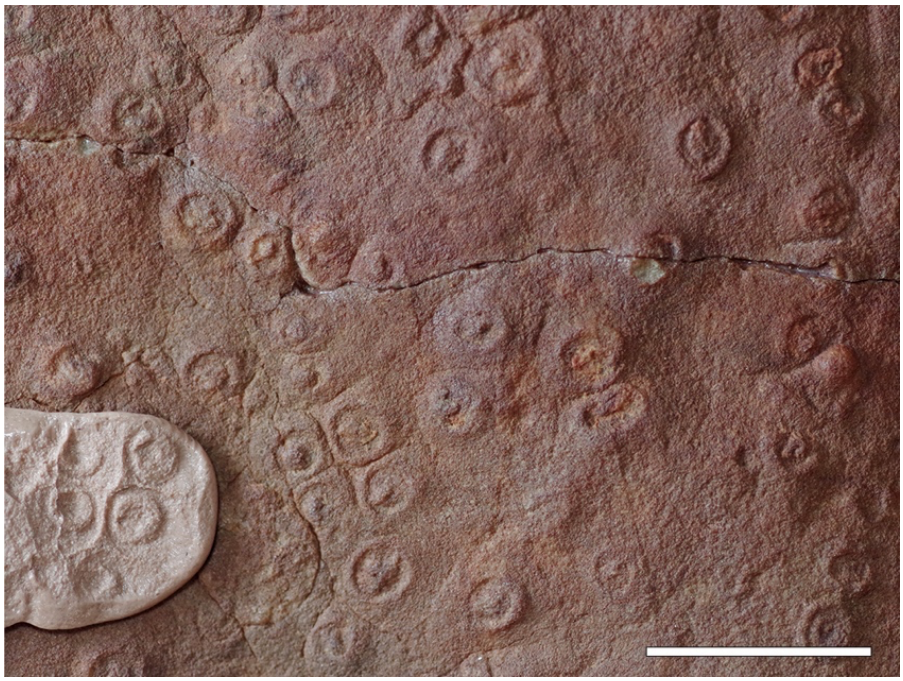

Figure 23. Cluster of *Funisia dorothea* holdfasts from the former Ediacara Conservation Park preserved on the base of a bedding plane and a putty mold of the holdfasts demonstrating what they would have looked like on the Ediacaran seafloor (bottom left) (SAM P55236). Note that isolated holdfasts are circular, while the shared edges of closely packed holdfasts are symmetrically flattened. Scale bar = 2 cm.

Insertional growth

The insertion of modular elements in modular Ediacaran organisms (e.g., *Dickinsonia, Charnia, Wutubus*) has been well-documented and appears to be a required mechanism for growth in relatively simple, nonbiomineral, and modular organisms, even in the absence of clear phylogenetic similarity (Braiser et al., 2012; Chen et al., 2014; Evans et al., 2017; Dunn et al., 2021). Thus, even without direct evidence for insertional growth in *Funisia*, it is likely that it occurred. While few complete *Funisia* specimens are known, the longest incomplete specimen reaches a length of ~20 cm (Figure 24).

When considering the fact that the width of *Funisia* modular elements is demonstrated to increase more quickly than length, it is likely that modular element insertion occurred in addition to inflation to reach the considerable length of some specimens.

Figure 24. The longest known *Funisia dorothea*, note transition from preservation in positive hyporelief (left) to negative hyporelief (right) corresponding to the loss of preserved modular element preservation (specimen located on bed LV-FUN at NNHS). Scale bar = 5 mm.

However, the rarity of complete *Funisia* prevents direct testing of whether insertion of modular elements occurred, because the total number of modular elements in large and small individuals is unknown. With that being said, one of the smallest known *Funisia* individuals is identified as a highly probable complete specimen, with clear apical and abapical ends (Figure 20a). Unfortunately, this small individual does not preserve well-defined modular elements along its entire length, again precluding direct assessment of the total number of modular elements. The complete preservation of this specimen, however, allows for the estimation of the total number of modular elements it possessed

by dividing the total length of the fossil by the average length of the well-preserved modular elements. This is a viable method for estimating the total number of modular elements in an individual only if modular elements are found to be similar in size along the length of individual *Funisia*.

Figure 21 supports the reconstruction of modular elements in individual *Funisia* as having a consistent size because most modular elements in individual *Funisia* have similar area values. While the relative placement of each modular element along the length of an individual cannot be used to designate apical- or abapical-most modular elements, if consistent tapering in size of modular elements was present along the length of *Funisia* it should still be evident (i.e., the first and last measured modular elements should have the highest or lowest area values). As discussed above, the modular elements that have notably larger or smaller areas than the other modular elements within an individual are randomly distributed along the length of the individual and the first and last measured modular elements are not consistently larger or smaller in area than other modular elements (Figure 21, Appendix C Figure 29). This provides no evidence for consistent size variation in modular elements along the length of individual *Funisia*.

Given the lack of a relationship between the size of modular elements and their relative placement along the length of an individual, the observed range of modular element areas within individuals is more consistent with small-scale size changes related to soft-bodied deformation during collapse. This is further supported by the fact that only specimens in

the intermediate to large size classes exhibit a wide range of modular element area values. Larger individuals would have necessarily had a higher amount of fluid in their hydrostatic skeleton and were thus likely more prone to deformation as a result of fluid loss and collapse. As such, the observed variability in modular element area is here interpreted as a result of taphonomic overprint, and the size of modular elements is considered to be consistent along the length of individual *Funisia*. Thus, the total number of modular elements in the small, complete individual—hereafter referred to as Specimen A— can be estimated by dividing the total preserved length of the specimen by the average length of its preserved modular elements.

Specimen A has a total length of 34.55 mm and preserves four modular elements with an average length of 2.81 mm per modular element (Table 4). When these average length values are used to estimate the total number of modular elements in each specimen, including the portion of the organism with no well-preserved modular elements, the small specimen is estimated to have had a total of 12 modular elements (Table 4).

To address whether there is evidence for insertional growth in *Funisia*, the estimated total number of modular elements in Specimen A can be compared to the longest known *Funisia* fossil, hereafter referred to as Specimen B. The longest specimen is used because all larger specimens within the dataset are not complete individuals, so the closest estimate to the maximum number of modular elements present in *Funisia* is from the longest known specimen.

Specimen	Number of modular elements preserved	Average modular element length	Total length	Estimated total number of modular elements
A	4	2.81	34.55	12
B	10	6.43	202.86	32

Table 4. Number of modular elements preserved, average modular element length, and total specimen length data used to estimate the total number of modular elements in the smallest and the longest known *Funisia dorothea* specimens, labelled Specimen A and Specimen B, respectively, units = mm.

Specimen B is incomplete, with no clear evidence of an apical or abapical end, and a little less than half of its total length preserves modular elements, after which the preservational mode changes and modular elements are no longer preserved (Figure 24). However, the portion of the tube with clear modular elements preserves a total of 10 complete modular elements, only two fewer than what is estimated for the total number of modular elements in Specimen A. Given that the portion of Specimen B that does not preserve modular elements makes up ~13 cm of the specimen's total length, Specimen B had to have greater than 12 modular elements. This provides clear evidence for insertional growth in *Funisia*.

The extent to which insertional growth contributed to the overall height of *Funisia* cannot be directly addressed, but estimation of the total number of modular elements likely to have been present in Specimen B can provide an underestimate for the number of modular elements added through insertional growth when compared with Specimen A.

The total number of modular elements present across the preserved length of Specimen B is estimated using the same formula as was used for Specimen A; the resultant estimate represents an underestimate because Specimen B is not complete, so it was likely comprised of more modular elements. Specimen B preserves 10 modular elements with an average length of 6.43 mm per modular element and a total preserved length of 202.86 mm (Table 4). Based on these values, Specimen B is estimated to have had 32 modular elements along its preserved length (Table 4). This is ~2.7 times the number of modular elements estimated to be present in Specimen A, suggesting that insertional growth contributed greatly to the height of the organism.

The generative zone of inserted modular elements, however, remains untestable due to a lack of specimens with clearly preserved apical and abapical ends. While the possibility of modular elements being added via the splitting of large modular elements in the middle of the tube can be disregarded due to a lack of fossil evidence showing partially split and variably sized modular elements, both an apical and abapical generative zone for *Funisia* modular elements remain as possibilities. Furthermore, results presented here cannot be used to directly test for determinate (i.e., growing to a set number of modular elements) or indeterminate (i.e., continual addition of modular elements) growth in *Funisia* due to the lack of complete specimens. However, the linear regression model for *Funisia* modular elements does not plateau (Figure 22), indicating that there was not a maximum length to width ratio for *Funisia* modular elements. This is consistent with, but not direct proof of, indeterminate growth in *Funisia*.

Growth model

To establish a holistic model for the growth of *Funisia*, the interplay of insertional and inflational growth processes must be considered. As demonstrated in Figure 21, *Funisia* modular elements were the same size along the length of the organism, but a suite of other fossil evidence suggests that *Funisia* did grow, in part, via insertion of new modular elements (Figures 20a, 24, Table 4). The timing and nature of insertional growth in *Funisia*, however, remains unclear, but the fact that tapering of modular elements along the length *Funisia* is not observed indicates that newly inserted modular elements inflated at a different rate than pre-existing modular elements. If all modular elements had a similar rate of inflation, they should be preserved as smaller modular elements followed by progressively larger modular elements, resulting in a tapered morphology towards the generative zone. This is not observed in *Funisia*. Therefore, inflation of newly inserted modular elements and pre-existing modular elements had to occur at different rates to maintain a broadly cylindrical form.

This growth process is here proposed to proceed via the initial insertion of a new modular element, either apically or abapically, that then inflated at a higher rate relative to the rest of the tube until it reached the same size as the pre-existing modular elements, after which inflational growth rates equalized with pre-existing modular elements to maintain the same size along the length of the organism.

This would require a newly inserted modular element to briefly experience an elevated rate of inflational growth relative to the pre-existing modular elements and suggests that growth processes in *Funisia* were highly regulated to maintain a broadly cylindrical form.

The timing of 'inflation rate equalization' (i.e., when new modular elements started to grow at the same rate as pre-existing modular elements) relative to when new modular elements were inserted is unclear. For example, did a newly inserted modular element have to reach a size similar to the pre-existing modular elements and equalize its inflation rate prior to initiation of insertion of another modular element, or was the process more continuous? However, the timing between new modular element insertion and 'inflation rate equalization' with pre-existing modular elements had to be great enough to prevent tapering of the organism. If these newly inserted modular elements inflated at a high rate, the probability of the preservation of these smaller, newly added modular elements would likely be low, because the majority of *Funisia* specimens are incompletely preserved. Regardless, the presence of similarly sized modular elements along the length of *Funisia* and its cylindrical morphology indicates that the inflation rates of their modular elements were variable relative to the timing of their insertion.

Based on evidence presented above, a new growth model for *Funisia* is proposed. This growth model is based on this study as well as on pre-existing understanding of *Funisia* reproduction, which holds that their occurrence in densely packed populations of similarly sized individuals is evidence for *Funisia* reproducing sexually via the

fertilization of eggs in the water column followed by settlement of these embryos on the organic mat (Droser and Gehling, 2008). The following subsections outline a three-stage growth model, beginning after fertilization, for *Funisia.*

Stage 1: Establishment of embryos

Fossil evidence for the first stage of growth in *Funisia*, representing early stages of development after the initial settlement of embryos, is non-existent, likely due to the inability to differentiate this growth stage from organic mat textures. However, the presence of closely packed *Funisia* holdfasts with symmetrically flattened shared edges (Figure 23), along with several other lines of evidence supporting inflational growth in *Funisia* (e.g., Figures 21, 22)*,* indicates that the size of *Funisia* at the time of settlement was smaller in all dimensions than in later growth stages. This precludes settlement of embryos with a wide circumference that only increased in height with growth and informs the reconstruction of newly settled *Funisia* as small spheres (Figure 25a).

Stage 2: Rapid insertion of modular elements

The second proposed stage of growth for *Funisia* is characterized by rapid insertion of modular elements with little to no inflational growth. The smallest known *Funisia* are relatively long and are comprised of many modular elements but remain very narrow (average W = 2.27 mm, ~ 11.13 mm smaller in width than the largest known *Funisia*) (Figure 20a, c). Larger specimens have both a higher number of modular elements and they are considerably larger than those in small individuals (Figure 25d, e, Table 4). This

indicates that early on in *Funisia's* growth, they likely had a phase wherein insertional growth was more prominent than inflational growth, with minimal to no inflation (Figure 25b, d). This is consistent with models of *Funisia* as a suspension feeder (Droser and Gehling, 2008), because the rapid addition of modular elements early in life would have elevated the organism above the mat-water interface to access more nutrients.

Stage 3: Combined insertional and inflational growth

The third and final growth stage likely occurred for the majority of *Funisia's* life. In this stage, *Funisia* grew via a consistent rate of inflational growth in pre-existing modular elements (Figure 22) and the periodic insertion of new modular elements with temporarily higher rates of inflation (Figure 25c, e). Once the size of the newly inserted modular element reached that of pre-existing modular elements, the inflation rate of the newly inserted modular element equalized to that of pre-existing modular elements to maintain a cylindrical, non-tapered form. In this stage, inflational growth contributed strongly to expansion of the organism into the horizontal plane, with minor contributions to expansion into the vertical plane, whereas insertional growth contributed most prominently to the height of the organism.

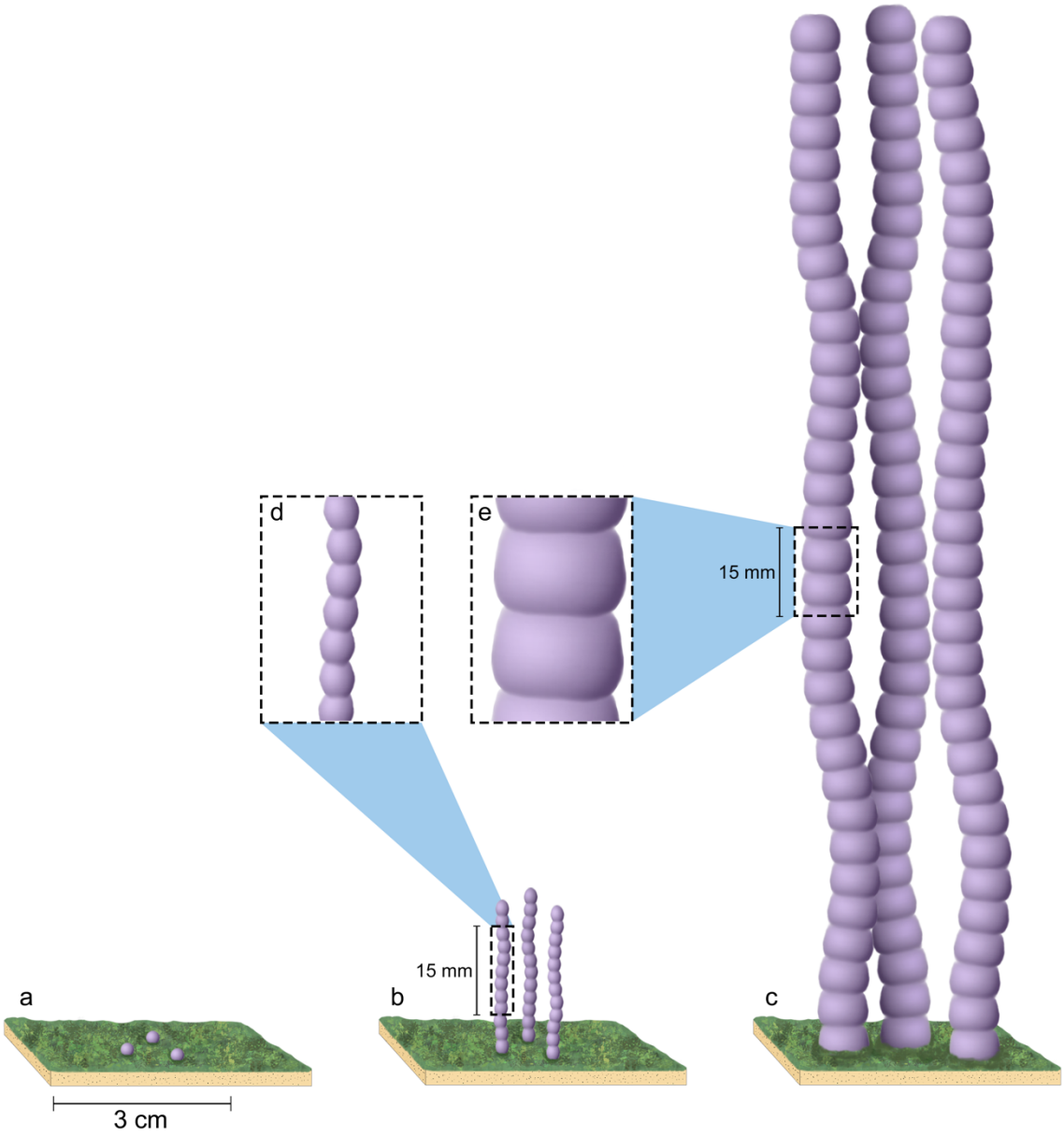

Figure 25. Schematic illustration of the proposed three-stage growth model for *Funisia dorothea.* (a) Establishment of spheroid embryos on the organic mat. (b) The early growth phase of *Funisia* wherein modular elements were rapidly inserted with little to no inflation of modular elements. (c) The later growth stage in which *Funisia* grew via combined insertional and inflational growth. (d) A 15 mm length of a *Funisia* individual in the early growth stage magnified to show detail. (e) A 15 mm length of a *Funisia* individual in the later growth stage magnified to show detail. Note that the *Funisia* in the later growth stage has increased substantially in width and in height of modular elements.

Comparative growth analysis

Funisia is one of two Ediacaran tubular organisms that are comprised of uniserially repeating modular elements, with the second being *Wutubus annularis* (Chen et al., 2014). The modular elements in both taxa are interpreted as hollow, fluid-filled structures (Droser and Gehling, 2008; Chen et al., 2014). While *Funisia* is endemic to the Ediacara Member of South Australia, *Wutubus* occurs more broadly, with specimens found in South China, North America, Ukraine, and South Australia (Chen et al., 2014; Smith et al., 2016; Gehling and Droser, 2018; Netrerovsky et al., 2018). In the Ediacara Member of South Australia, *Wutubus* is known only from a single specimen which, notably, occurs on the same fossiliferous slab as *Funisia* (Gehling and Droser, 2018).
Chen et al., (2014) suggested that the shared modular construction of *Wutubus* and *Funisia* may be a homologous trait. In the same study, an analysis of *Wutubus* growth processes was conducted on material from limestones of the Dengying Formation, South China (~541 Ma). While the identification of homologous traits in the fossil record is tenuous without phylogenetic information (Wright, 2015), the growth strategies and paleoecologies of the two taxa can be compared to assess overall similarity.

The growth model proposed for *Wutubus* has two stages: (1) initial insertional growth to a set number of modular elements and (2) isometric inflation of existing modular elements (Chen et al., 2014). Notably, both *Funisia* and *Wutubus* appear to have had an initial growth phase dominated by the insertion of modular elements that inflated at a later point. A key difference between *Wutubus* and *Funisia* is that *Wutubus* had a set

number of modular elements established in an early growth phase whereas *Funisia* likely did not have a set number of modular elements and is found to have inserted new modular elements throughout its life, not just in early growth stages. Further, the variability in the rate of inflation of modular elements in *Funisia* relative to the timing of modular element insertion demonstrated here is distinct from the consistent isometric growth of *Wutubus.* This distinction in growth processes of the two taxa results in an overall conical morphology in *Wutubus* and a cylindrical morphology in *Funisia.* Thus, when the growth strategies of these morphologically similar taxa are compared, they are clearly disparate and were regulated in different ways to maintain distinct gross morphologies.

The differences in the growth strategies of these two taxa is further bolstered by their holdfast morphologies. Both *Wutubus* and *Funisia* are preserved with associated holdfast structures, however, the morphology of these structures is distinct. In *Wutubus* this structure is described as a smooth conical termination that is narrower in width than the remaining tube and is hypothesized to be evidence of an embryonic test (Chen et al., 2014). In comparison, the holdfast of *Funisia* is a disk-shaped structure with a central circular divot (Figure 23). If these holdfast structures are indeed relics of embryonic tests, the two taxa had drastically different embryonic morphologies.

Further differences between *Funisia* and *Wutubus* are made evident when comparing their paleoecological strategies. *Wutubus* are reported to occur as multiple individuals of

different sizes on the same bedding plane (Chen et al., 2014). This is presented as a common occurrence in *Wutubus,* but in *Funisia* the occurrence of multiple different sized individuals on the same bedding plane is the exception, not the rule, and is only observed on one bed at NNHS where *Funisia* occur in clusters spread out across multiple square meters of bedding plane (Surprenant et al., 2020). In this case, *Funisia* within individual clusters are similar in size, but the size of *Funisia* between clusters is variable. Additionally, *Funisia* is found to occur in very densely packed populations that can cover multiple square meters of fossilized bedding plane (Surprenant et al., 2020). This contrasts starkly with *Wutubus,* which occur in more sparsely distributed populations (Chen et al., 2014). While these observed characteristics of *Wutubus* from the Dengying Formation could be telling an incomplete story due to the lack of meter-scale bedding plane preservation, the isolated occurrence of *Wutubus* in South Australia bolsters the hypothesis that they did not occur in densely packed aggregates similar to *Funisia.*

Given that the common occurrence of *Funisia* in populations of densely packed, similarly sized individuals is invoked as evidence for sexual reproduction via spatfall, these paleoecological differences could indicate distinct reproductive strategies in *Wutubus* and *Funisia*. Additionally, the differences in population structure of the two taxa demonstrates that they functioned differently within their paleoenvironments. For example, the dense packing of *Funisia* over multiple square meters of preserved seafloor has been demonstrated to preclude the establishment of other organisms, resulting in low diversity ecosystems (Surprenant et al., 2020). In comparison, *Wutubus* were more

sparsely distributed across the seafloor and are preserved in association with abundant trace fossils (Chen et al., 2014). Therefore, the two organisms clearly had drastically different impacts on the ecosystems in which they lived.

The above comparison demonstrates that, despite similarities in their constructional morphologies, *Funisia* and *Wutubus* share few other traits and grew via distinct developmental processes. The differences in modular element insertion and inflation, in holdfast morphology, and in population structure between the two taxa strongly suggests that their shared gross morphology is related to convergence and not phylogenetic similarity. However, direct testing for homology between these two taxa is not possible in the absence of a phylogenetic framework, so this remains an outstanding question. At the very least, the disparity between the developmental processes and the paleoecologies of the two taxa is notable and highlights the fact that shared gross morphology does not beget developmental or paleoecological similarity in the Ediacaran tubular morphogroup. As such, broad interpretations of the ecosystem impact of the total tubular morphogroup, without consideration of variability in the paleoecological strategies of individual tubular taxa, should be carried out with caution because, despite similar simple forms, certain tubular taxa functioned drastically differently within their paleoenvironments.

Conclusion

This study details the nature of modular element size change in the tubular organism *Funisia dorothea* to inform a new model for *Funisia* growth strategies. Description of the

relative contributions of inflational and insertional growth in *Funisia* contributes to understanding of the paleobiology of the most abundant organism in the Ediacara Member of South Australia and allows for comparison of its growth strategies with other modular tubular organisms. Results demonstrate that the growth of *Funisia* modular elements was variably regulated in different growth stages and relative to the timing of modular element insertion in order to maintain a similar size of all modular elements within individuals and a broadly cylindrical form. This demonstrates that, although *Funisia's* morphology is relatively simple, its growth was highly regulated. New insights into *Funisia* growth strategies and pre-existing understanding of its paleoecology are additionally compared to another modular tubular organism, *Wutubus annularis,* to assess similarity beyond constructional morphology. This comparative analysis reveals few other shared traits between the two taxa, highlighting the developmental and autecological disparity between members of the tubular morphogroup despite their shared morphologies.

CONCLUDING REMARKS AND FUTURE WORK

The Ediacara biota represent some of the most critical fossils for developing understanding of the origins of animal life because they preserve the first evidence for macroscopic, complex, community forming organisms—including animals. The tubular morphogroup is a subset of the Ediacara biota that includes all metazoan-grade Ediacara taxa with a hollow and elongate body plan and is of great interest to Ediacaran paleontologists because it is globally distributed, highly abundant, includes taxa that are aligned with metazoan phyla, and occurs commonly in the terminal Ediacaran despite the extinction of other Ediacaran morphogroups. These characteristics of the tubular morphogroup suggest that their fossil record has unique potential to provide insight into the paleobiological traits and paleoecological strategies that were advantageous to early animal life.

However, while these taxa do share a tubular form, they are not necessarily phylogenetically linked, and though paleobiological and paleoecological similarity between tubular genera is often assumed, there is no concrete evidence to support the hypothesis that their shared morphology begets further similarity. Additionally, there is no comprehensive understanding of the number of genera that comprise the tubular morphogroup or their temporal distributions. As such, the morphogroup holds little intrinsic meaning, and the fossil record of the tubular morphogroup cannot be leveraged for understanding the paleobiological drivers of their abundance, their paleoenvironmental impacts, or their macroevolutionary significance. The chapters

presented above provide a baseline understanding of what taxa comprise the morphogroup, what characters they possessed beyond a hollow and elongate morphology, their temporal distribution, and provides a framework for future investigation of tubular taxa that establishes methodologies for further elucidating their paleobiological traits and paleoecological strategies. This is achieved through generation and analysis of a database including occurrence and morphological data on all Ediacaran non-biomineral tubular taxa and through specimen-based analyses of individual tubular genera from taphonomic and developmental perspectives.

Synthesis of the global record of the tubular morphogroup further bolsters the group's significance within the Ediacaran by demonstrating that they are the most diverse Ediacaran morphogroup, were highly diverse for ~20 million years longer than was previously appreciated, and maintained this high diversity across the White Sea-Nama extinction while most other Ediacaran morphogroups did not. This provides the first concrete evidence of a tubular form being more common and more adaptable to ecosystem changes than other Ediacaran organisms, demonstrating that hypotheses pertaining to the nature of success of a tubular form and their impacts on Ediacaran ecosystems are worthwhile to pursue.

A secondary outcome of synthesizing the global Ediacaran tubular record, however, was the recognition of the fact that current understanding of the genera that comprise the tubular morphogroup is insufficient to address such questions. For example, the

morphogroup is found to encompass two distinct constructional morphologies: (1) a fluid-filled tubular morphology wherein the entire organism is comprised of a single integument that is supported by a hydrostatic skeleton and has a closed aperture, and (2) a tubicolous morphology wherein an organism excretes an external tube that it lives within, and that tube has an open aperture. The second constructional morphology is fundamentally more complex than the first, and organisms that had a tubicolous form likely had distinct paleobiological traits and paleoecological strategies. The inclusion of these two drastically different body plans without differentiation within the total tubular morphogroup obfuscates the relative importance of the two different forms within Ediacaran ecosystems and precludes effective use of their fossil record for testing macroevolutionary questions. To accurately subdivide tubular organisms into tubicolous and tubiform constructional morphologies, however, identification of a closed or open aperture in individual genera is essential. Unfortunately, this research demonstrates that this morphological information is not known for the majority of Ediacaran tubular organisms. Further, the question of whether shared constructional morphologies can be reliable indicators of shared paleobiological traits and paleoecological strategies is outstanding.

To this end, the second and third chapters of this dissertation take a specimen-based approach to develop an understanding of individual tubular genera that is adequate for informing comparative analyses of the paleobiological traits and paleoecological strategies possessed by tubular taxa and for addressing broader questions on the role of

the tubular morphogroup in Ediacaran ecosystems. Study of the taphonomy of the tubular organism *Aulozoon soliorum* demonstrates that detailed characterization of the modes of preservation and integument deformation in tubular genera with few diagnostic morphological features can provide essential insight into the morphology, life habit, and biomaterials of these organisms. Similar taphonomic investigations of all other tubular taxa are thus recommended because they would establish a baseline understanding of how these characteristics vary across taxa within the tubular morphogroup and would aid in developing classification schemes for the tubular morphogroup that would hold more intrinsic meaning.

Study of the growth of the tubular organism *Funisia dorothea*, which is characterized by uniserially arranged modular elements, demonstrates that its growth was highly regulated to maintain a cylindrical morphology. However, comparison of *Funisia's* growth strategies with another tubular organism comprised of modular elements, *Wutubus annularis*, demonstrates that they share few other characteristics despite a similar modular form. The two taxa both possessed regulated growth processes, but addition of new modular elements and growth of those modular elements is demonstrated to have been disparate between the two taxa. Further, comparison of their paleoecologies demonstrates that, beyond developmental differences, the two taxa functioned drastically differently within their environments.

This research establishes growth analysis as a viable methodology for discerning similarity between tubular genera that invokes more than gross morphological features and demonstrates that, even with a shared modular morphology, tubular taxa can be paleobiologically and paleoecologically distinct.

Ultimately, the research presented in this dissertation provides a clear picture of the tubular morphogroup as a group of organisms that were certainly dominant members of Ediacaran ecosystems but that do not represent a monolith of lifeforms with universal paleobiological traits or ecosystem functions. The investigative frameworks presented in chapters two and three provide novel insight into two of the most Ediacaran abundant tubular organisms and provide solutions for better describing, and differentiating between, the genera that comprise the tubular morphogroup. Future work to develop similar taphonomically and developmentally informed reconstructions of all known tubular genera that address fundamental traits such as aperture morphology and nature of growth is required to develop a holistic picture of the tubular morphogroup and to enable testing of hypotheses on their role in Ediacaran ecosystems.

REFERENCES

Babcock, L.E., Grunow, A.M., Sadowski, G.R., Leslie, S.A., 2005. *Corumbella*, an Ediacaran-grade organism from the Late Neoproterozoic of Brazil. Palaeogeography, Palaeoclimatology, Palaeoecology 220, 7–18. https://doi.org/10.1016/j.palaeo.2003.01.001

Bamforth, E.L., Narbonne, G.M., 2009. New Ediacaran rangeomorphs from Mistaken Point, Newfoundland, Canada. Journal of Paleontology 83, 897–913. https://doi.org/10.1666/09-047.1

Barnes, R.S., Olive, P.J., Calow, P.P., Golding, D.W., Spicer, J., 2009. Excretion, ionic and osmotic regulations, and buoyancy. In: The Invertebrates: A Synthesis. John Wiley and Sons, New Jersey, pp. 289–300.

Bobrovskiy, I., Nagovitsyn, A., Hope, J.M., Luzhnaya, E., Brocks, J.J., 2022. Guts, gut contents, and feeding strategies of Ediacaran animals. Current Biology 32, 5382-5389.e3. https://doi.org/10.1016/j.cub.2022.10.051

Bobrovskiy, I., Hope, J.M., Ivantsov, A., Nettersheim, B.J., Hallmann, C., Brocks, J.J., 2018. Ancient steroids establish the Ediacaran fossil *Dickinsonia* as one of the earliest animals. Science 361, 1246–1249. https://doi.org/10.1126/science.aat7228

Boddy, C.E., Mitchell, E.G., Merdith, A., Liu, A.G., 2022. Palaeolatitudinal distribution of the Ediacaran macrobiota. Journal of the Geological Society 179, jgs2021-030. https://doi.org/10.1144/jgs2021-030

Bowyer, F.T., Uahengo, C.-I., Kaputuaza, K., Ndeunyema, J., Yilales, M., Alexander, R.D., Curtis, A., Wood, R.A., 2023. Constraining the onset and environmental setting of metazoan biomineralization: The Ediacaran Nama Group of the Tsaus Mountains, Namibia. Earth and Planetary Science Letters 620, 118336. https://doi.org/10.1016/j.epsl.2023.118336

Brasier, M.D., Antcliffe, J.B., Liu, A.G., 2012. The architecture of Ediacaran Fronds. Palaeontology 55, 1105–1124. https://doi.org/10.1111/j.1475-4983.2012.01164.x

Budd, G.E., Jackson, I.S.C., 2016. Ecological innovations in the Cambrian and the origins of the crown group phyla. Philosophical Transactions of the Royal Society B: Biological Sciences 371, 20150287. https://doi.org/10.1098/rstb.2015.0287

Cai, Y., Schiffbauer, J.D., Hua, H., Xiao, S., 2012. Preservational modes in the Ediacaran Gaojiashan Lagerstätte: Pyritization, aluminosilicification, and carbonaceous compression. Palaeogeography, Palaeoclimatology, Palaeoecology 326–328, 109–117. https://doi.org/10.1016/j.palaeo.2012.02.009

Chen, Z., Zhou, C., Xiao, S., Wang, W., Guan, C., Hua, H., Yuan, X., 2014. New Ediacara fossils preserved in marine limestone and their ecological implications. Scientific Reports 4, 4180. https://doi.org/10.1038/srep04180

Cuadrado, D.G., Carmona, N.B., Bournod, C., 2011. Biostabilization of sediments by microbial mats in a temperate siliciclastic tidal flat, Bahia Blanca estuary (Argentina). Sedimentary Geology 237, 95–101. https://doi.org/10.1016/j.sedgeo.2011.02.008

Darroch, S.A.F., Smith, E.F., Laflamme, M., Erwin, D.H., 2018. Ediacaran extinction and Cambrian explosion. Trends in Ecology & Evolution 33, 653–663. https://doi.org/10.1016/j.tree.2018.06.003

Droser, M.L., Gehling, J.G., 2015. The advent of animals: The view from the Ediacaran. Proceedings of the National Academy of Sciences 112, 4865–4870. https://doi.org/10.1073/pnas.1403669112

Droser, M.L., Gehling, J.G., 2008. Synchronous aggregate growth in an abundant new Ediacaran tubular organism. Science 319, 1660–1662. https://doi.org/10.1126/science.1152595

Droser, M.L., Evans, S.D., Tarhan, L.G., Surprenant, R.L., Hughes, I.V., Hughes, E.B., Gehling, J.G., 2022. What happens between depositional events, stays between depositional events: The significance of organic mat surfaces in the capture of Ediacara communities and the sedimentary rocks that preserve them. Frontiers in Earth Science 10, 826353. https://doi.org/10.3389/feart.2022.826353

Droser, M.L., Gehling, J.G., Tarhan, L.G., Evans, S.D., Hall, C.M.S., Hughes, I.V., Hughes, E.B., Dzaugis, M.E., Dzaugis, M.P., Dzaugis, P.W., Rice, D., 2019. Piecing together the puzzle of the Ediacara Biota: Excavation and reconstruction at the Ediacara National Heritage site Nilpena (South Australia). Palaeogeography, Palaeoclimatology, Palaeoecology 513, 132–145. https://doi.org/10.1016/j.palaeo.2017.09.007

Droser, M.L., Gehling, J.G., Jensen, S.R., 2006. Assemblage palaeoecology of the Ediacara biota: The unabridged edition? Palaeogeography, Palaeoclimatology, Palaeoecology 232, 131–147. https://doi.org/10.1016/j.palaeo.2005.12.015

Dunn, F.S., Kenchington, C.G., Parry, L.A., Clark, J.W., Kendall, R.S., Wilby, P.R., 2022. A crown-group cnidarian from the Ediacaran of Charnwood Forest, UK. Nature Ecology and Evolution 6, 1095–1104. https://doi.org/10.1038/s41559-022-01807-x

Dunn, F.S., Liu, A.G., Grazhdankin, D.V., Vixseboxse, P., Flannery-Sutherland, J., Green, E., Harris, S., Wilby, P.R., Donoghue, P.C.J., 2021. The developmental biology of *Charnia* and the eumetazoan affinity of the Ediacaran rangeomorphs. Sci. Adv. 7, eabe0291. https://doi.org/10.1126/sciadv.abe0291

Dunn, F.S., Liu, A.G., Donoghue, P.C.J., 2018. Ediacaran developmental biology. Biological Reviews 93, 914–932. https://doi.org/10.1111/brv.12379

Elliott, D.A., Trusler, P.W., Narbonne, G.M., Vickers-Rich, P., Morton, N., Hall, M., Hoffmann, K.H., Schneider, G.I.C., 2016. *Ernietta* from the late Ediacaran Nama Group, Namibia. Journal of Paleontology. 90, 1017–1026. https://doi.org/10.1017/jpa.2016.94

Erwin, D.H., Laflamme, M., Tweedt, S.M., Sperling, E.A., Pisani, D., Peterson, K.J., 2011. The Cambrian Conundrum: Early divergence and later ecological success in the early history of animals. Science 334, 1091–1097. https://doi.org/10.1126/science.1206375

Evans, S.D., Tu, C., Rizzo, A., Surprenant, R.L., Boan, P.C., McCandless, H., Marshall, N., Xiao, S., Droser, M.L., 2022. Environmental drivers of the first major animal extinction across the Ediacaran White Sea-Nama transition. Proceedings of the National Academy of Sciences 119, e2207475119. https://doi.org/10.1073/pnas.2207475119

Evans, S.D., Droser, M.L., Erwin, D.H., 2021. Developmental processes in Ediacara macrofossils. Proceedings of the Royal Society B: Biological Sciences 288, 20203055. https://doi.org/10.1098/rspb.2020.3055

Evans, S.D., Hughes, I.V., Gehling, J.G., Droser, M.L., 2020. Discovery of the oldest bilaterian from the Ediacaran of South Australia. Proceedings of the National Academy of Sciences 117, 7845–7850. https://doi.org/10.1073/pnas.2001045117

Evans, S.D., Droser, M.L., Gehling, J.G., 2017. Highly regulated growth and development of the Ediacara macrofossil *Dickinsonia costata*. PLoS ONE 12, e0176874. https://doi.org/10.1371/journal.pone.0176874

Evans, S.D., Droser, M.L., Gehling, J.G., 2015. *Dickinsonia* liftoff: Evidence of current derived morphologies. Palaeogeography, Palaeoclimatology, Palaeoecology 434, 28–33. https://doi.org/10.1016/j.palaeo.2015.02.006

Fedonkin, M.A., Runnegar, B.N., 1992. Proterozoic metazoan trace fossils. In Schopf, J.W., Klein, C. (Eds.), The Proterozoic Biosphere: A Multidisciplinary Study. Cambridge University Press, Cambridge, pp. 389–395.

Gehling, J.G., 2000. Environmental interpretation and a sequence stratigraphic framework for the terminal Proterozoic Ediacara Member within the Rawnsley Quartzite, South Australia. Precambrian Research 100, 65–95. https://doi.org/10.1016/S0301-9268(99)00069-8

Gehling, J.G., 1999. Microbial mats in terminal Proterozoic siliciclastics: Ediacaran death masks. PALAIOS 14, 40. https://doi.org/10.2307/3515360

Gehling, J.G., 1991. The case for Ediacaran fossil roots to the metazoan tree. Geological Society of India Memoir 20, pp. 181–224.

Gehling, J.G., Droser, M.L., 2018. Ediacaran scavenging as a prelude to predation. Emerging Topics in Life Sciences 2, 213–222. https://doi.org/10.1042/ETLS20170166

Gehling, J.G., Droser, M.L., 2013. How well do fossil assemblages of the Ediacara Biota tell time? Geology 41, 447–450. https://doi.org/10.1130/G33881.1

Gehling, J.G., Droser, M.L., 2009. Textured organic surfaces associated with the Ediacara Biota in South Australia. Earth-Science Reviews 96, 196–206. https://doi.org/10.1016/j.earscirev.2009.03.002

Gehling, J.G., Runnegar, B., 2022. *Phyllozoon* and *Aulozoon*: Key components of a novel Ediacaran death assemblage in Bathtub Gorge, Heysen Range, South Australia. Geological Magazine 159, 1134–1147. https://doi.org/10.1017/S0016756821000509

Gehling, J.G., Runnegar, B.N., Droser, M.L., 2014. Scratch traces of large Ediacara bilaterian animals. Journal of Paleontology 88, 284–298. https://doi.org/10.1666/13-054

Glaessner, M.F., 1969. Trace fossils from the Precambrian and basal Cambrian. Lethaia 2, 369–393. https://doi.org/10.1111/j.1502-3931.1969.tb01258.x

Gnilovskaya, M.B., 1996. New Saarinids from the Vendian of Russian Platform. In Doklady Akademii Nauk 348, pp. 89-93.

Golubkova, E.Yu., Kuzmenkova, O.F., Laptsevich, A.G., Kushim, E.A., Vaskaboinikava, T.V., Silivanov, M.O., 2022. Paleontological characteristics of the Upper Vendian–Lower Cambrian sediments in the section of the North Polotsk Borehole of the East European Platform, Belarus. Stratigraphy and Geological Correlation 30, 457–474. https://doi.org/10.1134/S0869593822060077

Grazhdankin, D., 2014. Patterns of evolution of the Ediacaran soft-bodied biota. Journal of Paleontology 88, 269–283. https://doi.org/10.1666/13-072

Hall, C.M.S., Droser, M.L., Gehling, J.G., Dzaugis, M.E., 2015. Paleoecology of the enigmatic *Tribrachidium*: New data from the Ediacaran of South Australia. Precambrian Research 269, 183–194. https://doi.org/10.1016/j.precamres.2015.08.009

Hancy, A.D., Antcliffe, J.B., 2020. Anoxia can increase the rate of decay for cnidarian tissue: Using *Actinia equina* to understand the early fossil record. Geobiology 18, 167–184. https://doi.org/10.1111/gbi.12370

Ivantsov, A.I., 2015. Makrofossilii Verkhnego Venda Vostochnoĭ Evropy. PIN RAN, Moskva.

Ivantsov, A.Yu., 2011. Feeding traces of proarticulata—the Vendian metazoa. Paleontological Journal 45, 237–248. https://doi.org/10.1134/S0031030111030063

Ivantsov, A.Yu., Vickers-Rich, P., Zakrevskaya, M.A., Hall, M., 2019. Conical thecae of Precambrian macroorganisms. Paleontological Journal 53, 1134–1146. https://doi.org/10.1134/S0031030119110054

Jenkins, R., 1995. The problems and potential of using animal fossils and trace fossils in terminal Proterozoic biostratigraphy. Precambrian Research 73, 51–69. https://doi.org/10.1016/0301-9268(94)00071-X

Jensen, S., Droser, M.L., Gehling, J.G., 2006. A critical look at the Ediacaran trace fossil record. In Xiao, S., Kaufman, A.J. (Eds.), Neoproterozoic Geobiology and Paleobiology, Topics in Geobiology. Springer Netherlands, Dordrecht, pp. 115–157. https://doi.org/10.1007/1-4020-5202-2_5

Joel, L.V., Droser, M.L., Gehling, J.G., 2014. A new enigmatic, tubular organism from the Ediacara Member, Rawnsley Quartzite, South Australia. Journal of Paleontology 88, 253–262. https://doi.org/10.1666/13-058

Kontorovich, A.E., Varlamov, A.I., Grazhdankin, D.V., Karlova, G.A., Klets, A.G., Kontorovich, V.A., Saraev, S.V., Terleev, A.A., Belyaev, S.Yu., Varaksina, I.V., Efimov, A.S., Kochnev, B.B., Nagovitsin, K.E., Postnikov, A.A., Filippov, Yu.F., 2008. A section of Vendian in the east of West Siberian Plate (based on data from the Borehole Vostok 3). Russian Geology and Geophysics 49, 932–939. https://doi.org/10.1016/j.rgg.2008.06.012

McIlroy, D., Green, O.R., Brasier, M.D., 2001. Palaeobiology and evolution of the earliest agglutinated Foraminifera: P*latysolenites, Spirosolenites* and related forms. Lethaia 34, 13–29. https://doi.org/10.1080/002411601300068170

Merdith, A.S., Williams, S.E., Collins, A.S., Tetley, M.G., Mulder, J.A., Blades, M.L., Young, A., Armistead, S.E., Cannon, J., Zahirovic, S., Müller, R.D., 2021. Extending

full-plate tectonic models into deep time: Linking the Neoproterozoic and the Phanerozoic. Earth-Science Reviews 214, 103477. https://doi.org/10.1016/j.earscirev.2020.103477

Meyer, M., Schiffbauer, J.D., Xiao, S., Cai, Y., Hua, H., 2012. Taphonomy of the upper Ediacaran enigmatic ribbonlike fossil *Shaanxilithes*. PALAIOS 27, 354–372. https://doi.org/10.2110/palo.2011.p11-098r

Moczydłowska, M., Westall, F., Foucher, F., 2014. Microstructure and biogeochemistry of the organically preserved Ediacaran metazoan *Sabellidites*. Journal of Paleontology 88, 224–239. https://doi.org/10.1666/13-003

Narbonne, G.M., 2005. The Ediacara Biota: Neoproterozoic origin of animals and their ecosystems. Annual Review of Earth and Planetary Sciences 33, 421–442. https://doi.org/10.1146/annurev.earth.33.092203.122519

Nesterovsky, V.A., Martyshyn, A.I., Chupryna, A.M., 2018. New biocenosis model of Vendian (Ediacaran) sedimentation basin of Podilia (Ukraine). Journal of Geology, Geography and Geoecology 27, 95–107. https://doi.org/10.15421/111835

Osés, G.L., Wood, R., Romero, G.R., Evangelista Martins Prado, G.M., Bidola, P., Herzen, J., Pfeiffer, F., Stampar, S.N., Alves Forancelli Pacheco, M.L., 2022. Ediacaran *Corumbella* has a cataphract calcareous skeleton with controlled biomineralization. iScience 25, 105676. https://doi.org/10.1016/j.isci.2022.105676

Park, T.-Y.S., Jung, J., Lee, M., Lee, S., Zhen, Y.Y., Hua, H., Warren, L.V., Hughes, N.C., 2021. Enduring evolutionary embellishment of cloudinids in the Cambrian. Royal Society Open Science 8, 210829. https://doi.org/10.1098/rsos.210829

Reid, L.M., Holmes, J.D., Payne, J.L., García-Bellido, D.C., Jago, J.B., 2020. Taxa, turnover and taphofacies: A preliminary analysis of facies-assemblage relationships in the Ediacara Member (Flinders Ranges, South Australia). Australian Journal of Earth Sciences 67, 905–914. https://doi.org/10.1080/08120099.2018.1488767

Retallack, G.J., 2013. Ediacaran life on land. Nature 493, 89–92. https://doi.org/10.1038/nature11777

Retallack, G.J., 2007. Growth, decay and burial compaction of *Dickinsonia*, an iconic Ediacaran fossil. Alcheringa: An Australasian Journal of Palaeontology 31, 215–240. https://doi.org/10.1080/03115510701484705

Runnegar, B., 1994. Proterozoic eukaryotes: Evidence from biology and geology. In Bengston, S. (Ed.), Early Life on Earth. Nobel Symposium 84. Columbia University Press, New York, pp 287–297.

Runnegar, B., 2022. Following the logic behind biological interpretations of the Ediacaran biotas. Geological Magazine 159, 1093–1117. https://doi.org/10.1017/S0016756821000443

Sappenfield, A., Droser, M.L., Gehling, J.G., 2011. Problematica, trace fossils, and tubes within the Ediacara Member (South Australia): Eedefining the Ediacaran trace fossil record one tube at a time. Journal of Paleontology 85, 256–265. https://doi.org/10.1666/10-068.1

Schiffbauer, J.D., Selly, T., Jacquet, S.M., Merz, R.A., Nelson, L.L., Strange, M.A., Cai, Y., Smith, E.F., 2020. Discovery of bilaterian-type through-guts in cloudinomorphs from the terminal Ediacaran Period. Nature Communications 11, 205. https://doi.org/10.1038/s41467-019-13882-z

Schiffbauer, J.D., Huntley, J.W., O'Neil, G.R., Darroch, S.A.F., Laflamme, M., Cai, Y., 2016. The latest Ediacaran wormworld fauna: Setting the ecological stage for the Cambrian explosion. GSA Today 26, 11. https://doi.org/10.1130/GSATG265A.1

Seilacher, A., 2007. Trace fossil analysis. Springer, Berlin.

Seilacher, A., Grazhdankin, D., Legouta, A., 2003. Ediacaran biota: The dawn of animal life in the shadow of giant protists. Paleontological Research 7, 43–54. https://doi.org/10.2517/prpsj.7.43

Selly, T., Schiffbauer, J.D., Jacquet, S.M., Smith, E.F., Nelson, L.L., Andreasen, B.D., Huntley, J.W., Strange, M.A., O'Neil, G.R., Thater, C.A., Bykova, N., Steiner, M., Yang, B., Cai, Y., 2020. A new cloudinid fossil assemblage from the terminal Ediacaran of Nevada, USA. Journal of Systematic Palaeontology 18, 357–379. https://doi.org/10.1080/14772019.2019.1623333

Shore, A., Wood, R., 2021. Environmental and diagenetic controls on the morphology and calcification of the Ediacaran metazoan Cloudina. Scientific Reports 11, 12341. https://doi.org/10.1038/s41598-021-90768-5

Shore, A.J., Wood, R.A., Butler, I.B., Zhuravlev, A.Yu., McMahon, S., Curtis, A., Bowyer, F.T., 2021. Ediacaran metazoan reveals lophotrochozoan affinity and deepens root of Cambrian Explosion. Science Advances 7, eabf2933. https://doi.org/10.1126/sciadv.abf2933

Slagter, S., Tarhan, L.G., Blum, T.B., Droser, M.L., Valley, J.W., 2024. Silica cementation history of the Ediacara Member (Rawnsley Quartzite, South Australia): Insights from petrographic and in situ oxygen isotopic microanalyses. Precambrian Research 402, 107288. https://doi.org/10.1016/j.precamres.2024.107288

Slagter, S., Hao, W., Planavsky, N.J., Konhauser, K.O., Tarhan, L.G., 2022. Biofilms as agents of Ediacara-style fossilization. Scientific Reports 12, 8631. https://doi.org/10.1038/s41598-022-12473-1

Slagter, S., Tarhan, L.G., Hao, W., Planavsky, N.J., Konhauser, K.O., 2021. Experimental evidence supports early silica cementation of the Ediacara Biota. Geology 49, 51–55.

Smith, E.F., Nelson, L.L., Strange, M.A., Eyster, A.E., Rowland, S.M., Schrag, D.P., Macdonald, F.A., 2016. The end of the Ediacaran: Two new exceptionally preserved body fossil assemblages from Mount Dunfee, Nevada, USA. Geology 44, 911–914. https://doi.org/10.1130/G38157.1

Surprenant, R.L., Droser, M.L., 2024. New insight into the global record of the Ediacaran tubular morphotype: a common solution to early multicellularity. Royal Society Open Science 11, 231313. https://doi.org/10.1098/rsos.231313

Surprenant, R.L., Gehling, J.G., Hughes, E.B., Droser, M.L., 2023. Biostratinomy of the enigmatic tubular organism *Aulozoon soliorum*, the Rawnsley Quartzite, South Australia. Gondwana Research 122, 138–162. https://doi.org/10.1016/j.gr.2023.06.010

Surprenant, R.L., Gehling, J.G., Droser, M.L., 2020. Biological and ecological insights from the preservational variability of *Funisia dorothea*, Ediacara Member, South Australia. PALAIOS 35, 359–376. https://doi.org/10.2110/palo.2020.014

Tarhan, L.G., Droser, M.L., Gehling, J.G., Dzaugis, M.P., 2017. Microbial mat sandwiches and other anactualistic sedimentary features of the Ediacara Member (Rawnsley Quartzite, South Australia): Implications for interpretation of the Ediacaran sedimentary record. PALAIOS 32, 181–194. https://doi.org/10.2110/palo.2016.060

Tarhan, L.G., Hood, A. v.S., Droser, M.L., Gehling, J.G., Briggs, D.E.G., 2016. Exceptional preservation of soft-bodied Ediacara Biota promoted by silica-rich oceans. Geology 44, 951–954. https://doi.org/10.1130/G38542.1

Tarhan, L.G., Droser, M.L., Gehling, J.G., Dzaugis, M.P., 2015. Taphonomy and morphology of the Ediacara form genus *Aspidella*. Precambrian Research 257, 124–136. https://doi.org/10.1016/j.precamres.2014.11.026

Waggoner, B., 2003. The Ediacaran Biotas in space and time. Integrative and Comparative Biology 43, 104–113. https://doi.org/10.1093/icb/43.1.104

Wang, X., Zhang, X., Zhang, Y., Cui, L., Li, L., 2021. New materials reveal *Shaanxilithes* as a *Cloudina*-like organism of the late Ediacaran. Precambrian Research 362, 106277. https://doi.org/10.1016/j.precamres.2021.106277

Wood, R., Bowyer, F.T., Alexander, R., Yilales, M., Uahengo, C.-I., Kaputuaza, K., Ndeunyema, J., Curtis, A., 2023. New Ediacaran biota from the oldest Nama Group, Namibia (Tsaus Mountains), and re-definition of the Nama Assemblage. Geological Magazine 160, 1673–1686. https://doi.org/10.1017/S0016756823000638

Wood, R., Curtis, A., 2015. Extensive metazoan reefs from the Ediacaran Nama Group, Namibia: the rise of benthic suspension feeding. Geobiology 13, 112–122. https://doi.org/10.1111/gbi.12122

Wright, D.F., 2015. Fossils, homology, and "Phylogenetic Paleo-ontogeny": A reassessment of primary posterior plate homologies among fossil and living crinoids with insights from developmental biology. Paleobiology 41, 570–591. https://doi.org/10.1017/pab.2015.18

Xiao, S., Narbonne, G.M., Zhou, C., Laflamme, M., Grazhdankin, D.V., Moczydlowska-Vidal, M., Cui, H., 2016. Towards an Ediacaran time Scale: Problems, protocols, and prospects. Episodes 39, 540–555. https://doi.org/10.18814/epiiugs/2016/v39i4/103886

Xiao, S., Droser, M., Gehling, J.G., Hughes, I.V., Wan, B., Chen, Z., Yuan, X., 2013. Affirming life aquatic for the Ediacara biota in China and Australia. Geology 41, 1095–1098. https://doi.org/10.1130/G34691.1

Xiao, S., Dong, L., 2006. On the morphological and ecological history of Proterozoic Macroalgae. In Xiao, S., Kaufman, A.J. (Eds.), Neoproterozoic Geobiology and Paleobiology. Springer Netherlands, Dordrecht, pp. 57–90.

Xiao, S., Yuan, X., Steiner, M., Knoll, A.H., 2002. Macroscopic carbonaceous compressions in a terminal Proterozoic shale: A systematic reassessment of the Miaohe Biota, South China. Journal of Paleontology 76, 2, 347-376. https://doi.org/10.1666/00223360(2002)076<0347:MCCIAT>2.0.CO;2

Yang, B., Steiner, M., Schiffbauer, J.D., Selly, T., Wu, X., Zhang, C., Liu, P., 2020. Ultrastructure of Ediacaran cloudinids suggests diverse taphonomic histories and affinities with non-biomineralized annelids. Scientific Reports 10, 535. https://doi.org/10.1038/s41598-019-56317-x

Ye, Q., Tong, J., An, Z., Hu, J., Tian, L., Guan, K., Xiao, S., 2019. A systematic description of new macrofossil material from the upper Ediacaran Miaohe Member in South China. Journal of Systematic Palaeontology 17, 183–238. https://doi.org/10.1080/14772019.2017.1404499

APPENDIX A

Genus	Localities where present*
Annulatubus	Olenik Uplift (Siberia), NW Canada (Laurentia)
Archaeichnium	Kalahari, South Australia, Great Basin (Laurentia)
Aulozoon	South Australia
Calyptrina	White Sea, South China
Conotubus	South China
Convolutubus	Central Iran
Costatubus	White Sea, Great Basin (Laurentia)
Cucullus	South China, White Sea
Funisia	South Australia
Gaojishania	Kalahari, South China
Gyrichnites	Kalahari
Onuphionella	Great Basin (Laurentia)
Protechiurus	Kalahari
Protoconites	South China
Saarina	White Sea, Great Basin (Laurentia)
Sabellidites	White Sea, Avalonia
Sekwitubulus	NW Canada
Shaanxilithes	India, White Sea, North China, South China, Uchur-Maya (Siberia), Olenik Uplift (Siberia), Oulongbuluke
Sinospongia	South China, White Sea
Somatohelix	South Australia
Vaveliksia	White Sea
Vendoconularia	White Sea
Wutubus	South Australia, White Sea, Great Basin (Laurentia), South China
Zolotytsia	NW Canada (Laurentia)
Zuunia	Zavkhan Terrane (Siberia)

*Entries with parentheses represent fossil localities that were determined to be paleogeographically distinct but that are located on the same paleocontinents (e.g., "Olenik Uplift (Siberia)" and "Uchur-Maya (Siberia)" represent two paleogeographically distinct localities on the same paleocontinent). Entries with no parentheses represent paleocontinents that do not have more than one paleogeographically distinct fossil site in the database.

Table 5. List of all non-biomineral tubular genera and their associated localities/paleocontinents. Tubular genera that are singletons (i.e., *Buchholzbrunnichnus* and *Propaleolina)* are excluded from this table.

Morphogroup	Total no. genera	No. genera in Avalon	No. genera in White Sea	No. genera in Nama	No. genera with unknown age*
Arboreomorpha	3	3	2	2	0
Bilateromorpha	14	0	13	1	0
Dickinsoniomorpha	7	0	6	0	1
Erniettomorpha	10	0	6	6	1
Kimberellomorpha	3	0	3	1	0
Palaeopaschichnid	2	1	1	2	0
Pentaradialomorpha	1	0	1	0	0
Rangeomorpha	15	11	6	3	0
Tetraradialomorpha	2	0	1	0	1
Triradialomorpha	7	0	7	0	0
Tubular organisms	27	0	15	15	2

*Genera listed under "unknown age" represent fossil occurrences that cannot be resolved to a single assemblage.

Table 6. Number of total genera and numbers of genera in the Avalon, White Sea, and Nama assemblages of all major Ediacaran morphogroups.

Table 7. Ediacara non-biomineral tube database, including all metazoan-grade tubular organisms preserved in the Ediacaran fossil record from 575—538 Ma. The Site column reports the general name for the location of the fossil site where the taxon was recovered. The locality column reports the name of the paleogeographically distinct locality in which each genus is located. The Time Bin column reports the relative age of the formation in which the fossil was found based on the three assemblages of the Ediacara biota; WS = White Sea assemblage (560-550 Ma) , N = Nama assemblage (550-538 Ma). The External Features column describes the type of external features or constructional morphology of each genus; S = smooth, M = modules, A = annulations, L = longitudinal striae, Ret = reticulated pattern, R = rings, Bb = Barrel-in-barrel, Ff = funnel-in-funnel. The Form Subgrouping column characterizes each genus based on its growth morphology, The Inferred Original Composition column reports the type of material each genus is hypothesized to have been comprised of; WM = weakly to non-biomineral, NMRO = non-biomineral and rigid organic, NMNR = non-biomineral, non-rigid organic, A = agglutinated, NR = not reported or unknown, NMRO and NMNR = genera that are thought to be composed of both non-biomineral, rigid organic and non-biomineral, non-rigid organic material.

Genus	Species	Site	Finer stratigraphic subdivision	Formation	Locality	Paleocontinent	Time bin	External features	Form subgrouping	Inferred original composition	References
Annulatubus	*flexuosus*	Khorbusuonka River		Khatyspyt	Olenik Uplift	Siberia	WS or N	A	tubiform	NR	Grazhdankin et al. 2008; Carbone et al. 2015 Bykova et al. 2020
Annulatubus	*flexuosus*	Locality B, Sekwi Brook		Upper Blueflower	NW Canada	Laurentia	WS or N	A	tubiform	NR	Carbone et al. 2015
Archaeichnium	*haughtoni*	Grundorn	Kuibis Beds	Dabis or Zaris	Kalahari	Kalahari	N	A, L	conotubular	A	Haughton 1960; Glaessner 1963, 1977; Pickford 1995; Nelson et al. 2022
Archaeichnium	*haughtoni*	Koelkrans	Spitskof Member	Urusis	Kalahari	Kalahari	N	A, L	conotubular	A	Buatois el. 2018; Nelson et al. 2022

Archaeichnium	*haughtoni*	Koelkrans	Feldschuhorn Member	Urusis	Kalahari	Kalahari	N	A, L	conotubular	A	Jensen et al. 2000; Buatois er al. 2018; Nelson et al. 2022
Archaeichnium	*haughtoni*	Multiple	Huns Member	Urusis	Kalahari	Kalahari	N	A, L	conotubular	A	Glaessner 1963, 1977; Germs 1972, 1995; Hagadorn and Waggoner 2000; Jensen et al. 2000; Darroch et al. 2021; Nelson et al. 2022
Archaeichnium	*haughtoni*	Multiple	Nasep Member	Urusis	Kalahari	Kalahari	N	A, L	conotubular	A	Glaessner 1963, 1977; Germs 1972, 1995; Hagadorn and Waggoner 2000; Jensen et al. 2000, 2006; Freeman 2009; Darroch et al. 2021; Nelson et al. 2022
Archaeichnium	*haughtoni*	Nilpena Ediacara National Park	Ediacara Member	Rawnsley Quartzite	South Australia	South Australia	WS	A, L	conotubular	A	Gehling and Droser 2013
Archaeichnium	*haughtoni*	Johnnie		Lower Wood Canyon	Great Basin	Laurentia	N	A, L	conotubular	A	Corsetti and Hagadorn 2000; Hagadorn and Waggoner 2000; Smith et al. 2017

Aulozoon	*soliorum*	Devil's Peak	Ediacara Member	Rawnsley Quartzite	South Australia	South Australia	WS	S	tubiform	NMNR	Reid et al. 2020; Gehling and Runnegar 2022
Aulozoon	*soliorum*	Nilpena Ediacara National Park	Ediacara Member	Rawnsley Quartzite	South Australia	South Australia	WS	S	tubiform	NMNR	Reid et al. 2020; Surprenant et al. 2023
Buchholzbrunnichnus	*kroneri*	Farm Buchholzbrunn	Kliphoek Member	Dabis	Kalahari	Kalahari	N	A, L	tubiform	NR	Germs 1973; Darroch et al. 2021
Calyptrina	*striata*	Karakhta River	Syuzma Beds	Verkhovka	White Sea	Baltica	WS	A	tubiform	NMNR	Bobrovskiy et al. 2022
Calyptrina	*striata*	Miaohe Section	Miaohe Member	Doushantuo	South China	South China	WS	A	tubiform	NMNR	Xiao et al. 2002; Ana et al. 2015; Ye et al. 2019; Cui et al. 2021
Calyptrina	*striata*	Obozerskaya drillcore	Syuzma Beds	Verkhovka	White Sea	Baltica	WS	A	tubiform	NMNR	Bobrovskiy et al. 2022
Calyptrina	*striata*	Onega River		Lyamtsa	White Sea	Baltica	WS	A	tubiform	NMNR	Ivantsov and Grazhdankin 1997; Fedonkin 1990; Grazhdankin 2003; Grazhdankin et al. 2007; Fedonkin and Ivantsov 2007
Calyptrina	*striata*	Solza River	Syuzma Beds	Verkhovka	White Sea	Baltica	WS	A	tubiform	NMNR	Bobrovskiy et al. 2022

Calyptrina	*striata*	Zhimaping Section	Miaohe Member	Doushantuo	South China	South China	WS	A	tubiform	NMNR	Jiang et al. 2011; Zhou et al. 2018; Ye et al. 2019
Calyptrina	*striata*	Zimnie Gory	Erga Beds	Erga	White Sea	Baltica	WS	A	tubiform	NMNR	Bobrovskiy et al. 2022
Conotubus	*hemiannulatus*	Changpoya Section	middle Gaojiashan Member	Dengying	South China	South China	N	Ff, A	cloudinomorph	WM	Cai and Hua 2007; Cai et al. 2011, 2012; Chai et al. 2021; Cui et al. 2019; Hong et al. 2007; Selly et al. 2020; Wang et al. 2021; Yang et al. 2021
Conotubus	*hemiannulatus*	Gaojiashan Section	middle Gaojiashan Member	Dengying	South China	South China	N	Ff, A	cloudinomorph	WM	Cai and Hua 2007; Cai et al. 2011, 2012; Chai et al. 2021; Cui et al. 2019; Hong et al. 2007; Selly et al. 2020; Wang et al. 2021; Yang et al. 2021
Conotubus	*hemiannulatus*	Shengchangba	Gaojiashan Member	Dengying	South China	South China	N	Ff, A	cloudinomorph	WM	Chen et al. 2022

Conotubus	*hemiannulatus*	Tudimiao Section	middle Gaojiashan Member	Dengying	South China	South China	N	Ff, A	cloudinomorph	WM	Cai and Hua 2007; Cai et al. 2011, 2012; Chai et al. 2021; Cui et al. 2019; Hong et al. 2007; Selly et al. 2020; Wang et al. 2021; Yang et al. 2021
Conotubus	*hemiannulatus*	Youjiagou Section	middle Gaojiashan Member	Dengying	South China	South China	N	Ff, A	cloudinomorph	WM	Cai and Hua 2007; Cai et al. 2011, 2012; Chai et al. 2021; Cui et al. 2019; Hong et al. 2007; Selly et al. 2020; Wang et al. 2021; Yang et al. 2021
Convolutubus	*dargazinensis*	Chamir	Sub-Unit 6	Kushk Series	Central Iran	Unknown	N	Ff	cloudinomorph	WM	Vaziri et al. 2018, 2021
Convolutubus	*dargazinensis*	Kushk	Sub-Unit 6	Kushk Series	Central Iran	Unknown	N	Ff	cloudinomorph	WM	Vaziri et al. 2018, 2021
Costatubus	*bibendi*	Johnnie		lower Wood Canyon	Great Basin	Laurentia	N	Bb	cloudinomorph	WM	Selly et al. 2020
Costatubus	*bibendi*	Mount Dunfee	middle Esmeralda Member	Deep Spring	Great Basin	Laurentia	N	Bb	cloudinomorph	WM	Selly et al. 2020

Costatubus	*kirsanovi*	NR		Redkino Horizon	White Sea	Baltica	WS	Bb	cloudinomorph	WM	Gnilovskaya 1996; Marusin et al. 2011; Selly et al. 2020; Golubkova et al. 2022
Cucullus	*fraudulentus*	Miaohe Section	Miaohe Member	Doushantuo	South China	South China	WS	S	tubiform	NMNR	Xiao et al. 2002; Ana et al. 2015; Ye et al. 2019; Cui et al. 2021
Cucullus	*fraudulentus*	Sanlihuang Section	Miaohe Member	Doushantuo	South China	South China	WS	S	tubiform	NMNR	Jiang et al. 2011; Zhou et al. 2017; Ye et al. 2019
Cucullus	*sp.*	Shotkusa 1 Borehole		Starorusskaya	White Sea	Baltica	WS	S	tubiform	NMNR	Marusin et al. 2011; Grazhdankin 2014; Golubkova et al. 2018, 2021
Cucullus	*fraudulentus*	Wenghui Section		upper Doushantuo	South China	South China	WS	S	tubiform	NMNR	Jiang et al. 2011; Wang and Wang 2011; Wang et al. 2011, 2014, 2016
Cucullus	*fraudulentus*	Zhimaping Section	Miaohe Member	Doushantuo	South China	South China	WS	S	tubiform	NMNR	Jiang et al. 2011; Zhou et al. 2017; Ye et al. 2019
Funisia	*dorothea*	Nilpena Ediacara National Park	Ediacara Member	Rawnsley Quartzite	South Australia	South Australia	WS	M	tubiform	NMNR	Droser and Gehling 2008

Funisia	*dorothea*	Devil's Peak	Ediacara Member	Rawnsley Quartzite	South Australia	South Australia	WS	M	tubiform	NMNR	Droser and Gehling 2008; Reid et al. 2020
Funisia	*dorothea*	Reaphook Hill	Ediacara Member	Rawnsley Quartzite	South Australia	South Australia	WS	M	tubiform	NMNR	Droser and Gehling 2008; Reid et al. 2020
Funisia	*dorothea*	Ediacara Conservation Park	Ediacara Member	Rawnsley Quartzite	South Australia	South Australia	WS	M	tubiform	NMNR	Droser and Gehling 2008; Reid et al. 2020
Gaojishania	*cyclus*	Donkergange Farm	Hoogland Member	Zaris	Kalahari	Kalahari	N	R, A	tubiform	NMRO and NMNR	Smith et al. 2017
Gaojishania	*cyclus*	Gaojiashan Section	middle Gaojiashan Member	Dengying	South China	South China	N	R, A	tubiform	NMRO and NMNR	Cai et al. 2012, 2013; Cui et al. 2019
Gaojishania	*cyclus*	Shengchangba	Gaojiashan Member	Dengying	South China	South China	N	R, A	tubiform	NMRO and NMNR	Chen et al. 2022
Gaojishania	*cyclus*	Tudimiao Section	middle Gaojiashan Member	Dengying	South China	South China	N	R, A	tubiform	NMRO and NMNR	Cai et al. 2012, 2013; Cui et al. 2022
Gyrichnites	*sauberi*	Farm Haruchas	Vingerbreek Member	Nudaus	Kalahari	Kalahari	N	A	tubiform	NMNR	Darroch et al. 2021; Nelson et al. 2022
Onuphionella	*sp*	LACMNH loc. 17130		lower Wood Canyon	Great Basin	Laurentia	N	L	tubiform	A	Corsetti and Hagadorn 2000; Hagadorn et al. 2000
Onuphionella	*sp*	Salt Spring Hills		lower Wood Canyon	Great Basin	Laurentia	N	L	tubiform	A	Hagadorn et al. 2000

Funisia	*dorothea*	Devil's Peak	Ediacara Member	Rawnsley Quartzite	South Australia	South Australia	WS	M	tubiform	NMNR	Droser and Gehling 2008; Reid et al. 2020
Funisia	*dorothea*	Reaphook Hill	Ediacara Member	Rawnsley Quartzite	South Australia	South Australia	WS	M	tubiform	NMNR	Droser and Gehling 2008; Reid et al. 2020
Funisia	*dorothea*	Ediacara Conservation Park	Ediacara Member	Rawnsley Quartzite	South Australia	South Australia	WS	M	tubiform	NMNR	Droser and Gehling 2008; Reid et al. 2020
Gaojishania	*cyclus*	Donkergange Farm	Hoogland Member	Zaris	Kalahari	Kalahari	N	R, A	tubiform	NMRO and NMNR	Smith et al. 2017
Gaojishania	*cyclus*	Gaojiashan Section	middle Gaojiashan Member	Dengying	South China	South China	N	R, A	tubiform	NMRO and NMNR	Cai et al. 2012, 2013; Cui et al. 2019
Gaojishania	*cyclus*	Shengchangba	Gaojiashan Member	Dengying	South China	South China	N	R, A	tubiform	NMRO and NMNR	Chen et al. 2022
Gaojishania	*cyclus*	Tudimiao Section	middle Gaojiashan Member	Dengying	South China	South China	N	R, A	tubiform	NMRO and NMNR	Cai et al. 2012, 2013; Cui et al. 2022
Gyrichnites	*sauberi*	Farm Haruchas	Vingerbreek Member	Nudaus	Kalahari	Kalahari	N	A	tubiform	NMNR	Darroch et al. 2021; Nelson et al. 2022
Onuphionella	*sp*	LACMNH loc. 17130		lower Wood Canyon	Great Basin	Laurentia	N	L	tubiform	A	Corsetti and Hagadorn 2000; Hagadorn et al. 2000
Onuphionella	*sp*	Salt Spring Hills		lower Wood Canyon	Great Basin	Laurentia	N	L	tubiform	A	Hagadorn et al. 2000

Saarina	*hagadorni*	Johnnie		lower Wood Canyon	Great Basin	Laurentia	N	Ff, A	cloudinomorph	NMNR	Selly et al. 2020
Saarina	*hagadorni*	Mount Dunfee	middle Esmeralda Member	Deep Spring	Great Basin	Laurentia	N	Ff, A	cloudinomorph	NMNR	Selly et al. 2020
Saarina	*juliae*	NR		Redkino Horizon	White Sea	Baltica	WS	Ff, A	cloudinomorph	NMNR	Gnilovskaya 1996; Marusin et al. 2011; Selly et al. 2020; Golubkova et al. 2022
Sabellidites	*cambriensis*	Borehole 842-F1		Rovno	White Sea	Baltica	N	A	tubiform	NMRO	Moczydlowska et al. 2014
Sabellidites	*cambriensis*	Borehole 942-F3		Buiskaya	White Sea	Baltica	N	A	tubiform	NMRO	Moczydlowska et al. 2014
Sabellidites	*cambriensis*	Gavrilov-Yam Borehole		Nekrasova	White Sea	Baltica	N	A	tubiform	NMRO	Felytsin et al. 1998; Moczydlowska et al. 2014
Sabellidites	*cambriensis*	Guadalupe and Castanar de Ibors, Hospital del Obispo		AS5 Unit	Spain	Avalonia	N	A	tubiform	NMRO	Vidal et al. 1994; Vidal et al. 1999; Jensen et al. 2007; Herrero et al. 2011
Sabellidites	*spp*	Sierra de la Zarzuela, Orellana dam	Talarrubias Dolostone Bed	lower Villarta Formation	Spain	Avalonia	N	A	tubiform	NMRO	Jensen et al. 2007; Herrero et al. 2011; Alvaro et al. 2020; Cortijo et al. 2021

Sekwitubulus	*annulatus*	Locality D, Sekwi Brook		upper Blueflower	NW Canada	Laurentia	WS or N	A	tubiform	NMRO	Carbone et al. 2015
Shaanxilithes	*ningqiangensis*	Pitari Dochi	Earthy Dolomite Member	Krol E	India	India	N	Tt: Ff, A	cloudinomorph	NMRO and NMNR	Jiang et al. 2002; Tarhan et al. 2014
Shaanxilithes	*ningqiangensis*	Pitari Dochi	Earthy Siltstone Member	Shaliyan Formation	India	India	N	Tt: Ff, A	cloudinomorph	NMRO and NMNR	Jiang et al. 2002; Tarhan et al. 2014
Shaanxilithes	*ningqiangensis*	Bernashivka Village	Bronnitsa Beds	Yaryshev	White Sea	Baltica	WS	Tt: Ff, A	cloudinomorph	NMRO and NMNR	Nesterovsky et al. 2018; Soldatenko et al. 2019; Martyshyn and Uchman 2021; Maslov and Podkovyrov 2022; Francovschi et al. 2023
Shaanxilithes	*ningqiangensis*	Binggou Section		Tuerkeng	North China	North China Block	N	Tt: Ff, A	cloudinomorph	NMRO and NMNR	Yang et al. 2019
Shaanxilithes	*ningqiangensis*	Bogedong Section	lower-middle Gaojiashan Member	Dengying	South China	South China	N	Tt: Ff, A	cloudinomorph	NMRO and NMNR	Cai et al. 2010, 2012; Meyer et al. 2012; Cui et al. 2019
Shaanxilithes	*ningqiangensis*	Changpoya Section	lower Gaojiashan Member	Dengying	South China	South China	N	Tt: Ff, A	cloudinomorph	NMRO and NMNR	Cai et al. 2010, 2012; Meyer et al. 2012; Cui et al. 2019
Shaanxilithes	*ningqiangensis*	Feidation-Dongdahe Section	Jiucheng Member	middle Dengying	South China	South China	N	Tt: Ff, A	cloudinomorph	NMRO and NMNR	Yang et al. 2017; Chai et al. 2021

Shaanxilithes	*ningqiangensis*	Gaojiashan Section	lower Gaojiashan Member	Dengying	South China	South China	N	Tt: Ff, A	cloudinomorph	NMRO and NMNR	Cai et al. 2010, 2012; Meyer et al. 2012; Cui et al. 2019; Wang et al. 2021
Shaanxilithes	*ningqiangensis*	Jiangchuan	Jiucheng Member	middle Dengying	South China	South China	N	Tt: Ff, A	cloudinomorph	NMRO and NMNR	Yang et al. 2017; Chai et al. 2021
Shaanxilithes	*ningqiangensis*	Jiunvdong Section		Dongpo	North China	North China Block	N	Tt: Ff, A	cloudinomorph	NMRO and NMNR	Pang et al. 2021
Shaanxilithes	*ningqiangensis*	Lijiagou Section	lower-middle Gaojiashan Member	Dengying	South China	South China	N	Tt: Ff, A	cloudinomorph	NMRO and NMNR	Cai et al. 2010, 2012; Meyer et al. 2012; Cui et al. 2019
Shaanxilithes	*ningqiangensis*	Luoquan Section		Dongpo	North China	North China Block	N	Tt: Ff, A	cloudinomorph	NMRO and NMNR	Wang et al. 2021
Shaanxilithes	*ningqiangensis*	Luxishao Section	Jiucheng Member	middle Dengying	South China	South China	N	Tt: Ff, A	cloudinomorph	NMRO and NMNR	Yang et al. 2017, 2021; Chai et al. 2021
Shaanxilithes	*ningqiangensis*	Nuuchchalakh		Aim	Uchur-Maya	Siberia	WS or N	Tt: Ff, A	cloudinomorph	NMRO and NMNR	Zhuravlev et al. 2009; Cai et al. 2011; Ivantsov 2017
Shaanxilithes	*ningqiangensis*	Olenek Uplift		Khatyspyt	Olenik Uplift	Siberia	WS or N	Tt: Ff, A	cloudinomorph	NMRO and NMNR	Meyer et al. 2012; Rogov et al. 2012; Bykova et al. 2020
Shaanxilithes	*ningqiangensis*	Quanji Section		Zhoujieshan	Oulongbuluke microcontinent	Chaidam Block	N	Tt: Ff, A	cloudinomorph	NMRO and NMNR	Shen et al. 2007; Cai and Hua 2011; Wang et al. 2021

Shaanxilithes	*ningqiangensis*	Quanjishan Section		Zhoujieshan	Oulongbuluke microcontinent	Chaidam Block	N	Tt: Ff, A	cloudinomorph	NMRO and NMNR	Pang et al. 2021; Wang et al. 2021
Shaanxilithes	*ningqiangensis*	Schizhonggou Section	lower-middle Gaojiashan Member	Dengying	South China	South China	N	Tt: Ff, A	cloudinomorph	NMRO and NMNR	Cai et al. 2010, 2012; Cui et al. 2019
Shaanxilithes	*ningqiangensis*	Suyukou Section		Tuerkeng	North China	North China Block	N	Tt: Ff, A	cloudinomorph	NMRO and NMNR	Shen et al. 2007; Pang et al. 2021; Wang et al. 2021
Shaanxilithes	*ningqiangensis*	Taozichong Section		lower Taozichong	South China	South China	N	Tt: Ff, A	cloudinomorph	NMRO and NMNR	Cai and Hua 2011; An et al. 2020; Wang et al. 2021
Shaanxilithes	*ningqiangensis*	Tongshan		Laupo	South China	South China	N	Tt: Ff, A	cloudinomorph	NMRO and NMNR	Jinbaio et al. 1981; Wang et al. 2021
Shaanxilithes	*ningqiangensis*	Tuerkeng Section		Tuerkeng	North China	North China Block	N	Tt: Ff, A	cloudinomorph	NMRO and NMNR	Yang et al. 2007, 2019; Pang et al. 2021
Shaanxilithes	*ningqiangensis*	Wangjiawan Section	Jiucheng Member	middle Dengying	South China	South China	N	Tt: Ff, A	cloudinomorph	NMRO and NMNR	Zhang et al. 2015; Chai et al. 2021; Yang et al. 2017; Yang et al. 2022
Shaanxilithes	*ningqiangensis*	Xinji Section		Dongpo	North China	North China Block	N	Tt: Ff, A	cloudinomorph	NMRO and NMNR	Wang et al. 2021
Shaanxilithes	*ningqiangensis*	Youjiagou Section	lower-middle Gaojiashan Member	Dengying	South China	South China	N	Tt: Ff, A	cloudinomorph	NMRO and NMNR	Cai et al. 2010, 2012; Meyer et al. 2012; Cui et al. 2019
Shaanxilithes	*ningqiangensis*	Zhelinziwan Section	upper Shibantan Member	Dengying	South China	South China	N	Tt: Ff, A	cloudinomorph	NMRO and NMNR	An et al. 2020

Shaanxilithes	*ningqiangensis*	Zhujiaqing Section	Jiucheng Member	middle Dengying	South China	South China	N	Tt: Ff, A	cloudinomorph	NMRO and NMNR	Yang et al. 2017; Chai et al. 2021
Shaanxilithes	*ningqiangensis*	Zihuagou Section		Tuerkeng	North China	North China Block	N	Tt: Ff, A	cloudinomorph	NMRO and NMNR	Yang et al. 2077; Yang et al. 2019; Pang et al. 2021
Sinospongia	*typica*	Borehole C18		Lyamtsa	White Sea	Baltica	WS	A	tubiform	NMNR	Francovschi et al. 2003; Grazhdankin et al. 2007; Ye et al. 2019
Sinospongia	*chenjunyuani*	Maxi section	Miaohe Member	Doushantuo	South China	South China	WS	Ret	tubiform	NMNR	Jiang et al. 2011; Zhou et al. 2017; Ye et al. 2019
Sinospongia	*chenjunyuani*	Miaohe Section	Miaohe Member	Doushantuo	South China	South China	WS	Ret	tubiform	NMNR	Xiao et al. 2002; Ana et al. 2015; Ye et al. 2019; Cui et al. 2021
Sinospongia	*typica*	Shotkusa 1 Borehole		Starorusskaya	White Sea	Baltica	WS	A	tubiform	NMNR	Grazhdankin 2014; Golubkova et al. 2018, 2021
Sinospongia	*chenjunyuani*	Zhimaping Section	Miaohe Member	Doushantuo	South China	South China	WS	Ret	tubiform	NMNR	Jiang et al. 2011; Zhou et al. 2017; Ye et al. 2019
Somatohelix	*sinuosus*	Ediacara Conservation Park	Ediacara Member	Rawnsley Quartzite	South Australia	South Australia	WS	S	tubiform	NMNR	Sappenfield et al. 2011

Somatohelix	*sinuosus*	Nilpena Ediacara National Park	Ediacara Member	Rawnsley Quartzite	South Australia	South Australia	WS	S	tubiform	NMNR	Sappenfield et al. 2011
Somatohelix	*sinuosus*	Ediacara Conservation Park	Nilpena Member	Rawnsley Quartzite	South Australia	South Australia	WS	S	tubiform	NMNR	Sappenfield et al. 2011
Vaveliksia	*velikanovi*	Dniester Hydroelectric Power Station	Lomozov Beds	Mogilev	White Sea	Baltica	WS	S	ovatubular	NMNR	Ivantsov et al. 2004;Grazhdankin 2014; Ivantsov 2015; Soldatenko et al. 2019; Martyshyn and Uchman 2021
Vaveliksia	*svetozarovae*	Vinozh Village	Lomozov Beds	Mogilev	White Sea	Baltica	WS	S	ovatubular	NMNR	Ivantsov et al. 2004, 2015; Grazhdankin 2014; Soldatenko et al. 2019; Martyshyn and Uchman 2021
Vaveliksia	*vana*	Zimnie Gory	Yorgia Beds	Erga	White Sea	Baltica	WS	S	ovatubular	NMNR	Grazhdankin et al. 2007; Serezhnikova 2010; Ivantsov et al. 2004; Ivantsov 2013; Antcliffe et al. 2015; Zakrevskaya 2014

Vendoconularia	*triradiata*	Yarnema		Verkhovka	White Sea	Baltica	WS	A, L	conotubular	WM	Ivantsov and Fedonkin 2002; Grazhdankin 2003, 2014; Van Iten er al. 2005, 2014; Ivantsov et al. 2019; Ivantsov and Zakrevskaya 2021
Wutubus	*sp.*	Ediacara Conservation Park	Ediacara Member	Rawnsley Quartzite	South Australia	South Australia	WS	M	conotubular	NMNR	Gehling and Droser 2018
Wutubus	*annularis*	Lyadova Village	Dzhurzhevka Beds	Nagoryany	White Sea	Baltica	WS or N	M	conotubular	NMNR	Grazhdankin 2014; Nesterovsky et al. 2018; Francovschi et al. 2021, 2023
Wutubus	*annularis*	Mount Dunfee	Dunfee Member	Deep Spring	Great Basin	Laurentia	N	M	conotubular	NMNR	Smith et al. 2016
Wutubus	*annularis*	Wuhe Section	Shibantan Member	Dengying	South China	South China	N	M	conotubular	NMNR	Chen et al. 2014; Xiao et al. 2020
Zolotytsia	*sp.*	Locaity 4		upper Miette Group	NW Canada	Laurentia	N	S	tubiform	NMNR	Hofmann et al. 1991
Zolotytsia	*biserialis*	NR		Verkhovka	White Sea	Baltica	WS	S	tubiform	NMNR	Fedonkin et al. 2012
Zuunia	*chimidtsereni*	Bayan Gorge Section		Zuun-Arts	Zavkhan Terrane	Siberia	N	Ff	cloudinomorph	NMRO	Bold et al. 2016; Smith et al. 2016; Yang et al. 2020

REFERENCES

Álvaro, J.J., Cortijo, I., Jensen, S., Lorenzo, S., Pieren, A.P., 2019. Updated stratigraphic framework and biota of the Ediacaran and Terreneuvian in the Alcudia-Toledo Mountains of the Central Iberian Zone, Spain. Estudios Geologicos 75, 093. https://doi.org/10.3989/egeol.43620.548

An, Z., Zhao, X., Niu, Z., Li, Z., Ye, Q., 2020. Discovery of *Shaanxilithes* from the Dengying Formation in the Yangtze Gorges area, South China, and its stratigraphic significance. China Geology 3, 649–651. https://doi.org/10.31035/cg2020059

Antcliffe, J.B., Callow, R.H.T., Brasier, M.D., 2014. Giving the early fossil record of sponges a squeeze: The early fossil record of sponges. Biological Reviews 89, 972–1004. https://doi.org/10.1111/brv.12090

Bobrovskiy, I., Nagovitsyn, A., Hope, J.M., Luzhnaya, E., Brocks, J.J., 2022. Guts, gut contents, and feeding strategies of Ediacaran animals. Current Biology 32, 5382-5389.e3. https://doi.org/10.1016/j.cub.2022.10.051

Bold, U., Crowley, J.L., Smith, E.F., Sambuu, O., Macdonald, F.A., 2016. Neoproterozoic to early Paleozoic tectonic evolution of the Zavkhan terrane of Mongolia: Implications for continental growth in the Central Asian orogenic belt. Lithosphere 8, 729–750. https://doi.org/10.1130/L549.1

Buatois, L.A., Almond, J., Mángano, M.G., Jensen, S., Germs, G.J.B., 2018. Sediment disturbance by Ediacaran bulldozers and the roots of the Cambrian explosion. Scientific Reports 8, 4514. https://doi.org/10.1038/s41598-018-22859-9

Bykova, N., LoDuca, S.T., Ye, Q., Marusin, V., Grazhdankin, D., Xiao, S., 2020. Seaweeds through time: Morphological and ecological analysis of Proterozoic and early Paleozoic benthic macroalgae. Precambrian Research 350, 105875. https://doi.org/10.1016/j.precamres.2020.105875

Cai, Y., Hua, H., 2007. Pyritization in the Gaojiashan Biota. Chinese Science Bulletin 52, 645–650. https://doi.org/10.1007/s11434-007-0080-9

Cai, Y., Hua, H., Zhang, X., 2013. Tube construction and life mode of the late Ediacaran tubular fossil *Gaojiashania cyclus* from the Gaojiashan Lagerstätte. Precambrian Research 224, 255–267. https://doi.org/10.1016/j.precamres.2012.09.022

Cai, Y., Schiffbauer, J.D., Hua, H., Xiao, S., 2012. Preservational modes in the Ediacaran Gaojiashan Lagerstätte: Pyritization, aluminosilicification, and carbonaceous compression. Palaeogeography, Palaeoclimatology, Palaeoecology 326–328, 109–117. https://doi.org/10.1016/j.palaeo.2012.02.009

Cai, Y., Hua, H., Zhuravlev, A.Yu., Gámez Vintaned, J.A., Ivantsov, A.Yu., 2011a. Discussion of 'First finds of problematic Ediacaran fossil *Gaojiashania* in Siberia and its origin.' Geological Magazine 148, 329–333. https://doi.org/10.1017/S0016756810000749

Cai, Y., Schiffbauer, J.D., Hua, H., Xiao, S., 2011b. Morphology and paleoecology of the late Ediacaran tubular fossil *Conotubus hemiannulatus* from the Gaojiashan Lagerstätte of southern Shaanxi Province, South China. Precambrian Research 191, 46–57. https://doi.org/10.1016/j.precamres.2011.09.002

Cai, Y., Hua, H., Xiao, S., Schiffbauer, J.D., Li, P., 2010. Biostratinomy of the late Ediacaran pyritized Gaojiashan Lagerstätte from southern Shaanxi, South China: importance of event deposits. PALAIOS 25, 487–506. https://doi.org/10.2110/palo.2009.p09-133r

Carbone, C.A., Narbonne, G.M., Macdonald, F.A., Boag, T.H., 2015. New Ediacaran fossils from the uppermost Blueflower Formation, northwest Canada: Disentangling biostratigraphy and paleoecology. Journal of Paleontology 89, 281–291. https://doi.org/10.1017/jpa.2014.25

Chai, S., Wu, Y., Hua, H., 2021. Potential index fossils for the Terminal Stage of the Ediacaran System. Journal of Asian Earth Sciences 218, 104885. https://doi.org/10.1016/j.jseaes.2021.104885

Chen, W., Cai, Y., Liang, D., Wang, X., 2022. Two tubular fossil assemblages from the terminal Ediacaran Dengying Formation in southern Shaanxi Province of South China. Precambrian Research 378, 106762. https://doi.org/10.1016/j.precamres.2022.106762

Chen, Z., Zhou, C., Xiao, S., Wang, W., Guan, C., Hua, H., Yuan, X., 2014. New Ediacara fossils preserved in marine limestone and their ecological implications. Scientific Reports 4, 4180. https://doi.org/10.1038/srep04180

Corsetti, F.A., Hagadorn, J.W., 2000. Precambrian-Cambrian transition: Death Valley, United States. Geology 28, 4, 299-302.

Cortijo, I., Palacios, T., Jensen, S., Barrera, J.M., 2021. The Ediacaran-Cambrian Radiation of Animals within the Villuercas-Ibores-Jara UNESCO Global Geopark, Spain. Geoconservation Research 4, 1, 43-55. https://doi.org/10.30486/gcr.2021.1918395.1076

Cui, H., Kitajima, K., Orland, I.J., Xiao, S., Baele, J.-M., Kaufman, A.J., Denny, A., Zhou, C., Spicuzza, M.J., Fournelle, J.H., Valley, J.W., 2021. Deposition or diagenesis? Probing the Ediacaran Shuram excursion in South China by SIMS. Global and Planetary Change 206, 103591. https://doi.org/10.1016/j.gloplacha.2021.103591

Cui, H., Xiao, S., Cai, Y., Peek, S., Plummer, R.E., Kaufman, A.J., 2019. Sedimentology and chemostratigraphy of the terminal Ediacaran Dengying Formation at the Gaojiashan section, South China. Geological Magazine 156, 1924–1948. https://doi.org/10.1017/S0016756819000293

Darroch, S.A.F., Cribb, A.T., Buatois, L.A., Germs, G.J.B., Kenchington, C.G., Smith, E.F., Mocke, H., O'Neil, G.R., Schiffbauer, J.D., Maloney, K.M., Racicot, R.A., Turk, K.A., Gibson, B.M., Almond, J., Koester, B., Boag, T.H., Tweedt, S.M., Laflamme, M., 2021. The trace fossil record of the Nama Group, Namibia: Exploring the terminal Ediacaran roots of the Cambrian explosion. Earth-Science Reviews 212, 103435. https://doi.org/10.1016/j.earscirev.2020.103435

Droser, M.L., Gehling, J.G., 2008. Synchronous aggregate growth in an abundant new Ediacaran tubular organism. Science 319, 1660–1662. https://doi.org/10.1126/science.1152595

Fedonkin, M.A., Vickers-Rich, P., Swalla, B.J., Trusler, P., Hall, M., 2012. A new metazoan from the Vendian of the White Sea, Russia, with possible affinities to the ascidians. Paleontological Journal 46, 1–11. https://doi.org/10.1134/S0031030112010042

Fedonkin, M.A., Ivantsov, A.Y., 2007. *Ventogyrus* , a possible siphonophore-like trilobozoan coelenterate from the Vendian Sequence (late Neoproterozoic), northern Russia. Geological Society, London, Special Publications 286, 187–194. https://doi.org/10.1144/SP286.14

Felitsyn, S.B., Vidal, G., Moczydłowska, M., 1998. Trace elements and Sr and C isotopic signatures in late Neoproterozoic and earliest Cambrian sedimentary organic matter from siliciclastic successions in the East European Platform. Geological Magazine 135, 537–551. https://doi.org/10.1017/S0016756898001150

Francovschi, I., Grădinaru, E., Li, H., Shumlyanskyy, L., Ciobotaru, V., 2021. U–Pb geochronology and Hf isotope systematics of detrital zircon from the late Ediacaran Kalyus Beds (East European Platform): Palaeogeographic evolution of southwestern Baltica and constraints on the Ediacaran biota. Precambrian Research 355, 106062. https://doi.org/10.1016/j.precamres.2020.106062

Freeman, G., 2009. The rise of bilaterians. Historical Biology 21, 99–114. https://doi.org/10.1080/08912960903295843

Gehling, J.G., Droser, M.L., 2018. Ediacaran scavenging as a prelude to predation. Emerging Topics in Life Sciences 2, 213–222. https://doi.org/10.1042/ETLS20170166

Gehling, J.G., Droser, M.L., 2013. How well do fossil assemblages of the Ediacara Biota tell time? Geology 41, 447–450. https://doi.org/10.1130/G33881.1
Gehling, J.G., Runnegar, B., 2022. *Phyllozoon* and *Aulozoon* : Key components of a novel Ediacaran death assemblage in Bathtub Gorge, Heysen Range, South Australia. Geological Magazine. 159, 1134–1147. https://doi.org/10.1017/S0016756821000509

Germs, G.J.B., 1973. Possible Sprigginid worm and a new trace fossil from the Nama Group, south west Africa. Geology 1, 69-70. https://doi.org/10.1130/0091-7613(1973)1<69:PSWAAN>2.0.CO;2

Germs, G.J.B., 1972. Trace Fossils from the Nama Group, South-West Africa. Journal of Paleontology 46, 6, 864-870. https://www.jstor.org/stable/1302944

Glaessner, M.F., 1977. Re-examination of *Archaeichnium*, a fossil from the Nama Group. Annals of the South African Museum 74.
https://www.biodiversitylibrary.org/item/128445

Golubkova, E.Yu., Kuzmenkova, O.F., Laptsevich, A.G., Kushim, E.A., Vaskaboinikava, T.V., Silivanov, M.O., 2022. Paleontological characteristics of the upper Vendian–lower Cambrian sediments in the section of the North Polotsk Borehole of the East European Platform, Belarus. Stratigraphy and Geological Correlation 30, 457–474.
https://doi.org/10.1134/S0869593822060077

Golubkova, E.Yu., Bobrovskiy, I.M., Kushim, E.A., Plotkina, Yu.V., 2021. Fossil organisms of the Redkino Regional Stage of the Upper Vendian of the Northwestern Russian Platform (Leningrad Region). Paleontological Journal 55, 579–587.
https://doi.org/10.1134/S0031030121050051

Golubkova, E.Yu., Kushim, E.A., Kuznetsov, A.B., Yanovskii, A.S., Maslov, A.V., Shvedov, S.D., Plotkina, Yu.V., 2018. Redkinian Biota of Macroscopic Fossils from the Northwestern East European Platform (South Ladoga Region). Doklady Earth Sciences 479, 300–304. https://doi.org/10.1134/S1028334X18030169

Grazhdankin, D., 2014. Patterns of evolution of the Ediacaran soft-bodied Biota. Journal of Paleontology 88, 269–283. https://doi.org/10.1666/13-072

Grazhdankin, D.V., 2003. Structure and Depositional Environment of the Vendian Complex in the Southeastern White Sea Area. Stratigraphy and Geological Correlation 11, 4, 313-331.

Grazhdankin, D.V., Balthasar, U., Nagovitsin, K.E., Kochnev, B.B., 2008. Carbonate-hosted Avalon-type fossils in arctic Siberia. Geology 36, 803.
https://doi.org/10.1130/G24946A.1

Grazhdankin, D.V., Nagovitsin, K.E., Maslov, A.V., 2007. Late Vendian Miaohe-type ecological assemblage of the east European platform. Doklady Earth Sciences 417, 1183–1187. https://doi.org/10.1134/S1028334X07080107

Hagadorn, J.W., Waggoner, B., 2000. Ediacaran fossils from the Southwestern Great Basin, United States. Journal of Paleontology 74, 349–359. https://doi.org/10.1666/0022-3360(2000)074<0349:EFFTSG>2.0.CO;2

Hagadorn, J.W., Fedo, C.M., Waggoner, B.M., 2000. Early Cambrian Ediacaran-type fossils from California. Journal of Paleontology 74, 731–740. https://doi.org/10.1666/0022-3360(2000)074<0731:ECETFF>2.0.CO;2

Haughton, S.H., 1960. An Archaeocyathid from the Nama System. Transactions of the Royal Society of South Africa 36, 57–59. https://doi.org/10.1080/00359196009519032

Herrero, M.J., Martín-Pérez, A., Alonso-Zarza, A.M., Gil-Peña, I., Meléndez, A., Martín-García, R., 2011. Petrography and geochemistry of the magnesites and dolostones of the Ediacaran Ibor Group (635 to 542 Ma), Western Spain: Evidences of their hydrothermal origin. Sedimentary Geology 240, 71–84. https://doi.org/10.1016/j.sedgeo.2011.08.007

Hofmann, H.J., Mountjoy, E.W., Teitz, M.W., 1991. Ediacaran fossils and dubiofossils, Miette Group of Mount Fitzwilliam area, British Columbia. Canadian Journal of Earth Science 28, 1541–1552. https://doi.org/10.1139/e91-138

Hong, H., Zhe, C., Xunlai, Y., 2007. The advent of mineralized skeletons in Neoproterozoic Metazoa—new fossil evidence from the Gaojiashan Fauna. Geological Journal 42, 263–279. https://doi.org/10.1002/gj.1077

Ivantsov, A.Yu., 2013. Trace fossils of Precambrian metazoans “Vendobionta” and “Mollusks.” Stratigraphic Geologic Correlations 21, 252–264. https://doi.org/10.1134/S0869593813030039

Ivantsov AYu, Grazhdankin DV. 1997 A new representative of the Petalonamae from the Upper Vendian of the Arkhangelsk Region. Paleontological Journal 31, 3–18.

Ivantsov, A.Yu., 2017. Finds of Ediacaran-type fossils in Vendian deposits of the Yudoma Group, Eastern Siberia. Doklady Earth Science 472, 143–146. https://doi.org/10.1134/S1028334X17020131

Ivantsov, A.Yu., Zakrevskaya, M.A., 2021. Symmetry of Vendobionta (Late Precambrian Metazoa). Paleontological Journal 55, 717–726. https://doi.org/10.1134/S0031030121070054

Ivantsov, A.Yu., Vickers-Rich, P., Zakrevskaya, M.A., Hall, M., 2019. Conical thecae of Precambrian macroorganisms. Paleontological Journal 53, 1134–1146. https://doi.org/10.1134/S0031030119110054

Ivantsov, A.Y., Gritsenko, V.P., Paliy, V.M., Velikanov, V.A., Konstantinenko, L.I., Menasova, A.S., Fedonkin, M.A., Zakrevskaya, M.A. and Serezhnikova, E.A., 2015. Upper Vendian macrofossils of Eastern Europe. PIN RAS.

Ivantsov, A.Y., Malakhovskaya, Y.E., Serezhnikova, E.A., 2004, Some problematic fossils from the Vendian of the Southeastern White Sea Region. Paleontological Journal 38, 1.

Jensen, S., Palacios, T., Martí Mus, M., 2007. A brief review of the fossil record of the Ediacaran–Cambrian transition in the area of Montes de Toledo–Guadalupe, Spain. Geological Society, London, Special Publications 286, 223–235. https://doi.org/10.1144/SP286.16

Jensen, S., Droser, M.L., Gehling, J.G., 2006. A critical look at the Ediacaran trace fossil record. In Xiao, S., Kaufman, A.J. (Eds.), Neoproterozoic Geobiology and Paleobiology, Topics in Geobiology. Springer Netherlands, Dordrecht, pp. 115–157. https://doi.org/10.1007/1-4020-5202-2_5

Jensen, S., Saylor, B.Z., Gehling, J.G., 2000. Complex trace fossils from the terminal Proterozoic of Namibia. Geology 28, 143-146.

Jiang, G., Shi, X., Zhang, S., Wang, Y., Xiao, S., 2011. Stratigraphy and paleogeography of the Ediacaran Doushantuo Formation (ca. 635–551Ma) in South China. Gondwana Research 19, 831–849. https://doi.org/10.1016/j.gr.2011.01.006

Jiang, G., Christie-Blick, N., Kaufman, A.J., Banerjee, D.M., Rai, V., 2002. Sequence stratigraphy of the Neoproterozoic Infra Krol Formation and Krol Group, Lesser Himalaya, India. Journal of Sedimentary Research 72, 524–542. https://doi.org/10.1306/120301720524

Jinbiao, C., Huimin, Z., Yusheng, X., Guogan, M., 1981. On the upper Precambrian (Sinian Suberathem) in China. Precambrian Research 15, 207–228. https://doi.org/10.1016/0301-9268(81)90052-8

Martyshyn, A., Uchman, A., 2021. New Ediacaran fossils from the Ukraine, some with a putative tunicate relationship. PalZ 95, 623–639. https://doi.org/10.1007/s12542-021-00596-1

Marusin, V.V., Grazhdankin, D.V., Maslov, A.V., 2011. Redkino stage in evolution of Vendian macrophytes. Doklady Earth Science 436, 197–202. https://doi.org/10.1134/S1028334X11020176

Maslov, A.V., Podkovyrov, V.N., 2022. Sources of Fine-grained alumosiliciclastic material for the Vendian–Lower Cambrian rocks of the Podilian Transnistria: A synthesis of Lithogeochemical Data. Stratigraphic Geological Correlations 30, 127–146. https://doi.org/10.1134/S0869593822030029

Meyer, M., Schiffbauer, J.D., Xiao, S., Cai, Y., Hua, H., 2012. Taphonomy of the upper Ediacaran enigmatic ribbonlike fossil *Shaanxilithes*. PALAIOS 27, 354–372. https://doi.org/10.2110/palo.2011.p11-098r

Moczydłowska, M., Westall, F., Foucher, F., 2014. Microstructure and biogeochemistry of the organically preserved Ediacaran metazoan *Sabellidites*. Journal of Paleontology 88, 224–239. https://doi.org/10.1666/13-003

Nelson, L.L., Ramezani, J., Almond, J.E., Darroch, S.A.F., Taylor, W.L., Brenner, D.C., Furey, R.P., Turner, M., Smith, E.F., 2022. Pushing the boundary: A calibrated Ediacaran-Cambrian stratigraphic record from the Nama Group in northwestern Republic of South Africa. Earth and Planetary Science Letters 580, 117396. https://doi.org/10.1016/j.epsl.2022.117396

Nesterovsky, V.A., Martyshyn, A.I., Chupryna, A.M., 2018. New biocenosis model of Vendian (Ediacaran) sedimentation basin of Podilia (Ukraine). Journal of Geology, Geography and Geoecology 27, 95–107. https://doi.org/10.15421/111835

Pang, K., Wu, C., Sun, Y., Ouyang, Q., Yuan, X., Shen, B., Lang, X., Wang, R., Chen, Z., Zhou, C., 2021. New Ediacara-type fossils and late Ediacaran stratigraphy from the northern Qaidam Basin (China): Paleogeographic implications. Geology 49, 1160–1164. https://doi.org/10.1130/G48842.1

Pickford, M.H.L., 1995. Review of the Riphean, Vendian and early Cambrian palaeontology of the Otavi and Nama Groups, Namibia. Communications of the Geological Survey of Namibia 10, 57-81.

Reid, L.M., Holmes, J.D., Payne, J.L., García-Bellido, D.C., Jago, J.B., 2020. Taxa, turnover and taphofacies: A preliminary analysis of facies-assemblage relationships in the Ediacara Member (Flinders Ranges, South Australia). Australian Journal of Earth Sciences 67, 905–914. https://doi.org/10.1080/08120099.2018.1488767

Rogov, V., Marusin, V., Bykova, N., Goy, Y., Nagovitsin, K., Kochnev, B., Karlova, G., Grazhdankin, D., 2012. The oldest evidence of bioturbation on Earth. Geology 40, 395–398. https://doi.org/10.1130/G32807.1

Sappenfield, A., Droser, M.L., Gehling, J.G., 2011. Problematica, trace fossils, and tubes within the Ediacara Member (South Australia): Redefining the ediacaran trace fossil record one tube at a time. J. Paleontol. 85, 256–265. https://doi.org/10.1666/10-068.1

Selly, T., Schiffbauer, J.D., Jacquet, S.M., Smith, E.F., Nelson, L.L., Andreasen, B.D., Huntley, J.W., Strange, M.A., O'Neil, G.R., Thater, C.A., Bykova, N., Steiner, M., Yang, B., Cai, Y., 2020. A new cloudinid fossil assemblage from the terminal Ediacaran of Nevada, USA. Journal of Systematic Palaeontology 18, 357–379. https://doi.org/10.1080/14772019.2019.1623333

Serezhnikova, E.A., 2010. Colonization of substrates: Vendian sedentary benthos. Paleontological Journal 44, 1560–1569. https://doi.org/10.1134/S0031030110120117

Shen, B., Xiao, S., Dong, L., Chuanming, Z., Liu, J., 2007. Problematic macrofossils from Ediacaran successions in the North China and Chaidam blocks: implications for their evolutionary roots and biostratigraphic significance. Journal of Paleontology 81, 1396–1411. https://doi.org/10.1666/06-016R.1

Smith, E.F., Nelson, L.L., Tweedt, S.M., Zeng, H., Workman, J.B., 2017. A cosmopolitan late Ediacaran biotic assemblage: new fossils from Nevada and Namibia support a global biostratigraphic link. Proceedings of the Royal Society B: Biological Sciences 284, 20170934. https://doi.org/10.1098/rspb.2017.0934

Smith, E.F., Nelson, L.L., Strange, M.A., Eyster, A.E., Rowland, S.M., Schrag, D.P., Macdonald, F.A., 2016. The end of the Ediacaran: Two new exceptionally preserved body fossil assemblages from Mount Dunfee, Nevada, USA. Geology 44, 911–914. https://doi.org/10.1130/G38157.1

Soldatenko, Y., El Albani, A., Ruzina, M., Fontaine, C., Nesterovsky, V., Paquette, J.-L., Meunier, A., Ovtcharova, M., 2019. Precise U-Pb age constrains on the Ediacaran biota in Podolia, East European Platform, Ukraine. Scientific Reports 9, 1675. https://doi.org/10.1038/s41598-018-38448-9

Tarhan, L.G., Hughes, N.C., Myrow, P.M., Bhargava, O.N., Ahluwalia, A.D., Kudryavtsev, A.B., 2014. Precambrian-Cambrian boundary interval occurrence and form of the enigmatic tubular body fossil Shaanxilithes ningqiangensis from the Lesser Himalaya of India. Palaeontology 57, 283–298. https://doi.org/10.1111/pala.12066

Van Iten, H., De Moraes Leme, J., Coelho Rodrigues, S., Guimaraes Simoes, M., 2005. Reinterpretation of a Conulariid-like fossil from the Vendian of Russia. Palaeontology 48, 619–622. https://doi.org/10.1111/j.1475-4983.2005.00471.x

Vaziri, S.H., Majidifard, M.R., Darroch, S.A.F., Laflamme, M., 2021. Ediacaran diversity and paleoecology from central Iran. Journal of Paleontology 95, 236–251. https://doi.org/10.1017/jpa.2020.88

Vaziri, S.H., Majidifard, M.R., Laflamme, M., 2018. Diverse assemblage of Ediacaran fossils from Central Iran. Scientific Reports 8, 5060. https://doi.org/10.1038/s41598-018-23442-y

Vidal, G., Palacios, T., Moczydłowska, M., Gubanov, A.P., 1999. Age constraints from small shelly fossils on the early Cambrian terminal Cadomian Phase in Iberia. GFF 121, 137–143. https://doi.org/10.1080/11035899901212137

Vidal, G., Palacios, T., Gámez-Vintaned, J.A., Balda, M.A.D., Grant, S.W.F., 1994. Neoproterozoic-early Cambrian geology and palaeontology of Iberia. Geological Magazine 131, 729–765. https://doi.org/10.1017/S001675680001284X

Wang, Y., Wang, X., 2011. New observations on *Cucullus* Steiner from the Neoproterozoic Doushantuo Formation of Guizhou, South China. Lethaia 44, 275–286. https://doi.org/10.1111/j.1502-3931.2010.00241.x

Wang, X., Zhang, X., Zhang, Y., Cui, L., Li, L., 2021. New materials reveal *Shaanxilithes* as a Cloudina-like organism of the late Ediacaran. Precambrian Research 362, 106277. https://doi.org/10.1016/j.precamres.2021.106277

Wang, Ye, Wang, Yue, Du, W., Wang, X., 2016. New data of macrofossils in the Ediacaran Wenghui Biota from Guizhou, South China. Acta Geologica Sinica - English Edition 90, 1611–1628. https://doi.org/10.1111/1755-6724.12805

Wang, Y., Wang, Y., Du, W., Wang, X., 2014. The correlation between macroscopic algae and metazoans in the Ediacaran: A case study on the Wenghui biota in northeastern Guizhou, South China. Australian Journal of Earth Sciences 61, 967–977. https://doi.org/10.1080/08120099.2014.956231

Wang, Y., Chen, H., Wang, X., Huang, Y., 2011. Evolution of the Ediacaran Doushantuoian Meta-Paleo-Community in Northeast Guizhou, South China. Acta Geologica Sinica - English Edition 85, 533–543. https://doi.org/10.1111/j.1755-6724.2011.00448.x

Xiao, S., Gehling, J.G., Evans, S.D., Hughes, I.V., Droser, M.L., 2020. Probable benthic macroalgae from the Ediacara Member, South Australia. Precambrian Research 350, 105903. https://doi.org/10.1016/j.precamres.2020.105903

Xiao, S., Yuan, X., Steiner, M., Knoll, A.H., 2002. Macroscopic carbonaceous compressions in a terminal Proterozoic shale: A systematic reassessment of the Miaohe Biota, South China. Journal of Paleontology 76, 2, 347-376. https://doi.org/10.1666/00223360(2002)076<0347:MCCIAT>2.0.CO;2

Yang, B., Warren, L.V., Steiner, M., Smith, E.F., Liu, P., 2022. Taxonomic revision of Ediacaran tubular fossils: *Cloudina , Sinotubulites* and *Conotubus*. Journal of Paleontology 96, 256–273. https://doi.org/10.1017/jpa.2021.95

Yang, B., Steiner, M., Schiffbauer, J.D., Selly, T., Wu, X., Zhang, C., Liu, P., 2020. Ultrastructure of Ediacaran cloudinids suggests diverse taphonomic histories and affinities with non-biomineralized annelids. Scientific Reports 10, 535. https://doi.org/10.1038/s41598-019-56317-x

Yang, J., Lyons, T.W., Zeng, Z., Odigie, K.O., Bates, S., Hu, L., 2019. Geochemical constraints on the origin of Neoproterozoic cap carbonate in the Helan Mountains, North China: Implications for mid-late Ediacaran glaciation? Precambrian Research 331, 105361. https://doi.org/10.1016/j.precamres.2019.105361

Yang, C., Li, X.-H., Zhu, M., Condon, D.J., 2017. SIMS U–Pb zircon geochronological constraints on upper Ediacaran stratigraphic correlations, South China. Geological Magazine 154, 1202–1216. https://doi.org/10.1017/S0016756816001102

Ye, Q., Tong, J., An, Z., Hu, J., Tian, L., Guan, K., Xiao, S., 2019. A systematic description of new macrofossil material from the upper Ediacaran Miaohe Member in South China. Journal of Systematic Palaeontology 17, 183–238. https://doi.org/10.1080/14772019.2017.1404499

Zakrevskaya, M., 2014. Paleoecological reconstruction of the Ediacaran benthic macroscopic communities of the White Sea (Russia). Palaeogeography, Palaeoclimatology, Palaeoecology 410, 27–38. https://doi.org/10.1016/j.palaeo.2014.05.021

Zhang, Z.L., Hua, H., Zhang, Z.F., 2015. Problematic Ediacaran fossil *Shaanxilithes* from the Jiucheng Member of Wangjiawan section in Jinning, Yunnan Province. Acta Palaeontologica Sinica 54.

Zhou, C., Yuan, X., Xiao, S., Chen, Z., Hua, H., 2019. Ediacaran integrative stratigraphy and timescale of China. Science China Earth Sciences 62, 7–24. https://doi.org/10.1007/s11430-017-9216-2

Zhuravlev, A.Yu., Vintaned, J.A.G., Ivantsov, A.Yu., 2009. First finds of problematic Ediacaran fossil Gaojiashania in Siberia and its origin. Geological Magazine 146, 775–780. https://doi.org/10.1017/S0016756809990185

APPENDIX B

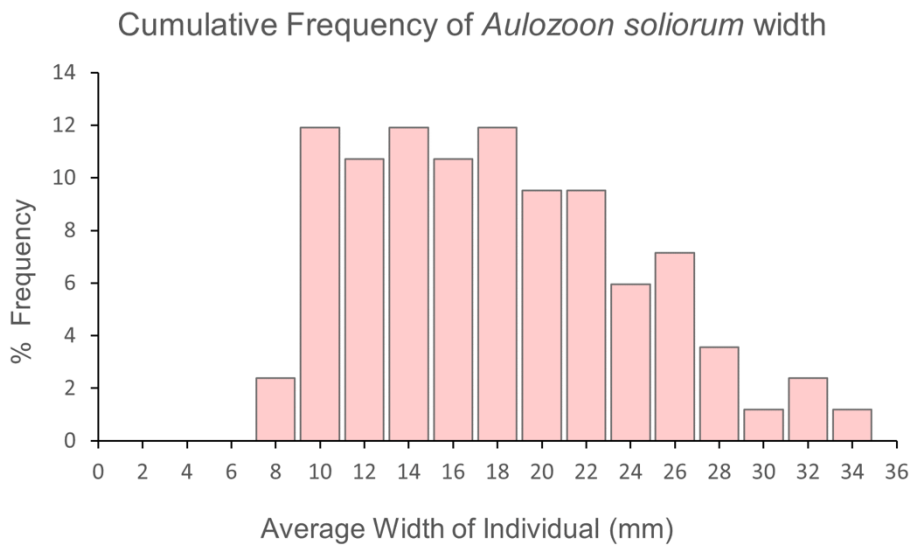

Figure 26. Size distribution of *Aulozoon soliorum* from Nilpena National Heritage Site.

No. of clusters identified from ten samples

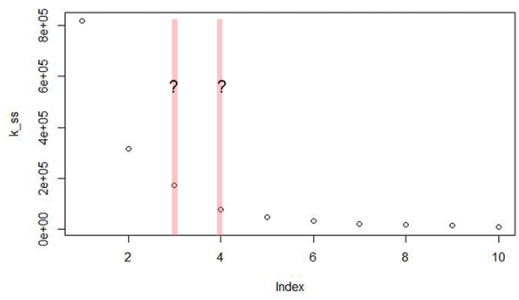

No. of clusters identified from thirty samples

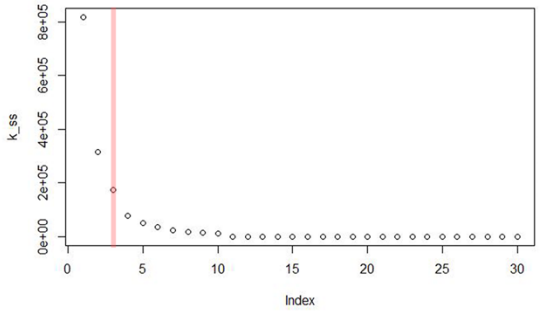

Color-coded clusters in averaged width values to identify the numerical ranges of the three clusters (0-14 mm; 15-21 m; > 22mm)

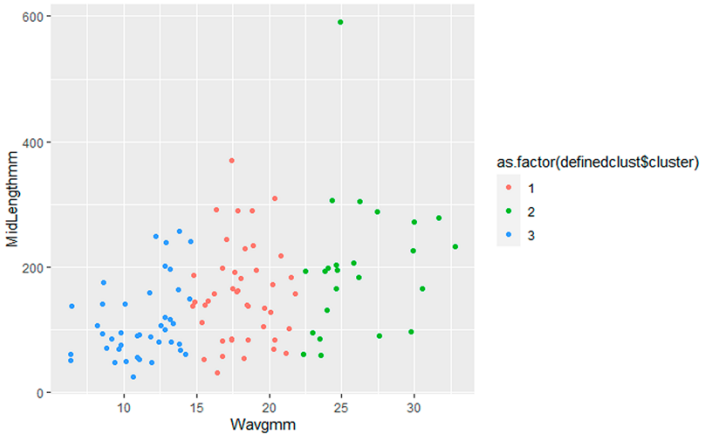

For cluster 1 (0-14 mm)

```
        Welch Two Sample t-test

data:  clust1_dat$Leftmostwmm and clust1_dat$Rightmostwmm
t = -0.41315, df = 73.994, p-value = 0.6807
alternative hypothesis: true difference in means is not equal to 0
95 percent confidence interval:
 -1.832052  1.202788
sample estimates:
mean of x mean of y
 18.08726  18.40189
```

For cluster 1 (15-21 mm)

```
        Welch Two Sample t-test

data:  clust2_dat$Leftmostwmm and clust2_dat$Rightmostwmm
t = -1.1401, df = 44.122, p-value = 0.2604
alternative hypothesis: true difference in means is not equal to 0
95 percent confidence interval:
 -4.039015  1.120181
sample estimates:
mean of x mean of y
 23.91429  25.37371
```

For cluster 1 (>22 mm)

```
        Welch Two Sample t-test

data:  clust3_dat$Leftmostwmm and clust3_dat$Rightmostwmm
t = -0.15422, df = 75.893, p-value = 0.8778
alternative hypothesis: true difference in means is not equal to 0
95 percent confidence interval:
 -1.541468  1.319907
sample estimates:
mean of x mean of y
 11.84512  11.95590
```

Figure 27. Results from *k*-means cluster analysis of *Aulozoon soliorum* width distributions and Welch Two Sample T-tests of the identified clusters.

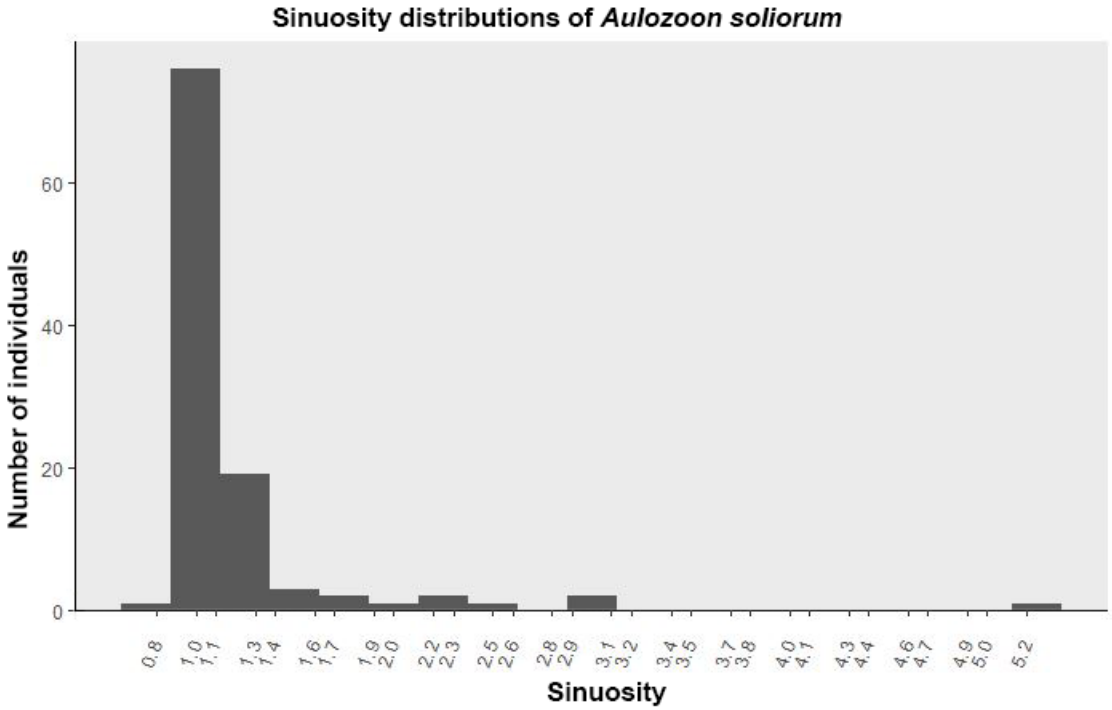

Figure 28. Sinuosity distributions of *Aulozoon soliorum* from Nilpena National Heritage Site.

		Right-hand termination						
		Circular	Rounded	Smooth blunt	Rough blunt	Flared	Ripped	Diffuse
Left-hand termination	Circular							
	Rounded		1	1				
	Smooth blunt		2	4			3	6
	Rough blunt	1	2	2	5		1	3
	Flared							
	Ripped					2		
	Diffuse		3	1		1	1	3

Table 8. Co-occurrence of termination types in *Aulozoon soliorum* individuals at Nilpena National Heritage Site.

APPENDIX C

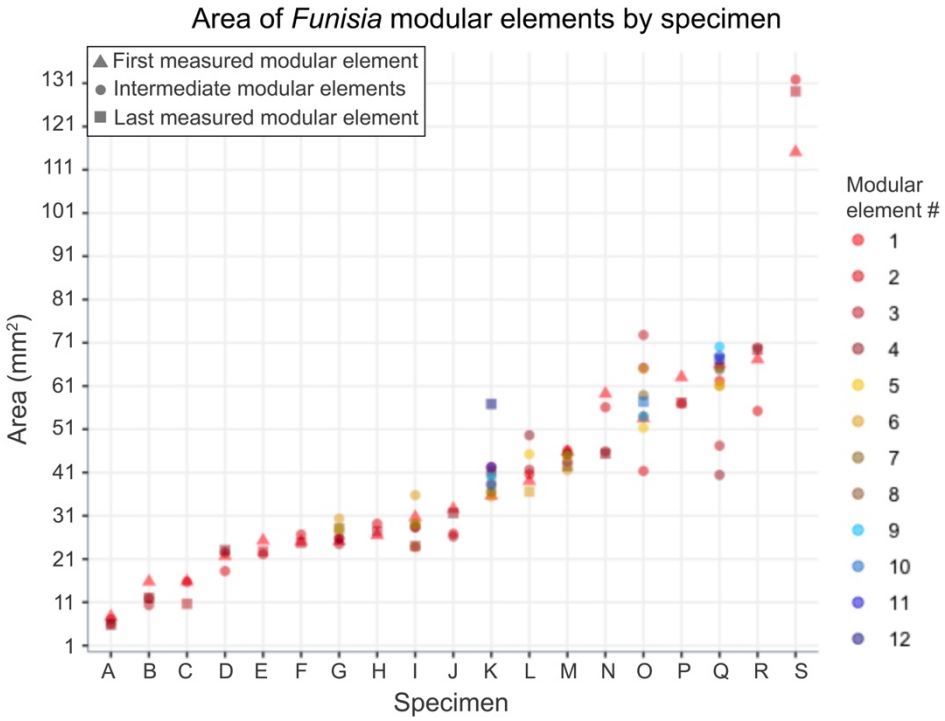

Figure 29. Area of individual modular elements by specimen with information pertaining to relative placement of all modular elements retained. First and last measured modular elements (i.e., those modular elements located at the left-most and right-most ends of the specimen when it is oriented horizontally) are denoted by triangles and squares, respectively. Data points are numbered and color coded based on their relative location within the individual. Modular element number 1 always represents the first measured modular element when the specimen is oriented horizontally and read from left to right; successive modular elements are designated as number two, three, and so on to represent the total number of modular elements within each individual. The maximum number of modular elements in an individual is 12, but most specimens preserved fewer than 12 modular elements, meaning that in some specimens cooler colors, representing modular elements 9-12, are not present because the specimen has fewer than 8 modular elements. For example, specimen "S" preserves only three modular elements, therefore its area values include two end-most elements (denoted by the triangle and the square) and one intermediate element (denoted by a red circle). In contrast, specimen "O" has 10 modular elements, resulting in its first and last measured modular elements having a warm and cool color, respectively, while intermediate values are plotted as a gradient from warm to cooler colors based on proximity to the first and last measured modular elements.